Magnetic field effects on *Drosophila melanogaster* and avian cryptochromes



Marco Bassetto

A thesis submitted in partial fulfilment of the requirements for the degree of Doctor of Philosophy

University of Oxford

Corpus Christi College

Hilary Term 2020

“In theory there is no difference between theory and practice.
In practice there is.”

- Lawrence Peter "Yogi" Berra -

ABSTRACT

One of the major challenges in the field of sensory biology is to understand the process by which migratory songbirds sense the direction of the Earth's magnetic field. This phenomenon, which has fascinated biologists for decades, has seen a growth of interest in the recent years. This poorly understood "sixth sense" has focused the attention of scientists from a variety of disciplines, from biology to theoretical physics. This multidisciplinarity is reflected in the work presented in this thesis, which spans animal behaviour, biochemistry, and spectroscopy. The common thread that links these experiments is the need to gain a better understanding of the radical pair mechanism of magnetoreception. According to this hypothesis, animals perceive magnetic fields by means of magnetically sensitive radicals formed by light-excitation of photosensitive flavoproteins called cryptochromes.

The first project, presented in Chapter 2, was an investigation of magnetic field effects on *Drosophila melanogaster* negative geotaxis. Two sets of equipment were built, experiments were conducted in a meticulously controlled environment, and strong statistical tests were applied to a large-scale dataset, but it proved impossible to reproduce the magnetic field effects reported in the literature.

The second project, presented in Chapter 3, was to test whether avian cryptochromes 1a and 1b could be the magnetoreceptor molecules. The proteins were expressed and purified and their binding affinity for flavin adenine dinucleotide, the chromophore responsible for light activation of the protein, was determined. It was concluded that cryptochromes 1a and 1b cannot be the magnetoreceptors, even though they have been considered ideal candidates for many years.

Finally, the third project, described in Chapter 4, was a comparative study of the spectroscopic properties and magnetic sensitivity of avian cryptochrome 4s from different species using Broadband Cavity-Enhanced Absorption Spectroscopy. This technique has the advantage of detecting the change in the optical absorbance of photo-induced radicals when the proteins are exposed to an external magnetic field. Striking differences were found between cryptochrome 4s from migratory and non-migratory birds.

TABLE OF CONTENTS

Introduction 1

1.1 The geomagnetic field 1

1.2 Electromagnetic induction 4

1.3 Magnetite based magnetoreception 4

1.4 The radical pair mechanism 5

1.4.1 General reaction scheme 7

1.5 Cryptochromes 9

1.5.1 Differences between animal cryptochromes 12

1.6 Evidence for the radical pair mechanism 14

1.6.1 Behavioural evidences 14

1.6.2 Neuroanatomical studies 16

1.6.3 Avian cryptochromes 16

1.6.4 Radiofrequency field effect 17

1.6.5 Magnetic field effects on *Drosophila melanogaster* 18

1.7 My project 25

Magnetic field effects on *Drosophila* negative geotaxis 27

2.1 Introduction 27

2.2 Material and Methods 28

2.2.1 Non-magnetic facility 28

2.2.2 *Drosophila* strains 28

2.2.3 Gravity apparatus 29

2.2.4 FlyVac apparatus 33

2.2.5 Static magnetic fields 35

2.2.6 Time-dependent electromagnetic fields 35

2.2.7 Data analysis 38

2.3 Results 43

2.3.1 Gravity apparatus 43
2.3.2 FlyVac apparatus 55
2.4 Discussion 65
2.4.2 Considerations on the set-ups 68
2.4.3 Statistical considerations on Fedele *et al.*[43] 69
2.4.4 Possible explanations for the lack of positive results 72
2.5 Conclusions 76
Avian Cry1s as putative magnetoreceptors 77
3.1 Introduction 77
3.1.1 Isothermal Titration Calorimetry (ITC) 77
3.1.2 Surface Plasmon Resonance (SPR) spectroscopy 78
3.2 Material and Methods 79
3.2.1 Cloning procedure 79
3.2.2 Expression and purification 80
3.2.3 SDS – PAGE and Western Blot 82
3.2.4 UV-Vis and Circular Dichroism (CD) spectroscopy 83
3.2.5 Isothermal Titration Calorimetry (ITC) 83
3.2.6 Surface Plasmon Resonance spectroscopy (SPR) 84
3.3 Results 86
3.3.1 *Er*Cry1a - Characterisation of the protein 86
3.3.2 *Er*Cry1a - Isothermal Titration Calorimetry 87
3.3.3 *Er*Cry1a - Surface Plasmon Resonance 88
3.3.4 *Er*Cry1b - Characterisation of the protein 90
3.3.5 *Er*Cry1b - Isothermal Titration Calorimetry 91
3.3.6 *Er*Cry1b - Surface Plasmon Resonance 92
3.4 Discussion 94
3.4.1 Considerations on the published results on Cry1s 95

3.5 Conclusions 97
Magnetic field effects on avian Cryptochrome 4s 98
4.1 Introduction 98
4.2 Material and Methods 102
4.2.1 Cloning, expression and purification of Cry4s 102
4.2.2 Broadband Cavity-Enhanced Spectroscopy (BBCEAS) 103
4.3 Results 105
4.3.1 Proteins characterisation 105
4.3.2 BBCEAS measurements 107
4.4 Discussion 110
4.5 Conclusions 112
Conclusions and future work 114
6. Appendix 116
6.1 Sequences alignments 125
7. Bibliography 130

Chapter 1

INTRODUCTION

Magnetoreception is the ability of certain organisms to perceive magnetic fields and use them for orientation and navigation purposes[108]. Many organisms belonging to different phyla, have been reported to be able to exploit the presence of a magnetic field and use it to their advantage: some organisms use it to navigate entire oceans, while others to find better conditions just a few centimetres away[72]. This phenomenon has fascinated biologists for decades and has seen an increased level of interest in the past few years. Scientists from diverse disciplines such as Biology, Biochemistry, Physical Chemistry and Theoretical Physics are now working together to try to solve the mystery of the "sixth sense". Despite the effort devoted to trying to solve this puzzle, so far nobody has found an exhaustive explanation that can fully explain how an organism can perceive magnetic fields as weak as the Earth's magnetic field[108].

1.1 The geomagnetic field

All organisms have evolved on a planet that has an intrinsic magnetic field[51]. Our planet possesses in its centre a massive magnet that produces a magnetic field extending from the Earth's core to the magnetosphere, a region above the ionosphere, several tens of thousands of kilometres into space. The magnitude of the field varies from ~25 μT at the equator to ~65 μT at the poles. As with all magnets, the geomagnetic field has North and South poles, which are tilted at an angle of 11° with respect to the Earth's rotational axis. Therefore, geographic and magnetic poles do not correspond. Moreover, the field lines enter the Northern and leave the Southern hemisphere: i.e. the magnetic field South pole is close to the Earth's geographic North pole and vice versa. As a consequence, the magnetic field lines point upward on the Southern hemisphere, run parallel to the Earth's surface at the magnetic equator and point downward in the Northern hemisphere (Figure 1.1)[109,172,173] The most accepted theory explaining the origin of the geomagnetic field is the so-called geodynamo effect[30]. Like in a normal dynamo, a conductive fluid can induce an electromagnetic field if kept in constant rotation. The conductive liquid in this case is the molten iron within the liquid core of the planet, that is constantly rotating thanks to the Coriolis force. This will produce electric currents aligned with the rotational axis of the planet and thus, the geomagnetic field[30]. The field, however, is neither

uniform nor constant. In fact, not only does it change by 3nT km^{-1} and 0.009° km^{-1} on the North-South axis (and much less on the east-west axis), it also varies by a few nT (from 30 to 100 nT, less than 1% of the total field intensity) on a daily basis due to stochastic fluctuations[88].

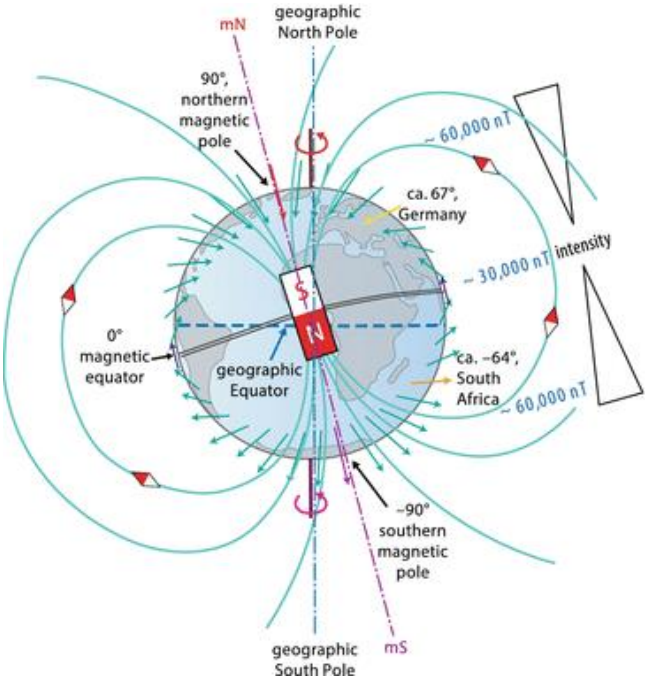


Figure 1.1. Depiction of the geomagnetic field. The field lines enter in the Northern hemisphere of our planet and leave in the Southern hemisphere. Noticeably, the geographical and the magnetic poles do not coincide, nor do the geographical and magnetic equators. Adapted from Mouritsen (2013)[110].

At any location, the geomagnetic field can be represented in Cartesian plan by dividing it in several components (Figure. 1.2):

- Declination (D): indicates the angle, in degrees, between the geographic North and the magnetic North.
- Inclination (I): is the angle, in degrees, between the field lines and the horizontal.
- Horizontal intensity (H): defines the horizontal component of the total field intensity.
- Vertical intensity (Z): defines the vertical component of the total field intensity.
- Total intensity (F): is the total strength of the geomagnetic field.

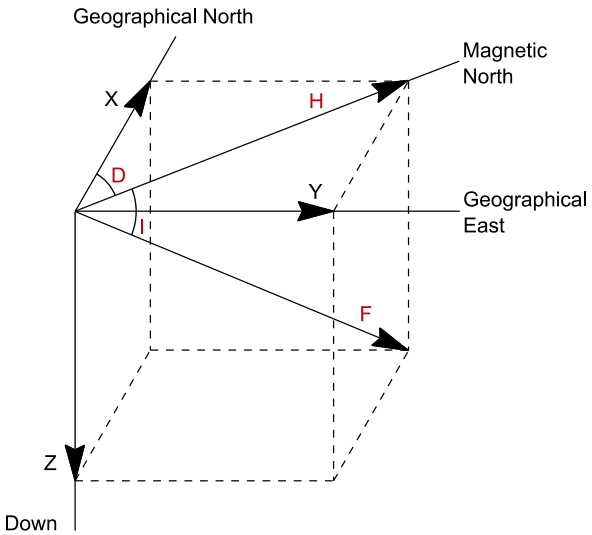


Figure 1.2. Vector representation of the geomagnetic field components. (X, Y, Z) define the Cartesian coordinate system (Geographical North, Geographical East, down). (H, D, Z) (horizontal intensity, declination, down) describe the components of the magnetic field. (I) represents the inclination of the field. (F) is the total intensity. Adapted from the National Oceanic and Atmospheric Administration (https://www.noaa.gov/).

Despite the small regional changes mentioned above, the geomagnetic field is a powerful source of navigational information[108]. The magnetic vector provides information that can be used as a compass[174], determining direction, or as a map[135], determining position (similarly to a GPS system)[172]. The direction of movement can be calculated by using the polarity of the field (H) and/or the inclination (I)[110,173,174], while position can be extrapolated by using the total magnetic intensity (F), the inclination angle (I) and the magnetic declination angle (D)[22,72,85,98,100]. Various behavioural studies have shown how fishes[16,89], sea turtles[99], amphibians[136] and birds[108,174,175] can use these different magnetic components to determine their direction and/or position. Moreover, a large number of organisms, from magnetotactic bacteria[14,71] to mammals[10], have been reported to be able to align themselves with the geomagnetic field. Even though behavioural studies clearly showed how animals can perceive and exploit the presence of magnetic fields and use them for navigational purposes, it is still not clear how they manage to do that[108]. Magnetic fields can penetrate biological materials, and therefore there is no obvious region where the primary sensory centre can be located inside the animal's body. To complicate the phenomenon even more, it is not clear how biological materials can accurately detect magnetic fields in the range of 25-60 μT, when parameters such as anatomical constrains and thermal noise are added to the equation. Currently, only three

mechanisms have been proposed to be physically viable: the first involves electromagnetic induction via highly sensitive electroreceptors[132], the second is based on magnetic particles[84], the third relies on a light-dependent chemical reaction involving pairs of radicals[67].

1.2 Electromagnetic induction

In 1831, Michael Faraday discovered that an electrical conductor moving through a static magnetic field produces a voltage. This effect is called electromagnetic induction and it has been proposed as an explanation for how some elasmobranchs (like sharks, skates and rays) can detect the geomagnetic field[132]. Such fishes possess several hundred pores, that are connected via highly conductive jelly-filled canals to the ampullae of Lorenzini, organs that are extremely sensitive to small changes in voltage (up to 2μV/m)[75,76]. Therefore, voltage induced by the geomagnetic field at the level of the pores could be measured comparing it against seawater, which acts as a reference potential. Nevertheless, it is not clear whether these structures are used for perceiving magnetic fields in elasmobranchs[72,132]. Recently, it has been proposed that pigeons (*Columba livia*) can perceive magnetic fields via electromagnetic induction. According to the authors, these birds possess a population of electrosensory hair cells that express a splice isoform of a voltage-gated calcium channel ($Ca_V1.3$) that has been shown to mediate electroreception in elasmobranchs. These hairs are present in the semi-circular canals of the inner ear and these structures have been shown to be neuronally activated once the bird was exposed to an external magnetic field stimulus[124].

1.3 Magnetite based magnetoreception

The second model that has been proposed revolves around the idea that endogenous magnetite crystals (Fe_3O_4) could be affected by the presence of an external magnetic field and therefore be the primary sensor for magnetoreception[31,81]. Magnetism is generated by the alignment of the electrons spin in the material. Normally, the atoms of a substance have an even number of electrons, so the magnetic moment of one electron cancels that of another. However, in magnetite, the crystal structure aligns the unpaired electrons in series, giving magnetization to the crystal. The magnetic properties of magnetite are due to the structure, size and shape of the crystals[82]. Crystals that roughly measure 50 nm are called single domain and retain a net

magnetic moment. These particles are large enough to be able to align to fields as small as the geomagnetic field[180]. On the other hand, superparamagnetic particles are too small (~ 20 nm) to retain a magnetic moment (due to thermal agitation) but can be temporarily magnetized as long as an external magnetic field is present[29].

Originally, endogenous magnetite crystals were found in bacteria[14]. These peculiar prokaryotes can synthesize magnetosomes, (chains of magnetite crystals) that allow them to swim according to the direction of an external magnetic field[9,71]. Since then, magnetite crystals have been found in nematodes[27], molluscs[161], insects[1,52,91], crustaceans[41] and various vertebrates, such as salmons[31,102], sea turtles[70] and birds[42,45]. This, however, should not come as a surprise. Iron is a fundamental metal for the proper function of the organism, and magnetite crystals could be a form of iron storage that can help with iron homeostasis[166].

In fact, even though magnetosomes prove that organisms are indeed able to synthetize magnetite, this is no evidence for it to be relevant for magnetoreception. To be relevant, magnetite would be needed to be expressed in consistent and specific locations and be associated with the nervous system via, for example, mechanoreceptors (and related ion channels) able to perceive the rotation of the magnetite crystals once aligned to an external magnetic field[111]. Previous reports of magnetite clusters present bilaterally and associated with dendrites in the upper beaks of pigeons (*Columba livia*)[42,45], were not independently confirmed. In fact, such structures were not consistently present in the 200 birds studied, and what were thought to be magnetite clusters were actually iron-rich macrophages[162,163]. This however does not necessary mean that a magnetite-based compass could not possibly exist. In fact, mole rats, fishes and sea turtles use a polarity compass that is independent of the presence of light (see below)[179], making possible the existence of a magnetite-based compass in these animals.

1.4 The radical pair mechanism

The third proposed model for animal magnetoreception revolves around the idea that the magnetic compass could be based on a chemical reaction involving pairs of radicals that are formed upon light excitation[67]. In 1978 Schulten *et al.*,[151] proposed that a photo-sensitive molecule, once activated by a photon, can form magnetically sensitive radical pairs as transient intermediates of the photochemical reaction. If the yield of the products of such a reaction is

dependent on the direction of an external magnetic field with respect to the reactants, one would have the basis for a magnetic compass[151].

A radical is a molecule that contains an unpaired electron and radical pairs are two radicals that are formed simultaneously, normally by a chemical reaction or by electron transfer. They possess a property known as spin angular momentum (or simply spin) that confers magnetic properties on the radicals[67].

Generally speaking, the spins of the radical pairs can be aligned in two states: singlet (S) and triplet (T). In the singlet state the spins of the two unpaired electrons are paired (antiparallel ↑↓), while in the triplet state they are unpaired (parallel ↑↑). Usually, when a radical pair is formed in an organic molecule, not only the formation of the radicals is spin-selective, but the reaction also conserves spin. Therefore, a radical in an overall singlet state can trigger reactions that are forbidden in a triplet state. A fundamental parameter that needs to be taken into consideration when calculating Earth-strength magnetic field effects on a radical pair reaction is the hyperfine interaction, i.e. the magnetic interaction between the spin of the nucleus and the spin of the unpaired electron. Hyperfine interactions must be present in at least one of the radicals, otherwise a radical pair reaction will not be affected by the presence of a small magnetic field. Two isotopes that possess strong nuclear magnetic fields are ^{1}H and ^{14}N, which are found in almost every biologically relevant radical[67].

The formation of the radical pair is not a static process. In fact, once the radical pair is formed in the singlet state, it oscillates in a band of frequencies (normally in the MHz range) and coherently interconverts to the triplet state. The frequency of this process is dependent on the strength of the hyperfine interactions. The singlet-triplet interconversion can be affected by the presence and direction of an external magnetic field due to the Zeeman interaction and the anisotropy of the hyperfine interactions. The anisotropy of the hyperfine interactions derives from the asymmetry of the molecular orbitals that contain the unpaired electron, and therefore, the probability to find an electron in the neighbourhood of a nucleus is not the same in all directions. Thus, the radical pair reaction will be affected by the direction of the magnetic field, giving the basis for a magnetic compass. The Zeeman effect is the interaction of an isolated spin with an external magnetic field that causes the direction of the magnetic moment of the electron to oscillate at a frequency proportional to the strength of the field. For a 50 μT magnetic field the frequency of this motion, also called the Larmor frequency, is 1.4 MHz, corresponding of a period of ~700 ns[67].

1.4.1 General reaction scheme

A general reaction scheme can be described as in Figure 1.3. We can imagine two reactants A and B that once photoexcited, form a radical pair [$A^{\bullet+}$ $B^{\bullet-}$]. The radical pair is formed instantaneously in a singlet state and it is imagined to have two possible reaction pathways. The first is a reverse electron transfer that will regenerate the reactants A and B with a rate constant k_S. This reaction can only happen in the singlet state and it is spin forbidden for the triplet state. The second pathway will convert both the singlet and triplet state of [$A^{\bullet+}$ $B^{\bullet-}$] into a product C, with a constant rate k_C. While the reaction proceeds along one of the two pathways, the remaining radical pairs [$A^{\bullet+}$ $B^{\bullet-}$] will interconvert coherently between their singlet and triplet states. The yield of the product C will not only depend on the rate constants k_S and k_C, but also on the kinetics of the singlet-triplet interconversion. In the presence of an external magnetic field, the Zeeman interaction could increase the fraction of radical pairs in the triplet state so that more radical pairs will form the product C. If the increase in the yield of C is dependent on the direction of the applied magnetic field, then we will have the basis for a magnetic compass. Importantly, for the magnetic field to affect the spin interconversion the radical pair must exist for at least the Larmor period (~ 700 ns). This, however, is not a problem, as the time constants for electron transfers in proteins can be as long as seconds[107]. Another process that needs to be considered, is spin relaxation. To be magnetically sensitive, the radical pair not only needs to have a certain lifetime, but it also needs to maintain its spin-coherence long enough for an external magnetic field to modify the singlet-triplet interconversion[77].

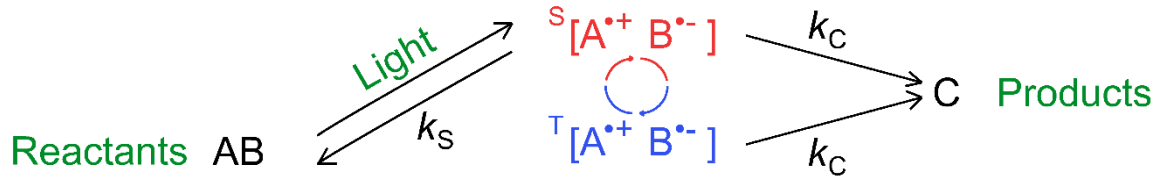


Figure 1.3 General scheme of a radical pair reaction. When reactants AB are photoexcited they are converted into product C via the formation of a radical pair [$A^{\bullet+}$ $B^{\bullet-}$]. The two rate constants k_S and k_C indicate the spin-selective back reaction (towards the reactants AB) and the non-spin-selective forward reaction (towards the product C) of the radical pair. The red and blue arrows indicate the coherent interconversion of the singlet (S) and triplet (T) states of the radical pair [$A^{\bullet+}$ $B^{\bullet-}$]. It is important that the two rate constants k_S and k_C are not too dissimilar. If there were no direct competition between the two pathways, all the radicals would react along one of the

two pathways, not allowing an external magnetic field to influence the reaction[63]. Figure modified from Hore and Mouritsen (2016)[67].

To sum up, radical pairs can be magnetically sensitive and provide directional information when the reaction is spin selective and it conserve spin, there are anisotropic hyperfine interactions in at least one of the radicals, and the radical pair lifetime and its spin-coherence are long enough to allow a magnetic field to affect the singlet-triplet interconversion.

At first sight, this mechanism does not seem realistic since, under physiological conditions, the thermal energy of a molecule, k_BT, would be a million times larger than the interaction between the geomagnetic field and the molecule itself. The thermal energy k_BT (Boltzmann's constant times temperature in Kelvin) describes the energy associated with the random motion of molecules as they vibrate, rotate and collide with each other. In normal conditions (i.e. if the system is in an equilibrium state), one would need to provide an amount of energy that is at least comparable to these random motions to successfully modify the yield of the products of a reaction. However, when a system is brought in a non-equilibrium state thanks to a supply of external energy, tiny interactions (as small as that with the Earth's magnetic field) can have profound effects. In our case, the state far from equilibrium is the transient radical pair, while the energy necessary to bring the system into that state is given by a photon of light[67].

These theoretical considerations are supported by experimental evidence. Since the early studies in the 1970s, the radical pair mechanism has been recognized as a genuine phenomenon, and hundreds of laboratory studies on organic radicals have demonstrate how relatively small magnetic fields (in the range 1-100 mT) can influence radical pair reactions[145,157,181] What has not been proven yet, is whether the radical pair mechanism is indeed the mechanism behind the animals' magnetic compass[108]. In 2012, Maeda *et al.*[101] showed that a photoinduced intramolecular electron transfer within a carotenoid-porphyrin-fullerene molecule can form radical pairs whose lifetime can be modified by applying a 40-50 μT magnetic field. Moreover, when a stronger magnetic field was applied, the yield of the radical pair reaction was dependent on the direction of the field, thus demonstrating a proof of principle for a radical-pair-based magnetic compass[101]. Further studies on the carotenoid-porphyrin-fullerene system confirmed that a radical pair reaction can be affected by the direction of an external magnetic field with a strength comparable to the geomagnetic field[80].

Even though the theoretical assumptions for a quantum compass are clear and a synthetic compound was shown to possess such properties, it is still not clear how this mechanism should work in a physiological environment. In 2000, Ritz and co-workers[143] suggested that a class of photoreceptors known as cryptochromes[2,21] could be the magnetoreceptor molecules. Twenty years later, these proteins are still the only candidates[32,97,114] The other known photosensitive molecules in vertebrates are opsins (the visual photoreceptors) which isomerize retinal without formation of radical pairs[13]. Chlorophylls (the only other protein known to form long lived radical pairs) are not expressed in animals[5].

1.5 Cryptochromes

Cryptochromes are a family of proteins that are ubiquitous among different phyla and are mostly known for their role in plant growth and in the entrainment of animal and plants circadian clocks[21,28]. They have evolved from photolyases[148], DNA repairing enzymes, but possess low or no DNA repair ability[17]. Cryptochromes consists of a highly conserved photolyase homology region (the PHR domain) and highly varying N and C-termini[149]. These proteins can be divided in two sub-families: actual flavoproteins and vestigial ones[90]. The actual flavoproteins noncovalently bind in the PHR domain a redox-active flavin adenine dinucleotide cofactor (FAD), which absorbs blue light when in its fully oxidized state. Cryptochromes also noncovalently bind a second cofactor, either 8-hydroxy-5-deazariboflavin or 5,10-methenyltetrahydrofolate[148]. Proteins belonging to this subcategory include plant cryptochrome 1 (e.g. as *Arabidopsis thaliana* Cry1)[2], insect cryptochrome 1 (e.g. *Drosophila melanogaster* Cry[156]) and vertebrate cryptochrome 4 (e.g. *Gallus gallus* Cry4[105,127]).

Vestigial flavoproteins, on the other hand, have lost the ability to bind FAD due a series of amino acidic mutations in the PHR domain that prevent a strong interaction between the protein and the chromophore. Vertebrate cryptochromes 1 and 2 belong to this category[90]. For details, see chapter 1.5.1.

In photosensitive cryptochromes, the absorption of light in the blue range leads to the formation of the flavosemiquinone radical ($FAD^{\bullet -}$) via electron transfers along a series of conserved tryptophans (Trp) that culminate in the formation of a Trp radical ($TrpH^{\bullet +}$)[12]. Interestingly, while animal photolyases and animal cryptochromes present a chain of four conserved

tryptophans (the Trp-tetrad)[19,116], plant cryptochromes and bacterial photolyases only possess a triad of conserved amino acids (the Trp-triad)[50,188]. Studies on *Arabidopsis thaliana* cryptochrome 1 (*At*Cry1) and *Escherichia coli* photolyase (*Ec*PL) have shown that the [$FAD^{\bullet-}$ $TrpH^{\bullet+}$] radical pair is magnetically sensitive[59,101,167]. As shown in Figure 1.4 once *At*Cry1 is photoexcited, the oxidized form [FAD^{OX}] produces an excited singlet state $^{S}FAD^{*}$ that is rapidly reduced by electron transfer from the Trp-triad to form the radical pair $^{S}[FAD^{\bullet-}\ TrpH^{\bullet+}]$. This radical is indicated as radical pair 1 (RP1). RP1 either undergoes spin-selective reverse electron transfer to regenerate the ground state [FAD^{OX} + TrpH], or coherently interconverts with the triplet state $^{T}[FAD^{\bullet-}\ TrpH^{\bullet+}]$. Both the singlet and the triplet state of RP1 can form a secondary radical pair called RP2 [$FADH^{\bullet}\ Trp^{\bullet}$], in which both radicals have been (de)protonated. Both the recombination of RP1 to the ground state and the conversion of RP1 to RP2 occur on a 1µs timescale. On the other hand, RP2 has a lifetime of up to 1 ms. The magnetically sensitive state RP1 can affect the total amount of RP2 that is produced depending on the strength of the applied magnetic field (1-25 mT)[101].

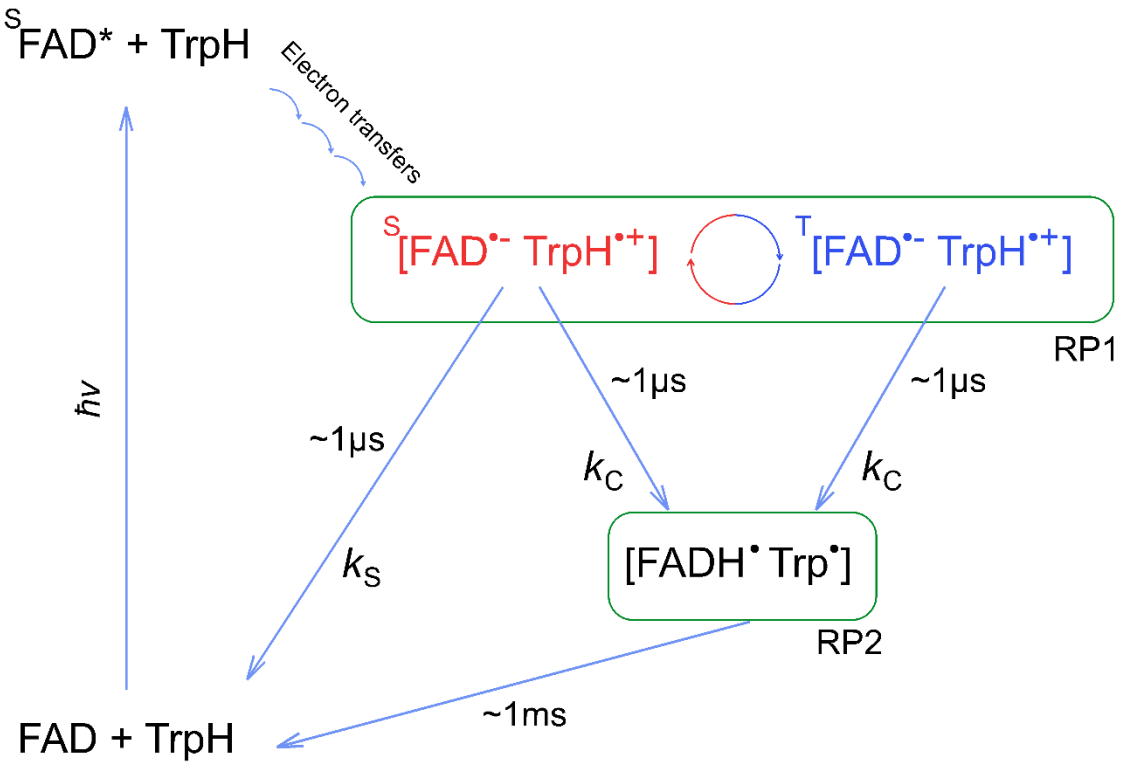


Figure 1.4. Photochemical reaction scheme that depicts the magnetic field effects on long-lived radical pairs observed in *At*Cry1 and *Ec*PL. RP1 is the magnetically sensitive state. RP2 is produced by the (de)protonation of one or both radicals and it is not influenced by a magnetic field. Red and blue arrows indicate the S-T interconversion. Approximate timescales for each

reaction step are indicated. k_S and k_C indicate the spin-selective back reaction and the non-spin selective forward reaction respectively. Adapted from Hore and Mouritsen (2016)[67].

Drosophila cryptochrome has been shown to produce magnetically sensitive radicals as well[153]. However, compared to *Ec*PL and *At*Cry1, it has an extra Trp at the end of the Trp chain, thus forming a Trp-tetrad. This fourth Trp, called Trp_D, causes a further electron transfer along the Trp-chain, creating a [$FAD^{\bullet-}$ $Trp_DH^{\bullet+}$] radical pair. Consequently, there are major differences in the chemical reactions between *Dm*Cry and *At*Cry1: a) the magnetic field effect reported in *Dm*Cry is smaller than that of *At*Cry1 (~2% versus ~20%); b) the $TrpH^{\bullet+} \rightarrow Trp^{\bullet}$ reaction is much slower in *Dm*Cry (~36 µs against ~1 µs); c) in *Dm*Cry in the first 70 µs there is no recovery of FAD^{OX}, while in both *Ec*PL and *At*Cry1 there is more than a 50% recovery; d) the electron transfer between Trp_C and Trp_D takes ~3 µs. However, like in *Ec*PL and *At*Cry1, the magnetically sensitive radical pair is [$FAD^{\bullet-}$ $Trp_CH^{\bullet+}$], since the radical form of Trp_D is too long lived for spin-selective recombination to compete with its spin relaxation[153].

These experiments proved that in principle cryptochrome could be the magnetoreceptor molecule[32]. However, things are not as simple as they might seem to be. One must bear in mind that these results were obtained while studying proteins *in vitro*. *In vivo* experiments showed that other electron-transfer pathways are possible in the cellular environment, since a substitution of Trp_C with a Phe (which is structurally similar, but unable to transfer electrons) did not affect the biological activity of *Arabidopsis*[39,94] and *Drosophila* cryptochromes[128,129]. Furthermore, magnetic field effects on *Drosophila* behaviour were reported when the flies were expressing Trp_C to Phe cryptochrome mutants (for details see chapter 1.5.5)[43,44,48,49]. It may also be that these evidences are misleading. Both *Arabidopsis* and *Drosophila* Cryptochromes have evolved to be part of the circadian clock of these organisms. Possibly, a Cryptochrome that has evolved to be a magnetoreceptor, shows completely different properties.

Other issues were raised in theoretical work. While FAD possesses strong anisotropic hyperfine interactions, due to its ^{14}N nuclei, making it an ideal component for a source of directional information[92,154], this stays true if the second radical has no or just a few hyperfine interactions. In fact, spin dynamics simulations have shown that an asymmetrical distribution of the hyperfine interactions within the radical pair gives larger magnetic field effects compared to one in which the two radicals have a similar number of hyperfine interactions (such as in the [$FAD^{\bullet-}$ $TrpH^{\bullet+}$] radical pair)[35,142,146] However, it is almost impossible to imagine an almost

hyperfine coupling-free radical that can be suitable in a biological environment, since most organic radicals contain one or more ^{14}N or ^{1}H[92]. The superoxide radical $O_2^{\bullet-}$ has been proposed as a possible alternative candidate[66,115,155,169]. Unfortunately, $O_2^{\bullet-}$ has extremely fast spin relaxation, leading to a loss of coherence in a matter of nanoseconds, making any magnetic field effect almost impossible[92]. Furthermore, recent spin dynamics simulations have concluded that a [FAD $O_2^{\bullet-}$] radical pair would be plausible only under highly restrictive conditions and thus its existence should be only speculative[139].

The other alternative radical that has been proposed is that from ascorbic acid, a common biological reductant, which possesses only few ^{1}H hyperfine interactions[92]. However, molecular dynamics simulations suggest that this is also an unlikely candidate due to the low rate at which cryptochromes and the ascorbyl radical interact in a cellular environment[118].

To summarize, the radical pair mechanism seems to be a plausible theory to describe how animals can perceive the Earth's magnetic field. So far, there has not been an experiment that has definitely proven the model to be the right one. However, there has been an increasing amount of evidences that points towards the possibility of the existence of a radical pair based magnetic compass.

1.5.1 Differences between animal cryptochromes

As stated in the previous paragraph, cryptochromes are proteins involved in the entrainment of the animal circadian clock. In this context, cryptochromes have been divided in two different subgroups: Type I animal Cry and Type II. The first group, to which proteins such as *Dm*Cry belong, are primary blue-light photoreceptors that entrain the circadian clock of invertebrates to the light/dark cycle of their environment[36,156]. On the other hand, Type II Crys are found both in invertebrates[189] and vertebrates[68] and they work as transcriptional repressors in the negative feedback loops of the central and peripheral clocks, and this appears to happen in a light-independent manner[158]. Proteins belonging to this subgroup are mammalian Cry1 and Cry2 and all the avian Cry1 and Cry2. While it has been demonstrated that Type I Crys can bind FAD and therefore be light-activated[11,28], this cannot be said for Type II. In fact, for many years they have been described as difficult to express and isolate with bound FAD[28,95,126]. According to Kutta *et al*.[90], Type II cryptochromes lost their ability to bind FAD due to amino acid substitutions in the PHR domain, and therefore should be considered vestigial

flavoproteins. The authors of the study pinpointed a series of crucial residues that can cause these dramatic changes in the FAD binding pocket.

Importantly, in *Dm*Cry Asn419 is highly conserved across all Type I Crys and in Type II it is replaced by a serine or methionine. This residue is known to form two hydrogen-bonds with the adenine component of FAD[28,93], thus stabilizing the cofactor in its distinctive U-shape. This, however, does not happen in Type II Crys[183]. Furthermore, in *Dm*Cry Arg237 is highly conserved among Type I Crys, but it is substituted by a histidine in Type II. This replacement has the effect of reducing the stability of the pyrophosphate group present in FAD[90]. Futhermore, in *Dm*Cry the residues between 295 and 307 form a loop region that covers the FAD-binding pocket[28]. This region acts as a lid and it is present in all Type I Crys. However, it is truncated in Type II Crys[28,183]. In conclusion, these changes in the PHR domain, which greatly reduce the strength with which FAD binds to the protein, make Type II Crys unlikely photoreceptors.

On the other hand, Cry4s, which are present in vertebrates such as fishes and birds, have yet to be categorized in a circadian context since their function is still unknown. Importantly, these proteins are known to be able to bind FAD and therefore can be light-activated[105,127]. Interestingly, of all the residues deemed important by Kutta *et al.*[90], Cry4s only include Asn419 (Figure 1.5).

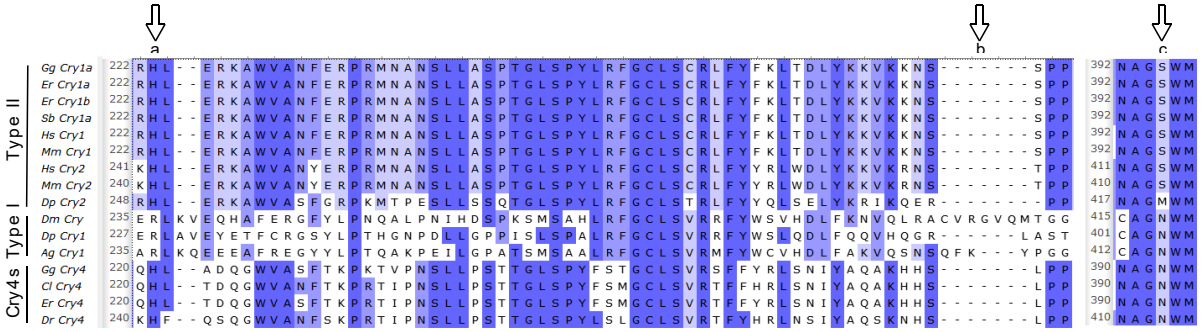


Figure 1.5. Partial sequence alignment of different cryptochromes belonging to Type I Crys, Type II Crys and Cry4s. The arrows highlight regions of the sequences deemed important by Kutta *et al.*[90] to explain the different binding properties of Type I and Type II Crys. In *Dm*Cry these residues are: **a.** Arg237 which increases the stability of the FAD pyrophosphate group, **b.** the loop region (residues 295- 307) forming the lid covering FAD, **c**. Asn419, which forms two hydrogen bonds with the adenine component of FAD. Interestingly, Cry4s are known to be flavoproteins, but they only present the Asn419 residue. The colour coding is determined

by shades of blue. Dark blue indicates 100% identity, while white indicates no identity. The full alignment and the species name can be found in Chapter 6.1.

1.6 Evidence for the radical pair mechanism

1.6.1 Behavioural evidences

In 1972 Wiltschko *et al.*[174], reported that the night-migratory songbird, the European robin (*Erithacus rubecula*) possesses an inclination compass instead of a polarity compass. When tested in the Emlen funnels[38], the birds were not able to distinguish between North and South magnetic directions but were sensitive to the inclination of the magnetic field, i.e. the angle between the field lines and the horizontal (Figure 1.6)[174]. Further studies have shown that this kind of compass is wavelength dependent as well. Robins were better oriented in light at shorter wavelengths (400-565 nm)[171,179], while they appeared to be disoriented when exposed to longer wavelengths (> 580 nm)[177]. Similar results were also found in the red-spotted newt (*Notophthalmus viridescens*) which also possesses a light-dependent inclination compass[136].

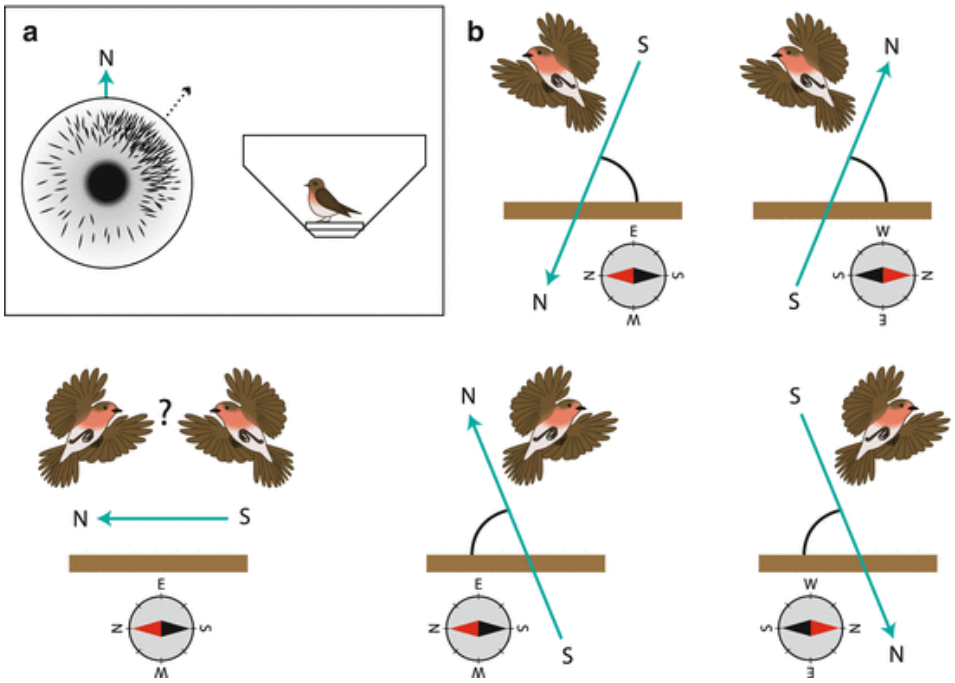


Figure 1.6 - The inclination compass of night-migratory songbirds. **a.** Birds are tested inside Emlen funnels[38], containing scratch-sensitive paper. The birds are prevented from having any directional cues other than the geomagnetic field. Therefore, they will try to jump in their

migratory direction and in doing so will leave scratches on the paper. **b.** Inclination compass. The birds measure the angle between the magnetic field lines and the Earth's surface. Therefore, the birds can distinguish between a poleward and equatorward direction, but they cannot distinguish between the magnetic North and the magnetic South (like in the case of a polarity compass). If, on the other hand, birds would be able to use a polarity compass, they would orient parallel to the horizontal component of the magnetic field. Furthermore, birds are disoriented when the inclination is equal to zero, like at the magnetic equator. The green arrow indicates the direction of the magnetic field, N and S indicate the magnetic North and South respectively, the brown bar indicates the Earth's surface. Adapted from Mouritsen (2013)[110].

It may seem somewhat counterintuitive that night-migratory songbirds need a light-dependent mechanism to be able to properly orient in the Earth's magnetic field. This paradox is however only apparent, since a state of absolute darkness never occurs at night. In fact, there is always some light, whether from the moon or the stars. Moreover, birds need to see to be able to fly and it has been reported that they tend to be less well oriented when there are periods of prolonged overcast skies[37]. Furthermore, birds tend to fly either above or below the clouds to have access to information coming from the sky or landmarks, respectively. When this is not the case due to prolonged unfavourable weather conditions, birds have been reported to have catastrophic mortality rates[4].

Normal vision is achieved in vertebrates thanks to two main photoreceptors present in the retina: rods and cones. The first are active at night in low light conditions, while the second are sensitive to higher light intensities during the day. Therefore, birds can see at night thanks to the activation of the rod pathway, which relies on rhodopsin photopigments. These are remarkably sensitive photoreceptors, which only need a few photons to detect light. Therefore, it is expected that cryptochromes could also work near this physical detection limit. Thus, in principle, the radical pair mechanism could require only tens or few thousands of photons in order to build up a signalling state necessary to determine the axis of the magnetic-field lines. According to theoretical calculations[67], the amount of photons hitting the retina on a starry night would be enough to activate such mechanism. Therefore, night migration and light-dependent magnetoreception don't necessarily need to be mutually exclusive.

1.6.2 Neuroanatomical studies

The light dependence of the magnetic compass has been further investigated in neuroanatomical studies of the avian brain[113]. These studies have demonstrated that the magnetic compass information is processed in a region of the brain named Cluster N[96,112]. In fact, once the retina absorb light, the signal is propagated via the thalamofugal visual pathway to Cluster N, a small area of the visual wulst[60,61,86]. Cluster N requires light to be activated and once destroyed, night-migratory songbirds lose their ability to use their magnetic compass, while keeping their sun and star compasses[187]. This is strong evidence supporting the idea that the avian magnetic compass is indeed light-dependent, that birds perceive the magnetic information as a light stimulus, and that the primary sensor needs to be located in the retinas[113]. Interestingly, early studies reported that birds can perceive magnetic stimuli only via the right eye[178]. These data were subsequently contradicted by studies reporting that there is no visual lateralization in magnetic compass perception[55,56].

1.6.3 Avian cryptochromes

Other indirect evidence for a radical-pair-based magnetic compass is the expression of at least four different cryptochromes in the avian retina. The cryptochromes found so far are the two isoforms of Cry1 (a and b), Cry2 and Cry4.

Cry1a was the first cryptochrome to be considered the ideal candidate because of its expression in the UV cones of chicken and European robins[119]. The localisation of the protein in that region of the eye would have matched the light-dependent magnetic orientation reported in behavioural experiments. Moreover, *Sylvia borin* (Garden warbler) Cry1a was reported to be successfully purified with bound FAD and once photoexcited could form FAD and Trp radicals with millisecond lifetimes[95]. Another study also reported successful expression and purification of *Columba livia* Cry1a with bound FAD[186]. Furthermore, immunohistochemical studies in the birds' retinas, reported a light driven conformational change in chicken Cry1a[120,122,170]. suggesting that Cry1s can bind FAD *in vivo*. Finally, Cry1a mRNA levels have been shown to have a cyclical circadian oscillation pattern but not a seasonal one[53].

Cry1b is the other isoform of Cry1[15,121]. In European robin, the two proteins are identical for the first 563 amino acids but have a different C-terminus, with Cry1b being 33 amino acids

shorter than Cry1a (587 vs 620 amino acids). This protein has also been described as a putative magnetoreceptor; since the PHR domain is identical to the one in Cry1a, Cry1b should have the same binding affinity for FAD as Cry1a. However, there is no empirical evidence for that. Cry1b is mainly expressed in the ganglion cell layer[15,121] and like Cry1a, has a circadian expression pattern but not a seasonal one[53].

On the other hand, Cry2 is expressed mainly in the inner nuclear cell layer of the retina (personal communication of Pranav Seth, University of Oldenburg). It shows circadian but not seasonal expression, and it is not considered a possible candidate magnetoreceptor given its nuclear expression[53].

The last possible candidate is Cry4. It is mainly expressed in the outer segments of the double cones and in the long wavelength cones in the birds' retina, it has a weak circadian expression pattern, but a strong seasonal one[53]. Finally, Cry4s from *Gallus gallus* and *Columba livia* have been expressed and isolated with bound FAD under physiological conditions[105,127,140].

1.6.4 Radiofrequency field effect

One of the most striking pieces of evidence for the existence of a radical-pair-based magnetic compass, are the reports of several species not being able to use their magnetic compass when exposed to weak time-dependent magnetic fields[40,78,131,142,144,152,159,164].

It has been shown in many laboratory studies how small organic radicals can be affected not only by static magnetic fields, but also by time-dependent ones[58]. This happens when the oscillation of the time-dependent magnetic field matches one of the frequencies at which the radical pair naturally oscillates between its singlet and triplet states in a static field. Therefore, if the time-dependent magnetic field is in resonance with the natural oscillation of the radical pair, it can modify the yield of the reaction products[67].

Spin dynamics calculations have predicted that the frequencies at which a time-dependent field can affect a radical pair are dependent on the number of hyperfine interactions considered in both radicals[64]. In the case in which one of the two radicals is devoid of hyperfine interactions, we would expect a strong resonance at the Larmor frequency. When one of the two radicals has only one or two hyperfine interactions, there will be a strong response only to a few

frequencies. Finally, if both radicals share a similar number of hyperfine interactions, the radical pair should be affected by a range of radiofrequencies, with no particular radiofrequency being much more sensitive than the other. The FAD-Trp radical pair is an example of this latter case, since both radicals have more than 10 nuclei with significant hyperfine interactions[64].

However, in 2009 Ritz *et al.*[142] reported that when tested in Emlen funnels, birds were disoriented if exposed to a 15 nT field at 1.315 MHz, the Larmor frequency in Frankfurt am Main, Germany. Effects at the Larmor frequency were found also in zebra finches[79], garden warblers[78] and cockroaches[164]. These results were interpreted as if one of the radicals did not have any hyperfine interactions, therefore excluding the FAD-Trp radical pair. The radical proposed was the superoxide radical, $O_2^{\bullet-}$, which as we as seen before, it is not a likely candidate.

Nevertheless, the radiofrequency effects at the Larmor frequency were challenged once these studies were repeated under more controlled conditions. In fact, Schwarze *et al*[152]. reported that there was no such effect at single frequencies, but instead birds were disoriented when exposed to weak broadband magnetic fields, ranging from 2 kHz to 9 MHz. Finally, a recent study showed that birds that were exposed to an electromagnetic field ranging from 0.1 to 100 kHz were not prevented from performing magnetic orientation. The authors concluded that the coherence lifetime of the radical pair is less than 10 μs[87].

The last findings supporting the existence of a radical pair mechanism are cryptochrome-dependent magnetic field effects reported in insects, such as cockroaches[8] and *Drosophila melanogaster*.

1.6.5 Magnetic field effects on *Drosophila melanogaster*

A series of studies have reported that the behaviour of the fruit fly *Drosophila melanogaster* can be affected by the presence of an external magnetic field, and that these effects seem to be cryptochrome-dependent. In *Drosophila*, cryptochrome is a UV-blue light photoreceptor that plays a central role in the entrainment of the circadian clock[36,133,156].

The first published study on electromagnetic field effects on *Drosophila melanogaster* goes back as far as 1966[137]. Picton reported a directional response of the flies depending on the direction of an applied 200 μT external magnetic field[137]. In 1970, Wehner and Lamhart[168] documented an effect of the geomagnetic field on the direction of geotactic orientation. More than twenty years later, Philips and Sayeed[134] trained flies to the ambient magnetic field with a horizontal gradient of 365 nm light, which emanated from one of the four cardinal compass directions. The flies were later tested in a radial 8-arm maze in which the magnetic field alignment could be varied. When tested under 365 nm light, flies showed a magnetic compass orientation in the direction from which light had previously emanated. Similar responses were also found in *Drosophila* second instar larvae[34,130]. However, under 500 nm light, flies showed a 90° shift in magnetic compass orientation with respect to the trained direction. Interestingly, only males seemed to orient properly, while females were completely disoriented (Figure 1.7). This work was the first one that showed how flies can perceive magnetic fields in a light-dependent manner[134].

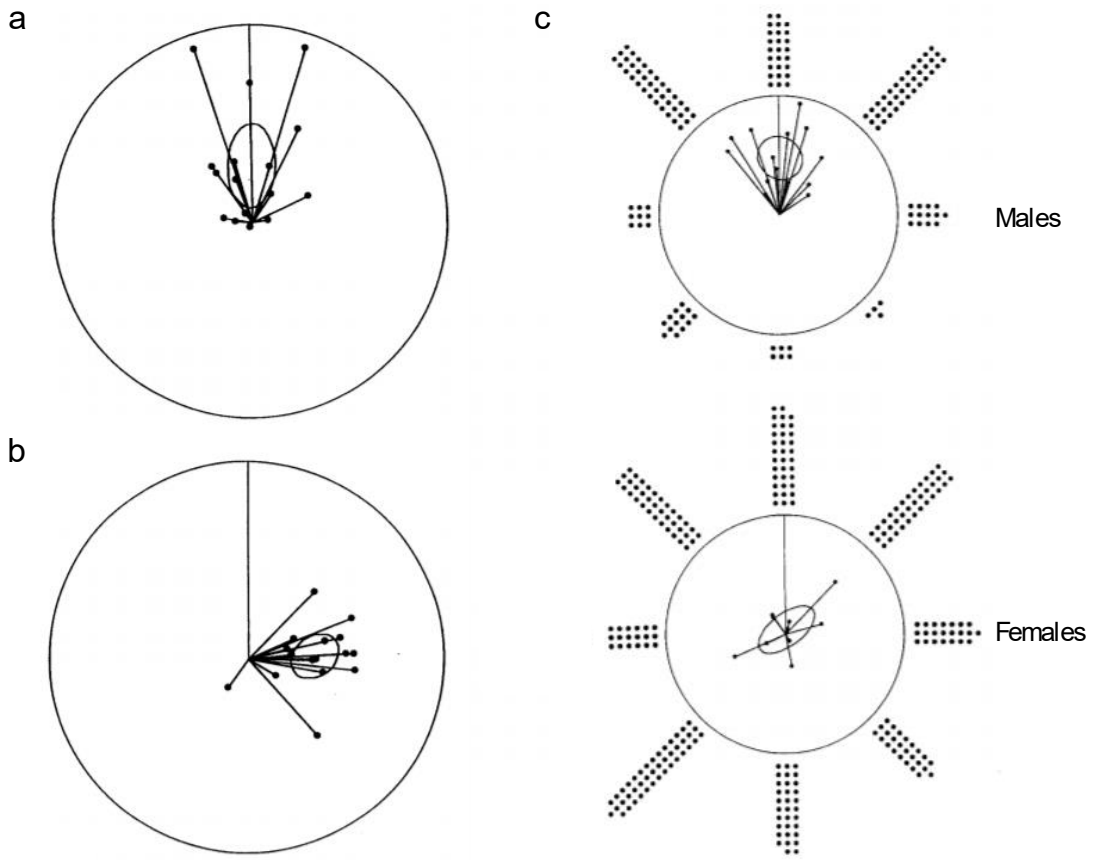


Figure 1.7. Magnetic compass orientation of *Drosophila*. **a.** Flies were exposed to 365 nm light. **b.** Flies show a 90° shift when exposed to 500 nm light. **c.** Magnetic compass orientation

of male and female *Drosophila* under 365 nm light. While males are properly oriented, females appear to be disoriented. Adapted from Phillips *et al.*[134]

On the other hand, Gegear and co-workers[46–48] were the first to show a cryptochrome-dependent magnetic field effect. They trained flies to associate a magnetic field with a sucrose reward and later tested them in a binary-choice T-maze. The experimental set-up consisted of an illuminated box containing a T-maze behavioural choice apparatus, which was positioned between two double-wrapped coils[83] that were rotated 45° with respect to the T-maze. The two coils produced a magnetic field only on one side of the T-maze, thus creating a field gradient. Under full spectrum light, trained wild type flies moved towards the magnetic field, while naïve flies (which had not been giving a sucrose reward), avoided the magnetic field. When the authors applied a filter that cut off wavelengths below 420 nm, the flies no longer showed a preference for the magnetic field. This was interpreted as inactivation of cryptochrome, since the protein is light activated in the blue region of the visible spectrum. Moreover, cry^{02} null and cry^{b} mutants failed to associate a magnetic field with the sucrose reward. cry^{02} mutants do not express cryptochrome, since *cry* has been substituted with the *mini-white* gene[33], while cry^{b} (*cry baby*) have a mutation in the FAD binding pocket (Asp 410 is substituted with Asn) that makes the protein unstable[156]. The lack of response in Cry-deficient flies suggested a putative role of Cry as magnetoreceptor. Furthermore, since cryptochrome interacts with Timeless to reset the clock mechanism[57], Gegear *et al.*[47], used clock mutants to show that an intact clock was not necessary for sensing a magnetic field. Subsequent work from the group showed that over-expressing cryptochrome in the clock neurons (using the UAS/GAL4 system) in a cry^{b} background, rescued the magnetosensitive behaviour in the flies. This also happened when they over-expressed the monarch butterfly *Danaus plexippus* (*Dp*) cryptochromes 1 and 2 in the clock neurons in cry^{b} flies[46,48]. Moreover, when over-expressing *Homo sapiens* (*Hs*) Cry2, in a *cry*-deficient background, the flies showed normal "trained and naïve" behaviour. The results on *Dp*Cry2 and *Hs*Cry2 are a bit surprising, since both proteins are thought not to be able to bind FAD, and therefore incapable of being light activated. Finally, they tested flies in which the third Trp in the Trp-tetrad was changed to a Phe (*Dm*Cry W342F), which is structurally similar, but unable to transfer electrons. Interestingly, flies showed again normal naïve and trained responses. These results opened the possibility of a different electron transfer pathway and therefore the existence of a different radical pair (Figure 1.8). [46,48]

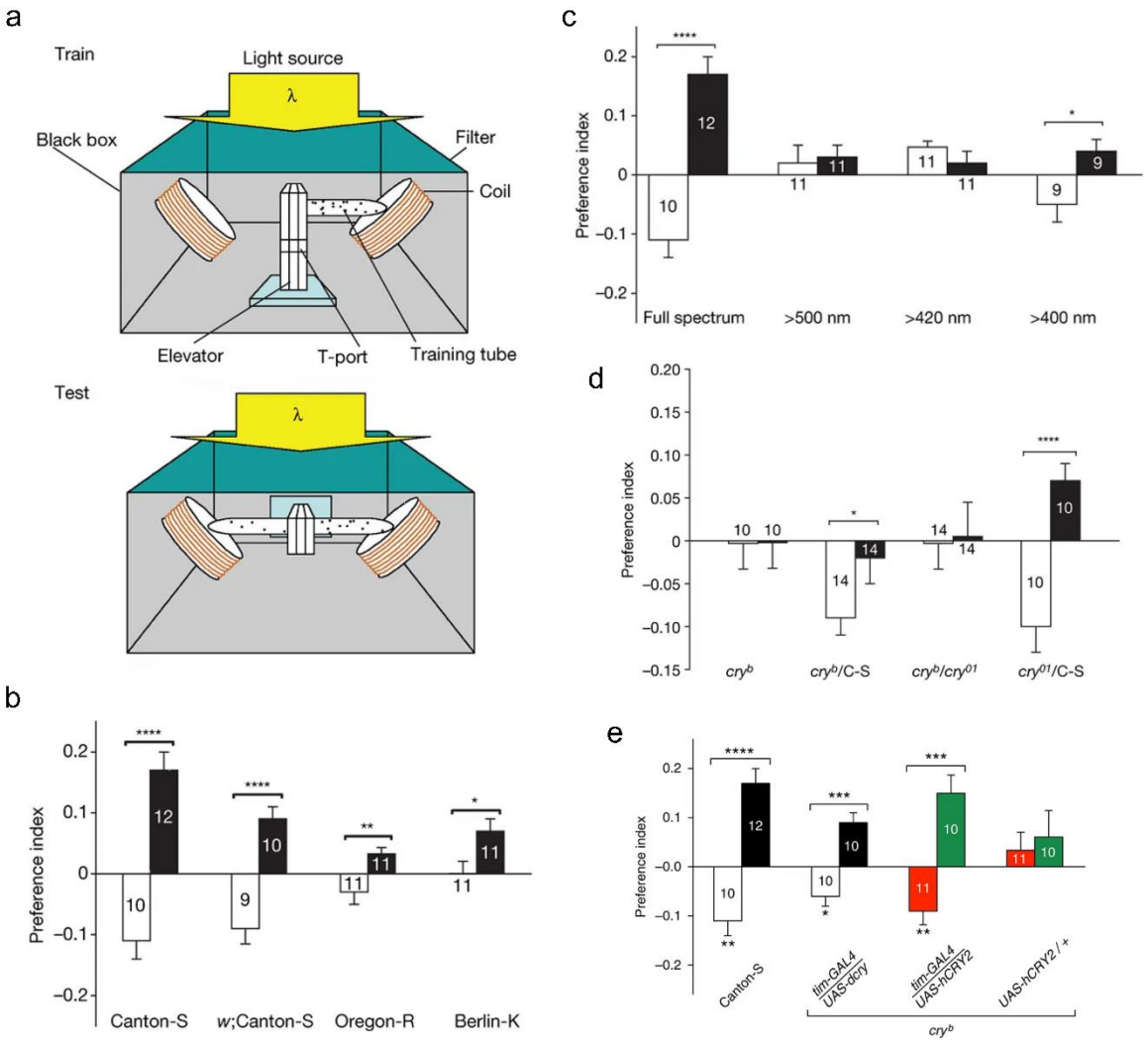


Figure 1.8. Set-up and results from Gegear *et al*[47]. and Foley *et al*[46]. **a.** T-maze set-up used to train the flies to associate a sucrose reward with a 500 µT magnetic stimulus. **b.** Different lines of wild-type flies. While trained flies tended to move towards the magnetic field, naïve flies tended to avoid it. **c.** Wavelength-dependence of the behaviours. Flies showed a normal response only when exposed to a full spectrum or when 400-420 nm wavelengths were included. **d.** Cryptochrome-dependence of the flies' behaviour. **e.** Flies showed normal "trained" and "naïve" behaviour when *Dm*Cry and *Hs*Cry2 were over-expressed in the clock neurons. White and red bars indicate "naïve" responses, while black and green bars indicate "trained" responses. Data shown as mean ± s.e.m.

Since cryptochrome in *Drosophila* plays a central role in the entrainment of the circadian clock, it seems plausible that an external magnetic field can interfere with the circadian rhythms. Yoshii *et al.*[185] measured the periods and rhythms of flies that were exposed in constant dim blue light to different magnetic field intensities (0 µT, 150 µT, 300 µT, 500 µT). The magnetic

field was produced by a set of two Helmholtz coils[83]. Interestingly, flies were affected only when exposed to a 300 μT field. Moreover, the magnetic field changed the free running period, predominantly by increasing it under blue light but not red light, a spectral region in which cryptochrome is not light activated. Furthermore, when *cry* mutants (*cry*^{b} and *cry*^{out}) were tested, the majority of the flies showed no magnetic field effect. On the other hand, over-expressing *cry* in all clock neurons showed an amplified response resulting in arrhythmia. To summarise, an external magnetic field seems to affect circadian clocks in a blue-light and cryptochrome-dependent manner[185].

Fedele *et al.*[43] also reported a cryptochrome-dependent magnetic field effect on *Drosophila* circadian rhythms. When exposed to a 300 μT field and to blue light, wild type flies showed a shortening of their period, while flies over-expressing cryptochrome showed an increase in rhythmicity. These results, opposite to those of Yoshii *et al*.[185], were explained by the different wavelength used (430–470 nm vs 445–495 nm). When flies were exposed to longer wavelengths (500 nm) the phenotype shown in Yoshii *et al*.[185] was restored. Interestingly, it was shown again that over-expressing *Dm*Cry W342F does not impair the circadian response to a magnetic field. Moreover, truncation of the cryptochrome C-terminus[147] attenuates the magnetic field effect. Furthermore, flies expressing the cryptochrome C-terminal residues 491–542 fused to GFP in a *cry*^{02} background, still showed a modest magnetic response. These results indicate the central role of the C-terminus of cryptochrome in mediating the magnetic field response. Finally, when expressing *Hs*Cry1 and *Hs*Cry2 in flies, only *Hs*Cry2 showed a magnetic field effect, confirming the data presented in Foley *et al*.[46]

Another behaviour that has been proven to be susceptible to the presence of an external magnetic field is negative geotaxis. Fedele *et al.*[44] built an experimental set-up that consisted of an aluminium box containing a homemade swinger mechanism placed in between two double wrapped Helmholtz coils producing a field of 500 μT. The mechanism held three tubes that were knocked on a surface at the same moment and with equal force. Ten flies were placed in each tube and the ones able to reach 15 cm in 15 s were considered "climbers". The flies were tested every 30 s for five time in a row, followed by a 15 min break, and then tested five times again. Under dim blue light (~ 0.25 μW/cm^2) but not under red light, the authors found that the magnetic field reduced the rate at which the flies ascended. This behaviour was shown to be cryptochrome-dependent and over-expression of Cry in the clock neurons in otherwise cry-null mutants recovered the magnetic field effect. Interestingly, the absence of the C-

terminus, did not rescue the magnetic field effect, indicating its role in mediating the magnetic stimulus. Finally, the over-expression of Cry W324F again rescued the magnetic field effect[44] (Figure 1.9).

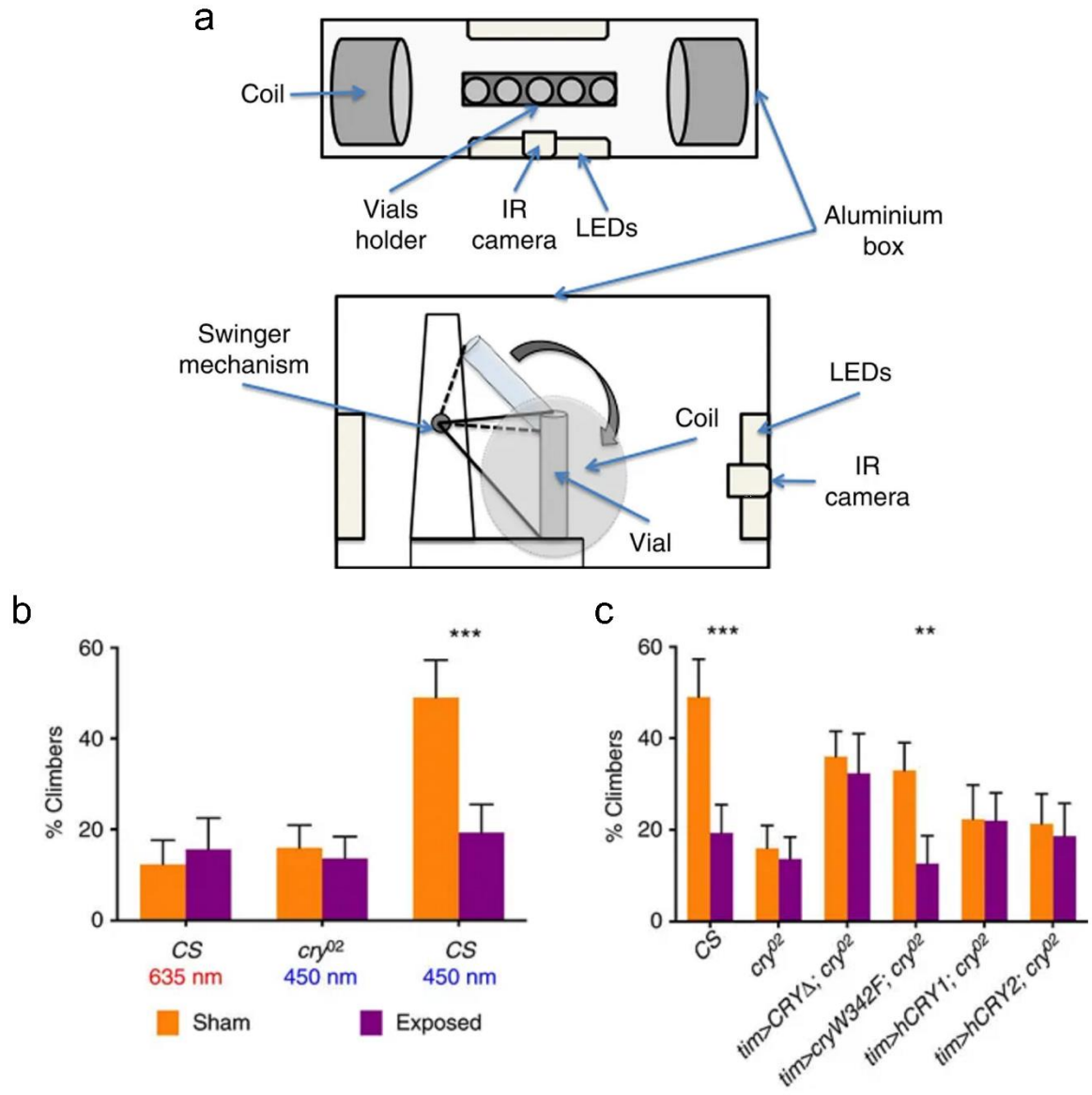


Figure 1.9. Set-up and results from Fedele *et al.*[44] **a.** The set-up used to test for negative geotaxis. **b.** Wild type Canton-S (CS) flies show an impairment in their climbing abilities when exposed to a 500 μT magnetic field. When exposed to red light, CS flies' ability to climb is reduced both under sham conditions and with a magnetic stimulus. *cry*^{02} flies perform the same way as CS flies exposed to red light, indicating that this is a blue-light cryptochrome-dependent behaviour. **c.** Over-expression of different cryptochrome constructs in the clock neurons. Data shown as mean ± s.e.m.

The data presented in Fedele *et al.*[44] were independently confirmed by Bae *et al.*[7] and recently expanded by the work of Oh *et al.*[125]. In the first study[7], *Drosophila* were tested in different assays: a tube positioning assay, a Y-maze assay, a free flight assay and an associative learning assay. Importantly, none of these assays resembled the one in Fedele *et al*[44]. However, independently from the assay used, the authors found that in a near-zero magnetic field (in which the *x*, *y* and *z* components of the geomagnetic field were cancelled by the magnetic field produced by 3-axis coils), the flies showed an increase in their negative geotaxis response. On the other hand, when exposed to stronger magnetic fields (up to 85 μT), the flies behaved in an opposite manner, showing a decrease in their negative geotaxis response. The authors also reported the lack of a magnetic field effect when flies were tested in darkness and in a *cry-null* mutant[7], thus confirming the importance of light and cryptochrome in mediating the geotactic response to an external magnetic stimulus. Furthermore, Oh *et al.*[125] have recently published a work in which they used a geotaxis assay to test whether *Drosophila* gets imprinted on the geomagnetic field present at birth. According to the authors, this imprinting process may help the flies to recognize locations that are favourable for foraging and reproduction[125].

In another study, Giacchello *et al.*[49] reported electrophysiological recordings from larval motor neurons ectopically expressing cryptochrome that showed a magnetic field response that was blue-light and cryptochrome-dependent. Once more, the results supported the importance of the C-terminus in mediating these responses and the proposal that an intact Trp-tetrad is not necessary for the magnetic sensitivity[49].

To summarize, a series of *Drosophila* behaviours such as learning[46–48,134], circadian timing[43,185], locomotor activity[43], geotaxis[44], gravitaxis[7,125], seizure response[103] and courtship activity[182] have been reported to be sensitive to magnetic fields in a blue-light and cryptochrome-dependent manner. While these results support the existence of a radical-pair-based magnetic sense, others, such as the lack of need of an intact Trp chain or the role of cry C-terminus, challenge our current understanding of the model.

1.7 My project

Since magnetoreception is a highly interdisciplinary subject, the aim of my project was to analyse how animals perceive magnetic fields from three different perspectives: animal behaviour, biochemical assays and spectroscopic measurements.

The first project, presented in Chapter 2, was an investigation of magnetic field effects on *Drosophila melanogaster*. The original idea was to test for possible radiofrequency field effects that could give better insights of the radical pair mechanism. As a testing paradigm, we decided to use negative geotaxis, based on the results published in Fedele *et al*[44] and later in Bae *et al*[7]. In fact, this behaviour not only has been shown to be sensitive to the presence of an external magnetic field, but the reported magnetic field effect was up to 25-30%[44]. Therefore, we designed, built and optimized two different set-ups. The first one was designed to test multiple individuals, while the second one was designed to test single flies. Unfortunately, even though the experiments were conducted in a meticulously controlled environment and strong statistical tests were applied to a large-scale dataset, it proved impossible to reproduce the magnetic field effects reported in the literature.

The second project, presented in Chapter 3, was to test whether *Er*Cry1a and *Er*Cry1b could be the magnetoreceptor molecules. In fact, even though these proteins have been considered the ideal candidates for many years (see chapter 1.6.3), all the evidence supporting this thesis were circumstantial[119], or not independently replicated[120,122], or both[95]. Therefore, the proteins were expressed and purified and their binding affinity for FAD was determined using two different biochemical assays: Isothermal Titration Calorimetry (ITC) and Surface Plasmon Resonance (SPR) spectroscopy. From the results of these experiments, we can exclude a role as a primary magnetoreceptor for *Er*Cry1a and *Er*Cry1b.

The third project, described in Chapter 4, is a comparative study of the spectroscopic properties and magnetic sensitivity of *Erithacus rubecula* Cry4, *Gallus gallus* Cry4 and *Taeniopygia guttata* Cry4. These proteins belong to a night-migratory passerine (the European robin), to an ancient species of birds (the common chicken) and to an early non-migratory passerine (zebra finch), respectively. The absorption measurements were done using Broadband Cavity-Enhanced Absorption Spectroscopy (BBCEAS). This technique has the advantage of detecting the change in the optical absorbance of photo-induced radicals when the proteins are exposed to an external magnetic field. We found striking differences between cryptochrome 4s from

migratory and non-migratory birds, thus supporting the idea that Cry4s might be the magnetoreceptor molecule.

Finally, Chapter 5 summaries all the obtained results and contains suggestions for future work.

Chapter 2

MAGNETIC FIELD EFFECTS ON *DROSOPHILA* NEGATIVE GEOTAXIS

2.1 Introduction

As described in chapter 1.6.5 *Drosophila melanogaster* is an ideal model organism to study magnetic field effects on animals. The advantages of using such animal are obvious when compared to testing night migratory songbirds such as the European robin. Unfortunately, at the moment is not possible to breed any songbird in captivity, no genetic tools are available, the number of birds that can be tested and sacrificed per year is limited, and the birds can be tested only twice per year, during their spring and autumn migratory seasons. *Drosophila* do not present any of such problems: the number of testable individuals is virtually unlimited, there are plenty of genetic and molecular tools available, different behaviours are affected by the presence of a magnetic field (albeit many times stronger than the geomagnetic field) and there are no constraints on when testing can be done. Therefore, we decided to exploit the many advantages offered by *Drosophila* to test for possible radiofrequency field effects that could give better insights of the radical pair mechanism.

As testing paradigm, we decided to use negative geotaxis. This behaviour has been shown to be sensitive to the presence of an external magnetic field with a surprisingly large, 25-30% magnetic field effect[44]. Moreover, negative geotaxis is a spontaneous behaviour and the genetic pathways of such behaviour have been extensively studied[62,69,160]. To test for negative geotaxis, we designed, built and optimized two different set-ups, the first one to test multiple individuals (the Gravity apparatus, described in chapter 2.2.3) and the second to test single flies (The FlyVac, described in chapter 2.2.4). The set-ups were built with the help of Dr Daniel Kattnig (a former post doc in Prof. Peter Hore's group, now at the University of Exeter) and the data analysis was performed by Dmitri Kobylkov (University of Oldenburg).

Originally, the experiments were supposed to be run in Oxford at the Centre for Neural Circuits and Behaviour under Prof. Scott Waddell's co-supervision. However, after few months of unsuccessful results, we decided to run these experiments at the Carl von Ossietzky University

of Oldenburg (Germany) under Prof. Henrik Mouritsen's co-supervision. The main advantage of moving to Germany was to have access to highly controlled behavioural facilities specifically built to test the magnetic compass sense of night-migratory songbirds[152]

2.2 Material and Methods

2.2.1 Non-magnetic facility

All experiments were conducted at the Carl von Ossietzky University of Oldenburg (Germany), inside a laboratory built to test night-migratory songbirds' magnetic compass. The building is fully described in Schwarze *et al.*[152], and here we highlight the main features. The laboratory was built only with magnetic-free materials (wood, copper, stainless steel and aluminium) and it contains four testing chambers. Each chamber had its own foundations to ensure that vibrations from people walking in the building were not propagated to the testing chamber. The chambers were individually electromagnetically screened (S101, ETS Lindgren) with attenuation factors of 10^5 at 10 kHz and $>10^6$ at frequencies above 150 kHz. This allowed to block time-dependent fields that are known to disrupt bird's orientation, but at the same time allowed the geomagnetic field to penetrate the aluminium shielding without distortion. At the centre of each testing chamber was placed a double-wrapped, three-dimensional Merritt four-coil system[187], with an average coil diameter of 2 m, inside which the *Drosophila* set-ups were placed (for details see sections 2.2.3 and 2.2.4). All *Drosophila* experiments were performed inside one of these electromagnetically shielded chambers.

2.2.2 *Drosophila* strains

The *Drosophila* stocks were reared in culture vials with standard maize. The genotypes of the flies in the negative geotaxis experiments were Canton-S LE, *pdf* ^{01} (from Professor C. P. Kyriacou, Department of Genetics, University of Leicester, UK) and Canton-S OX (from Professor S. Waddell, Centre for Neural Circuits and Behaviour, University of Oxford, UK). The vials were kept in incubators at 25 °C under a 12:12 h light:dark regime. The light was switched on at 8 a.m. The experiments were run at 25°C.

2.2.3 Gravity apparatus

Set-up

Negative geotaxis was studied using an experimental arrangement designed to resemble that used by Fedele *et al.*[44]. As shown in Figure 2.1, three cylindrical poly(methyl methacrylate) tubes (length 200 mm, inner diameter 20 mm, outer diameter 25 mm) were mounted on a support constructed of non-magnetic materials. The support could be lifted manually through 6 cm, by means of a handle, and then released to knock the flies down to the base of the tubes. This assured that the flies were exposed to the same amount of force every time they were tapped. A thin layer of rubber beneath the tubes acted as a shock absorber to reduce recoil. The apparatus was made entirely of Delrin and poly(methyl methacrylate) to avoid any distortion of the applied magnetic field. It was built in the mechanical workshop of the Department of Chemistry of the University of Oxford.

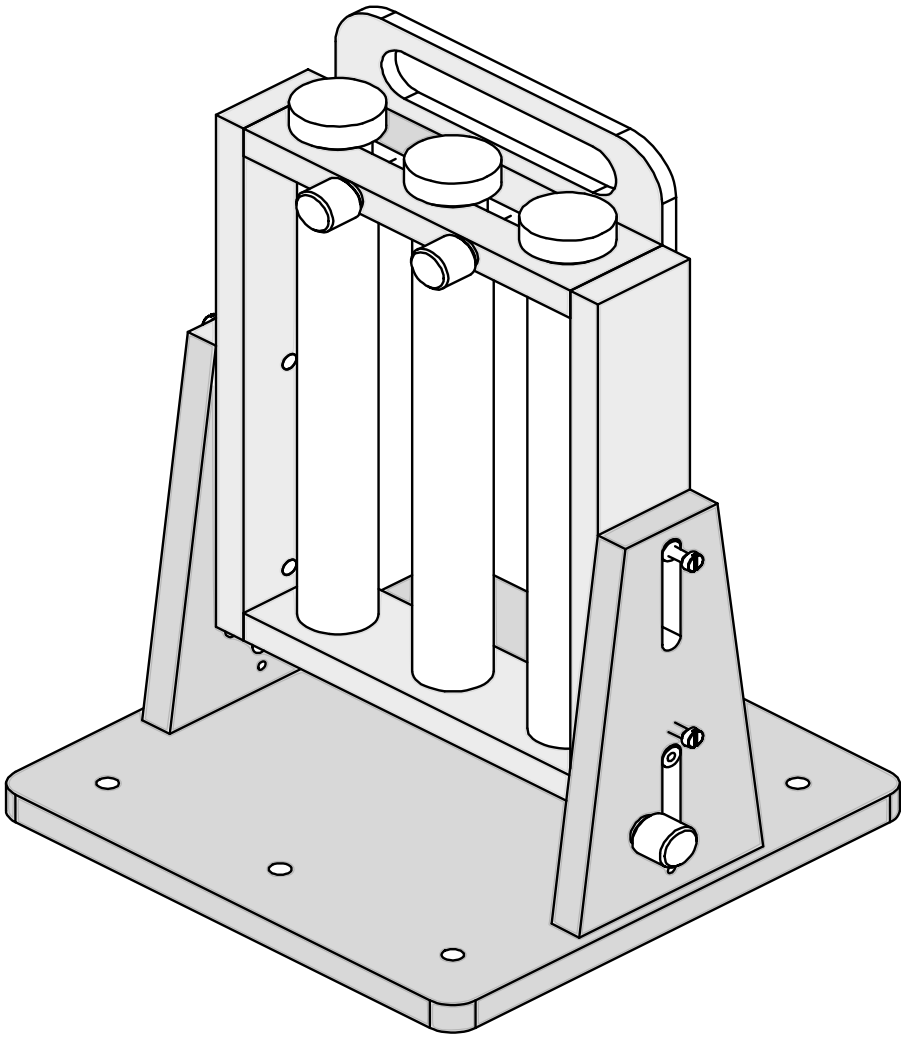


Figure 2.1. Schematic of the Gravity apparatus. Three cylindrical poly(methyl methacrylate) tubes were mounted on a support that could be lifted manually by the means of a handle.

The wavelength-dependence of the flies' ability to climb was investigated by uniformly illuminating the tubes using one of three purpose-built arrays of light emitting diodes (LEDs): UV-blue (380–450 nm, LHUV-0405-0600 Ultraviolet LUXEON Z LED), blue (410–490 nm, LXZ1-PR01 Royal-Blue LUXEON Z LED), and red (580–660 nm, LXZ1-PD02 Red LUXEON Z LED). Each LED plate had 20 LEDs separated 45 mm from each other. The LEDs arrays were built in the electronics workshop of the Department of Chemistry of the University of Oxford. The LED plates were supplied with DC current by a power supply unit (Manson SPS 9400). The spectral distributions of the three diode types in the range 300–700 nm were measured using a Maya2000 Pro spectrometer (Ocean Optics) with an integration time of 100 ms. Measurements were made in front of and behind the tubes to check for differential absorption at different wavelengths (Figure 2.2). Apart from some minor wavelength-independent attenuation, probably due to light scattering, no difference was detected. The light incident on the tubes was approximately 0.25 µW cm^{-2} and therefore comparable to Fedele *et al*. [44] (Figure 2.2).

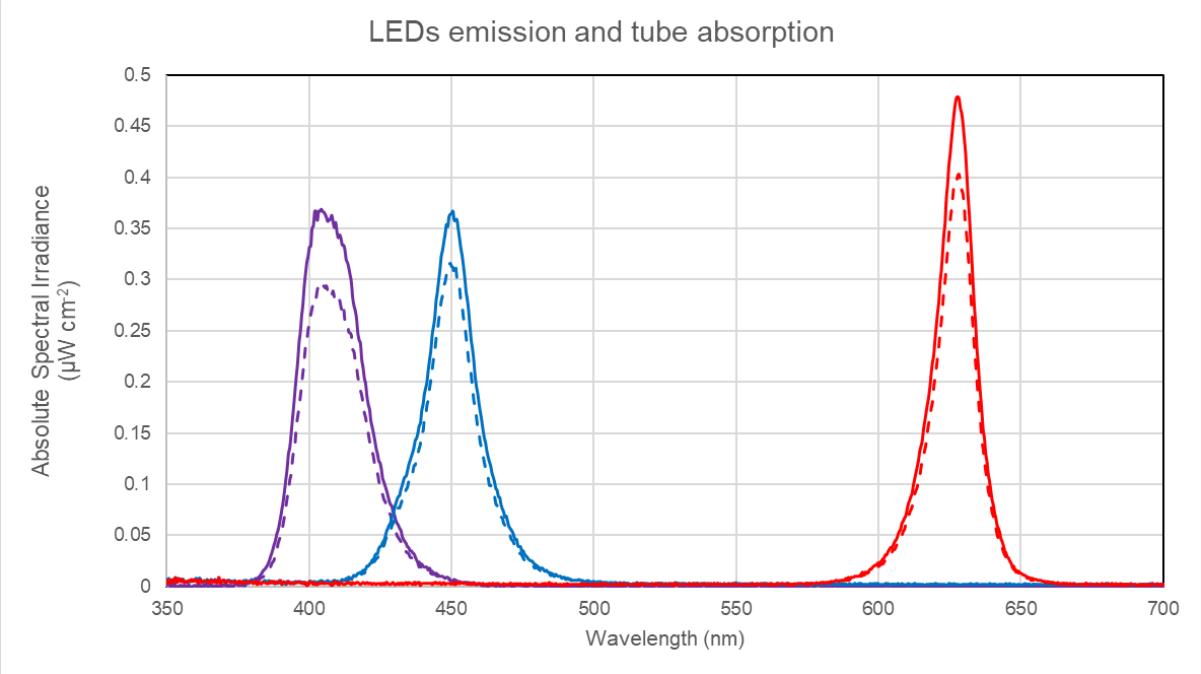


Figure 2.2. Emission spectra of the three LEDs arrays measured in front (continuous line) and behind (dashed line) the plastic tubes.

The flies were filmed using an infrared video camera (Thorlabs DCC1645C) at 10 frames s^{-1}. An infrared filter (Schott RG 780 filter 50 mm × 50 mm) was positioned in front of the camera and the tubes were back-lit with a purpose-built plate of infrared LEDs (≥ 850 nm, L1IZ-0850000000000 Infrared LUXEON IR LED). The LED plate had 20 LEDs separated 45 mm from each other. In the videos, the flies appeared black on a white background.

As a further control, we installed a magnetic sensor (SparkFun Triple Axis Magnetometer Breakout HMC588L), a light sensor (Adafruit TSL2591 High Dynamic Range Digital Light Sensor) and a temperature sensor (Maxim Integrated DS18B20). These were controlled by an Arduino-based data acquisition system with the Arduino board enclosed in an electrically shielded box. The sensors were placed on a poly(methyl methacrylate) cube placed close to the tubes, just out of view of the camera. During the behavioural experiments, the three sensors sampled at 1 Hz to check the constancy of environmental conditions and to provide feedback on the proper functioning of the magnetic field-exposure equipment without revealing the exposure conditions to the experimenter. The Gravity apparatus, LEDs panels and sensors were also placed inside the double-wrapped, three-dimensional Merritt four-coil system.

A LabVIEW program allowed to control the camera and the sensors. The information recorded by the magnetic field-sensor was encrypted and only revealed after completion of the data analysis. In this way, the experimenter was blind to the magnetic field condition. A common experiment MATLAB code was used to synchronize the data acquisition of the laptop (inside the shielded room) and the desktop computer (outside the room) that controlled the Merritt coils. The synchronisation was independently verified using the magnetic field registered by the HMC588L sensor. Thus, while hidden from the experimenter, the exposure settings were always traceable. A schematic of the set-up is shown in Figure 2.3.

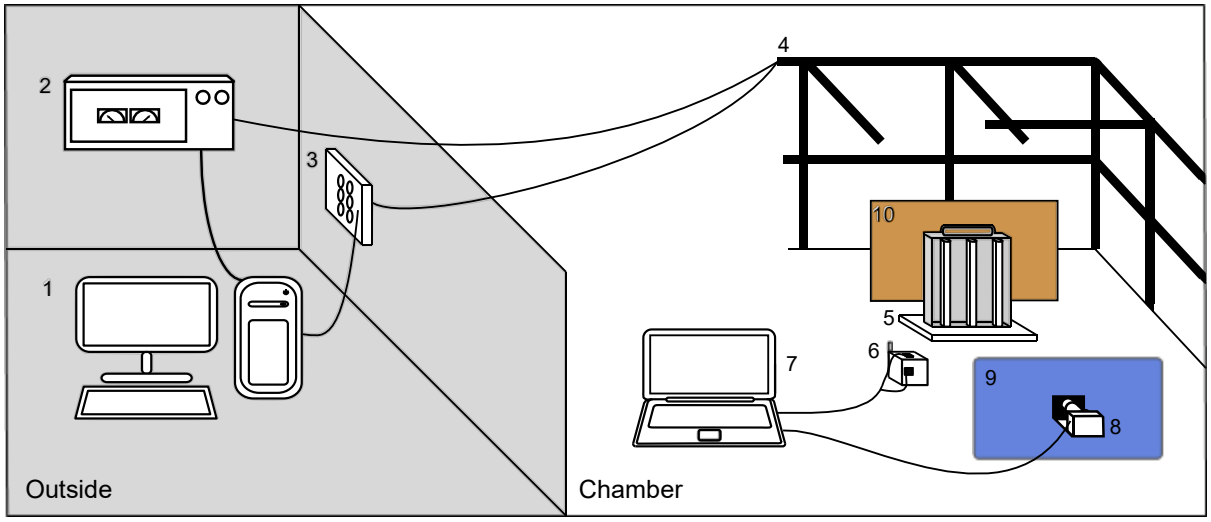


Figure 2.3. Schematic of the Gravity apparatus. The currents in the coils were controlled by an external computer (1) via two DAQ cards, programmed with a MATLAB script. The first DAQ card (National Instruments, USB- 9263) connected the computer to the power supplies (2) (BOP 50-4M, Kepco Inc.) and controlled the magnitudes of the currents in the coils. The second DAQ card (National Instruments USB-6051) controlled the switching box (3) responsible for the directions of the currents (parallel or antiparallel) through the windings of each coil (4). In the schematic, most of the 12 coils were omitted for clarity. A picture of the chamber and the coils is available in Schwarze *et al.*[152] The MATLAB script controlled the two DAQ cards (a) to provide an analogue output to the power supply and (b) to switch the direction of the currents via a digital output. The Gravity apparatus (5) was placed inside the coils inside the chamber. Sensors for temperature, light and magnetic field conditions (6) gave a constant feedback on the experiments. These sensors were connected to a laptop (7), which was controlling the camera (8) to film the flies as well. The set-up was illuminated with UV-blue or blue light via a LEDs plate (9). The other LEDs plate (10) shone infrared light that was used as a background for the videos. The Gravity apparatus, the LEDs plates, the camera and the sensors were placed on a table inside the coils.

Experimental procedure

In the gravity assay, ten flies were gently loaded into each of the three tubes and allowed to rest for at least 5 min before the tubes were clamped to the support. After additional 5 min rest, the flies were pre-exposed to the light and magnetic stimulus for 120 s. In each experiment, three tubes containing ten flies each were first tapped on the table five times in quick succession to knock the flies to the base of the tubes. This was repeated four times at 30 s intervals to give a total of five trials. Every single experiment was filmed and tracked. After each experiment, the tubes were washed with a 70% ethanol solution. Each group of flies was tested in a single

magnetic condition, either sham or exposed depending on the direction of the currents through the windings of Merritt coils (for details on the coils and the production of the static magnetic field see section 2.5).

For the negative geotaxis assays, only male flies (1–2 days old) were tested. Flies were collected at least 24 hours before the experiments after being anaesthetized on ice and kept in the incubators until the testing time. Tests were performed between 1 p.m. and 5 p.m. Four magnetic field conditions were used: 0 µT, 90 µT, 220 µT, and 300 µT. For each magnetic field strength, a sham exposure was performed (with antiparallel currents through the coil windings). A single set of experiments therefore comprised eight separate treatments. Each set of experiments was repeated five times independently, giving the total sample size of 15 independent biological replicas per treatment. In each set of experiments, the order of "Sham" and "Exposed" conditions was randomised and blinded so that it was impossible for the experimenter to know the magnetic field condition experienced by the flies.

2.2.4 FlyVac apparatus

Set-up

The "FlyVac" apparatus (see Kain *et al.*[74]) constructed to study *Drosophila* negative geotaxis comprised four vertical cylindrical polystyrene tubes (length 200 mm, inner diameter 5 mm, outer diameter 6 mm). Each tube was closed at the top by means of a small cap with air holes and connected at its base to a vacuum pump via a solenoid valve. Each tube contained one fly. When the valve was opened, the air vortex quickly and safely whisked the flies to the bottom of the tubes. On closing the valve after 3 s, the flies started to climb inside the tubes. The connections between the bottom of each tube and the vacuum system were stereolithographically printed using epoxy resin to avoid any distortion of the local magnetic field. The solenoid valve (SMC VT 307v- 50Z1-01F-Q) was connected to the vacuum pump (Vacuubrand, ME4CNT) via a tank (with an approximate volume of 30 L) to ensure that the flies were subject to a reproducible pressure.

The experiment used the same LED panels, sensors, camera, laptop and LabVIEW program as in the gravity experiments. The experiment was completely automated to remove any possible artefact due to human interaction. As in the previous experiment, the camera and the sensors

were connected to a laptop via USB cables. The solenoid valve was connected and controlled by a relay (Four Channel USB Relay Module, Numato Lab), which was connected to the laptop via USB. The laptop controlled the camera, the sensors and the relay. The laptop and the relay were placed in a grounded aluminium box placed inside the shielded room, as far as possible from the coils (Figure 2.4).

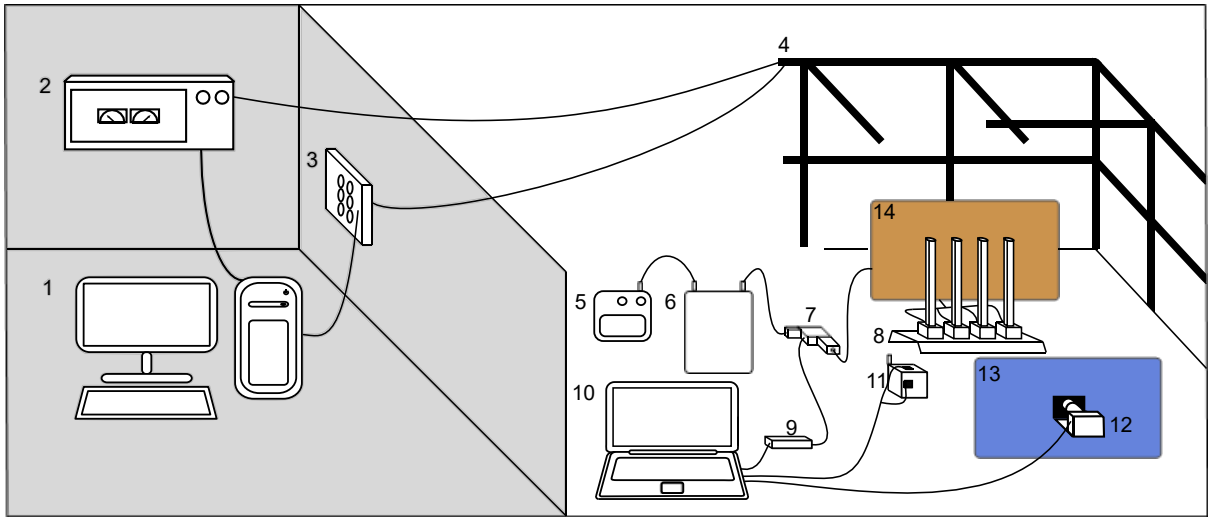


Figure 2.4. FlyVac apparatus schematic. A desktop computer (1) outside the chamber controlled the power supplies (2), the switching box (3) and the double-wrapped three-dimensional Merritt four-coil system (4). A vacuum pump (5) was connected to a vacuum tank (6) and thence to a solenoid valve (7). The valve was connected with the FlyVac apparatus (8) and to a relay (9). The relay was connected via USB to a laptop (10) that controlled the valve, the camera (10) and the sensors (11). The first LEDs plate (13) illuminated the apparatus with UV-blue, blue or red light, while the second one (14) shone infrared light that functioned as a background for the image. The FlyVac, the LEDs plates, the camera, the sensors and the valve were placed on a table inside the coils.

Experimental procedure

A single fly was transferred into each of the four FlyVac traps (formed by the base and the plastic tube) where they rested for 120 s before the FlyVac traps were connected to the set-up inside the screened chamber. The flies were then pre-exposed for 120 s to the magnetic field and light conditions in which they would be tested. At 30 s intervals, the flies were whisked to

the base with a 3 s vacuum pulse. This was repeated another four times to give a total of five trials. Each fly was tested in a single magnetic condition. All experiments were filmed and tracked. After each experiment, the tubes were washed with a 70% ethanol solution.

The gender of the flies, keeping and collecting, daily time of the experiments, magnetic field conditions, blinding and randomisation of the experiments were the same as in the previous negative geotaxis experiment.

2.2.5 Static magnetic fields

The static magnetic fields in all the negative geotaxis experiments were generated by a double-wrapped, three-dimensional Merritt four-coil system, with an average coil diameter of 2 m. Experiments were performed in the centre of the coils where the field homogeneity is better than 99%[83]. The currents in the magnetic coils ran through subsets of windings either in parallel or in antiparallel directions. When the currents were antiparallel, the flies experienced the normal geomagnetic field of Oldenburg (53.152437 N, 8.164159 E). ("Sham" exposure: 48.3 μT intensity, 67.7° inclination). When the currents ran parallel, the flies were exposed to four magnetic fields of different total intensity: 0 μT, 90 μT, 220 μT, and 300 μT (which was the highest producible field without risking damage to the coils). Apart from the 220 μT experiments, in which the magnetic field was applied in the horizontal plane (to mimic the conditions of the original report[44]), the magnetic field was applied on the vertical (*z*) axis.

The magnetic fields were measured either with a FVM 400 Vector Magnetometer (Meda), for fields below 100 μT or a Model 475 DSP Gaussmeter (Lake Shore Cryotronics) for stronger fields. For fields below 100 μT, it was possible to measure the *x*, *y* and *z* components, while for higher fields only the total intensity could be measured.

2.2.6 Time-dependent electromagnetic fields

Spectra of the electromagnetic fields in the immediate neighbourhood of the behavioural apparatus were measured when all electronic components were switched off (as a control) and during an experimental trial (when all equipment was running), using a signal analyser (Rohde and Schwarz, FSV 3 Signal and Spectrum Analyzer, 10 Hz–3.6 GHz). The magnetic

components were measured using a calibrated active loop antenna (Schwarzbeck Mess-Electronik, HFS 1546) between 150 kHz and 10 MHz. The electric components were measured using a calibrated active bi-conical antenna (Schwarzbeck Mess-Electronik, EFS 9218), between 9 kHz and 10 MHz as described in Engels *et al.*[40] (Figures 2.5 a, b, d).

The electromagnetic shielding of the room in which all experiments were performed very effectively excluded anthropogenic time-dependent fields, with attenuation factors of 10^5 at 10 kHz and $>10^6$ at frequencies above 150 kHz. To check whether the *absence* of this background electromagnetic noise affected the flies' ability to respond to static magnetic fields, in one experiment we introduced broadband electromagnetic noise in a range from ~2 kHz to ~10 MHz (20 Vpp) by means of a passive loop antenna (ETS Lindgren EMCO antennas, Model 6511, 20 Hz – 5 MHz) placed close to the Gravity apparatus. As described in Schwarze *et al.*[152], the antenna was driven by a RIGOL, DG1022 signal generator (Figure 2.5 c).

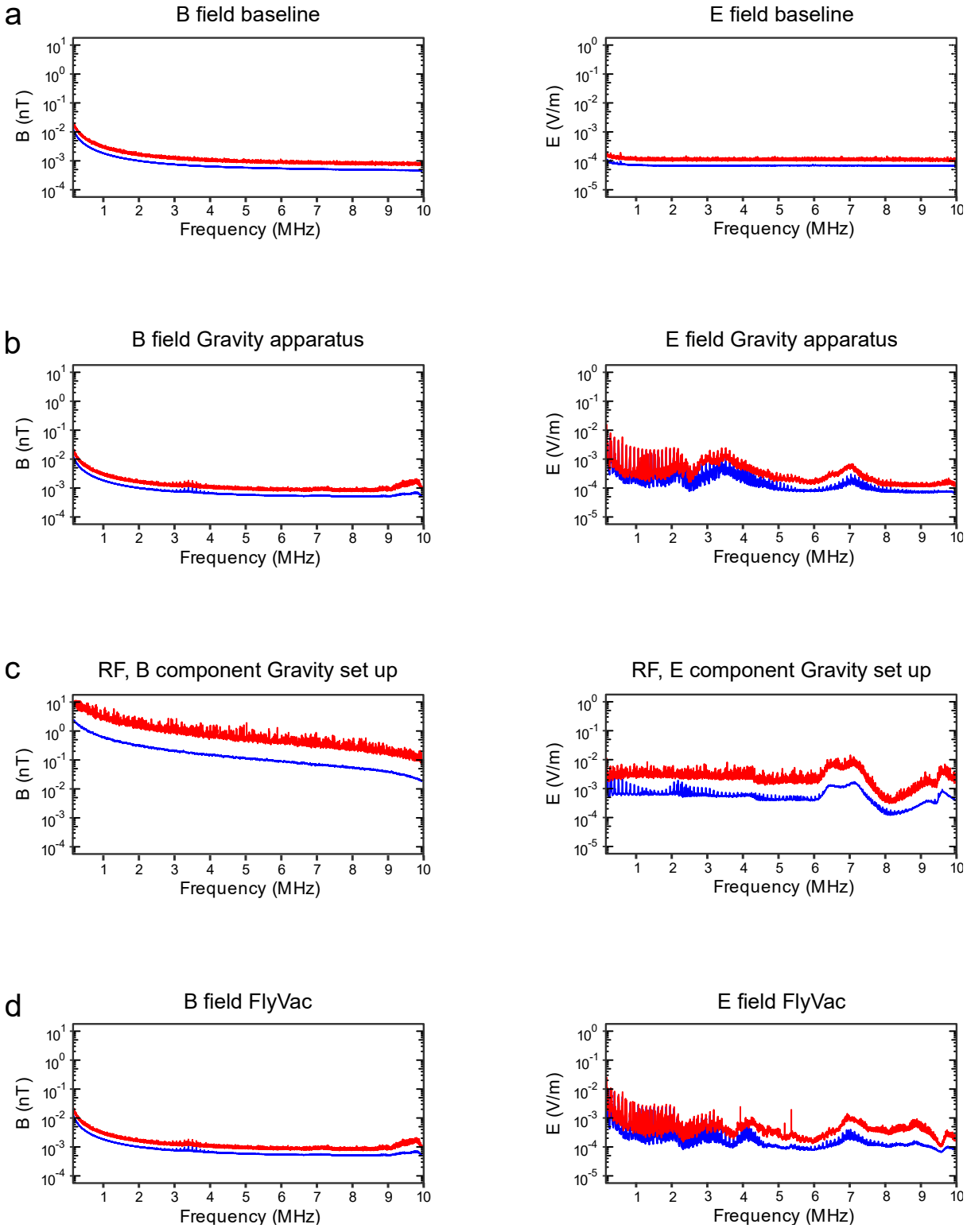


Figure 2.5. Spectra of measured electromagnetic fields. Blue line indicates average measurement, red line indicates max hold measurement. **a.** *Left*. Magnetic component of time-dependent field measured when the set-ups were switched off. *Right*. Electric component of time-dependent field measured when the set-ups were switched off. These measurements were considered as baseline. **b**. *Left*. Magnetic component of time-dependent field measured when all the Gravity apparatus electrical devices (LED plates, laptop, camera and sensors) were

switched on. *Right*. Electric component of time-dependent field measured when all the Gravity apparatus electrical devices (LED plates, laptop, camera and sensors) were switched on. **c**. *Left*. Magnetic component of time-dependent field measured when all the Gravity apparatus electrical devices (LED plates, laptop, camera and sensors) were switched on and broadband RF was reintroduced in the experimental chamber. *Right*. Electric component of time-dependent field measured when all the Gravity apparatus electrical devices (LED plates, laptop, camera and sensors) were switched on and broadband RF was reintroduced in the experimental chamber. **d**. *Left*. Magnetic component of time-dependent field measured when all the FlyVac electrical devices (LED plates, laptop, camera, sensors, vacuum pump, valve and relay) were switched on. *Right*. Electric component of time-dependent field measured when all the FlyVac electrical devices (LED plates, laptop, camera, sensors, vacuum pump, valve and relay) were switched on.

2.2.7 Data analysis

Video analysis

Every experiment was recorded with a 1280×1024 pixel resolution and the videos were analysed and tracked. To do so, as first step, all videos recorded were edited using Fiji (http://fiji.sc/Fiji; Schindelin *et al.*[150]) to produce high-contrast images in which it was easier to spot the flies inside the tubes. We corrected for the gamma (value = 0.45) and sharpened the image (unsharp mask - radius Sigma = 1.0, mask weight = 0.93).

The flies in the tubes were tracked using a MATLAB script to record their positions in each frame. To this end, a representative background image (i.e. a still image of the exposure apparatus without flies) was calculated from the entire recording. This was realized in a two-pass process. In the first step, the arithmetic average of all recorded frames was calculated. In a second iteration, a refined background value was calculated for each pixel individually by considering only those frames for which the pixel intensity did not fall short of the average from the first iteration by more than 20% (presumably due to the presence of a fly). Pixels with contributions from fewer frames than corresponded to the total length of the recording were not considered reliable. Instead, these pixels were filled in from neighbouring pixels based on the moving average with a window size of 10 pixels. The image so obtained was convoluted with a two-dimensional Gaussian with standard deviations of 1 pixel to obtain a faithful and smoothed representation of the background, i.e. the scene without flies. For the tracking, each frame was linearly scaled in intensity to match the background image in several regions

inaccessible to the flies, i.e. in between the tubes. The scaled image was then subtracted from the background to obtain a raw representation of the moving flies as bright pixels on a dark background. This raw image was subject to morphological opening using a disk of size comparable to the flies as structuring element. The dimensions of the disk were delimited as follows: major axis range between 4 and 20 pixels, minor axis between 3 and 20 pixels, surface area of the disk between 8 and 200 pixels. Binarization with a suitable threshold, followed by the removal of small connected regions yielded a representation of flies as white regions on a black background. The centroid, area, semi-major and semi-minor axes of these regions were calculated. Provided that the geometrical measures fitted the expected range, the centroid was recorded for further analyses. Regions that did not meet these criteria were disregarded (Figure 2.6).

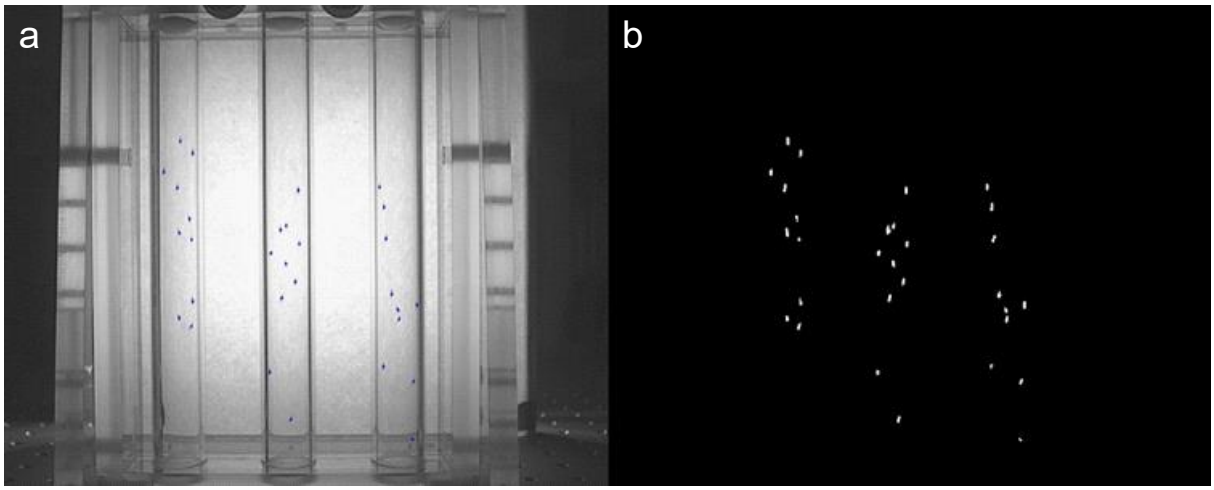


Figure 2.6. a. Videoframe of one of the experiments in the Gravity apparatus. **b.** Visual representation of how the tracking program detected the flies in the tubes.

To check the reliability of the tracking program in the Gravity apparatus assay, three random videos were chosen and the number of flies in each tube was counted every 5 frames (i.e. every 0.5 s) by eye. The lack of proper resolution in the first 4 s of each videos is mainly due to the difficulty of tracking singular flies when close to each other and due to reflections of the flies on the plastic surface of the tube (Figure 2.7). All these issues were solved once flies were tested and tracked individually in the FlyVac set-up (Figure 2.8).

In the Gravity apparatus all frames that detected more than ten flies were excluded from the statistical analysis and considered as false positives. In the FlyVac set-up, every fly that was

not whipped to the bottom by all five vacuum pulses or that showed no mobility in all five trials, was discarded.

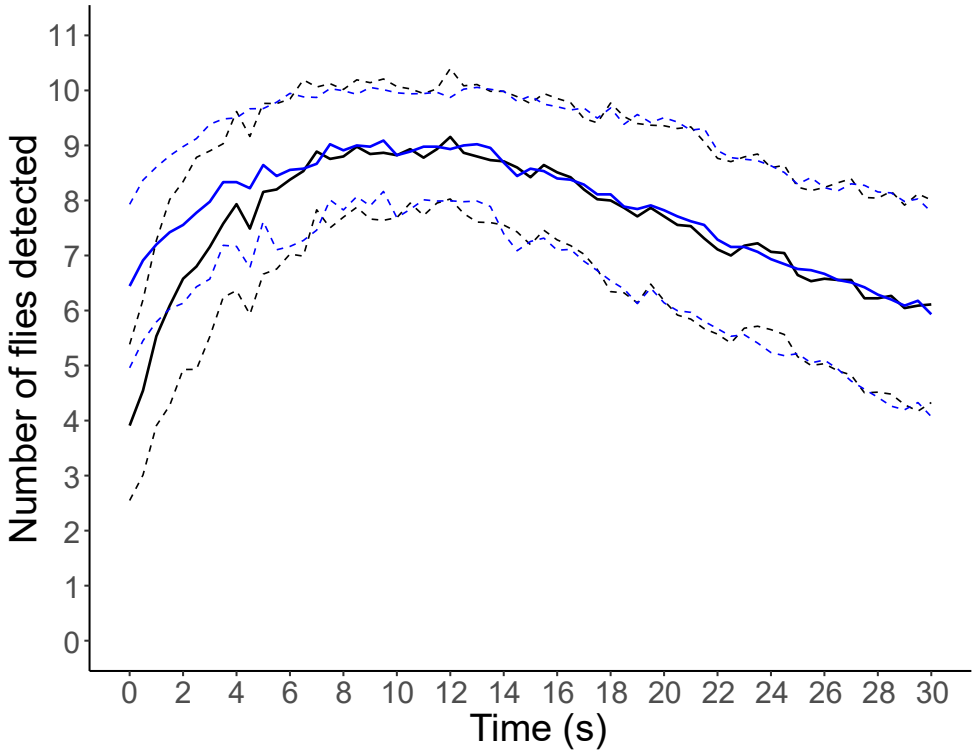


Figure 2.7. Comparison between manual and automated tracking in the Gravity apparatus. Three random videos were analysed by eye and then by the tracking software. The solid line shows the number of flies detected averaged over three randomly chosen videos with three tubes per video and ten flies per tube. Blue: counted by eye. Black: automatic counting. The dashed lines represent one standard deviation either side of the mean.

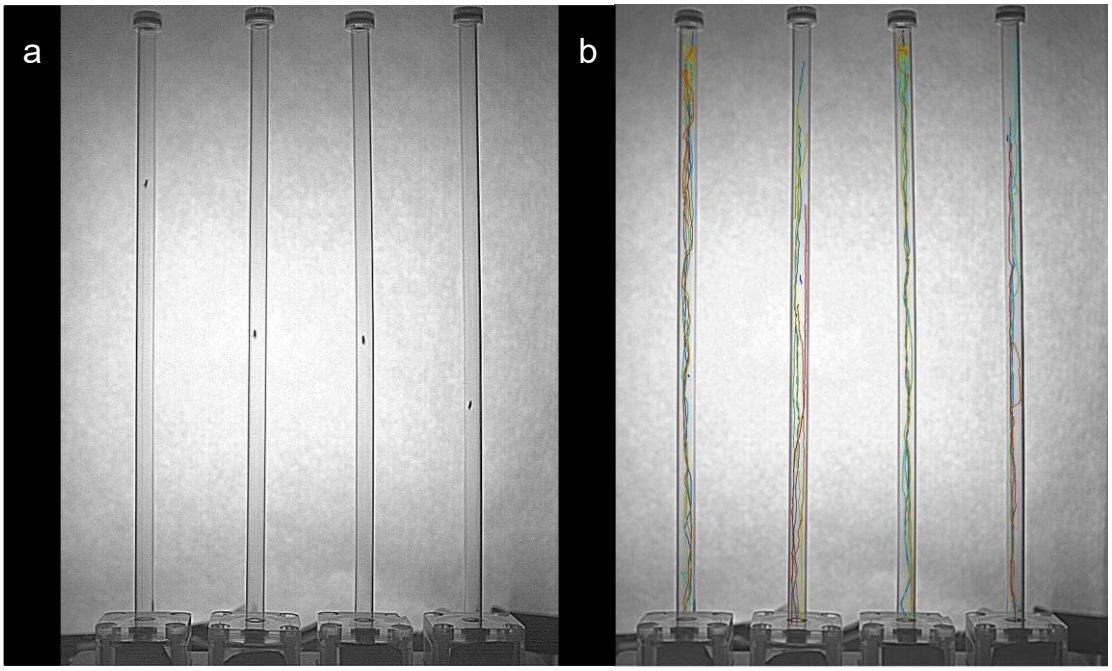


Figure 2.8. a. Videoframe of one of the experiments in the FlyVac set-up. **b.** Visual representation of how the tracking program detected the flies in the tubes. The different colours showed the different tracks performed by a single fly in the five repetitions.

Gravity apparatus

In each experiment three tubes containing ten flies each were tested in 5 consecutive trials, 30 s per trial. Before each trial, the tubes were manually tapped on the table five times to knock the flies to the bottom. This experiment was repeated with new flies for every magnetic field treatment (4 magnetic field condition + 4 corresponding shams = 8 treatments). Each set consisted of eight treatments and it was replicated five times.

All the statistical analyses were run using an R script (https://www.r-project.org/). To ensure a correct replication of the original study, we adopted the statistical test used in Fedele *et al* [44]. We initially evaluated the climbing behaviour as the percentage of flies that climbed 15 cm in 15 s and compared this ratio of climbers between experimental groups with repeated measurements ANOVA. To make sure that we did not overlook any possible magnetic field effect, we additionally analysed the difference in the climbing ratio of flies over the whole time of the trial, and not only for the time point of 15 s. We applied a Generalized Linear Mixed Model (GLM) to account for the binomial error structure of our data (climbing ratios) and for the repeated measurements (consecutive video frames). The random part of the model was

(1|id) + (1|trial/frame), where "*id*" is unique for each fly. Then ANOVA (from the package "car") was used to estimate the F-value and *p*-value for the factor "Exposure".

prop.glme = lme4::glmer(cbind(n,sum.n-n) ~ Exposure + (1|id) + (1|trial/frame), data=df, family=binomial, na.action=na.exclude)

Anova(prop.glme,type="III")

To analyse the negative geotaxis behaviour, we estimated the actual position of the flies during the trials. Since it was impossible to track every single fly independently from the others, we averaged the position of 10 flies per video frame (0.1 s). Then we applied Linear Mixed Effects model (LME) to analyse the effect of the magnetic field condition (0 µT, 90 µT, 220 µT or 300 µT) and of the exposure (Sham vs. Exposed) as well as of the interaction of these two factors on the average distribution of flies over time. The random part of the model was *(1|ID) + (1|trial/frame)*, where "*ID*" is unique for each independent biological replicate (tube with flies).

*fly.lme = lmerTest::lmer(Ycm ~ Exposure*condition + (1|ID) + (1|trial/frame), data=df, na.action=na.exclude)*

The LME model of the same structure was also applied to every independent set of experiments consisting of eight experimental treatments (4 magnetic field conditions times 2 exposures).

Then, ANOVA was used to estimate the F-value and *p*-value for each of the three factors ("Condition", "Exposure" and "Exposure:Condition") in every LME model.

FlyVac apparatus

In each experiment, four tubes containing one fly each were tested in 5 consecutive trials, 30 s per trial. Before each trial flies were whipped to the bottom of the tube by the means of a 3 s

vacuum pulse. This experiment was repeated with new flies for every magnetic field treatment (4 magnetic field condition + 4 corresponding shams = 8 treatments). For every magnetic field treatment ca. 50 flies were tested. The climbing behaviour of individual flies in the FlyVac set-up was analysed as the absolute position of a fly over time. We applied a LME of the same structure as for the Gravity apparatus data followed by the ANOVA to test for the effect of different magnetic field treatments. For the positive control of the climbing behaviour itself we included the factor "genotype" / "light condition" into the fixed part of the model.

2.3 Results

2.3.1 Gravity apparatus

To make sure to reproduce the original study as closely as possible, we tested the flies in different conditions. The parameters we looked at were: different static magnetic field intensities (0 µT, 90 µT, 220 µT and 300 µT), different light conditions (blue and UV-blue light) and absence or presence of re-introduced time-dependent magnetic fields. Whichever variable was changed, we were not able to elicit a magnetic field response. In this section we show the summary of all the experiments and corresponding statistical analysis. As an example for magnetic exposure, we show the results of the experiment in which flies were exposed at 300 µT in presence of blue light (410-490 nm).

As seen in Figure 2.9, initially we only looked at the proportion of flies that was able to climb 15 cm in 15 s (grey dotted line). Unfortunately, the ability of the flies to ascend the tube was not affected by an external magnetic field with an intensity of 300 µT when exposed to blue light (Repeated Measure ANOVA, $p = 0.827$, Table 2.1). Therefore, not to be restricted to a single time point, we looked at the proportion of flies able to reach 15 cm during the entire testing time of 30 s. Again, we saw no magnetic field effect (ANOVA of Generalized Linear Mixed Model, $p = 0.824$, Table 2.2). To make sure we did not miss even the slightest possible magnetic field effect, we decided to look at the average position of the flies over time. However, no magnetic field effect was detected (ANOVA of the Linear Mixed Effect Model, $p = 0.6289$, Table 2.3).

The same principle was applied to analyse all the data from the remaining experiments. As a further control we replicated all these experiments in two different *Drosophila* strains. The first

one, labelled Canton-S LE, was the same strain as in the original Fedele *et al* [44]. The second strain, labelled Canton-S OX, was kindly provided by Prof. Scott Waddell, Centre for Neural Circuits and Behaviour, University of Oxford.

The summary of all the experiments are showed from Figure 2.10 to Figure 2.15. The relative statistical analysis and *p*-values are collected in Table 2.4 and Table 2.5.

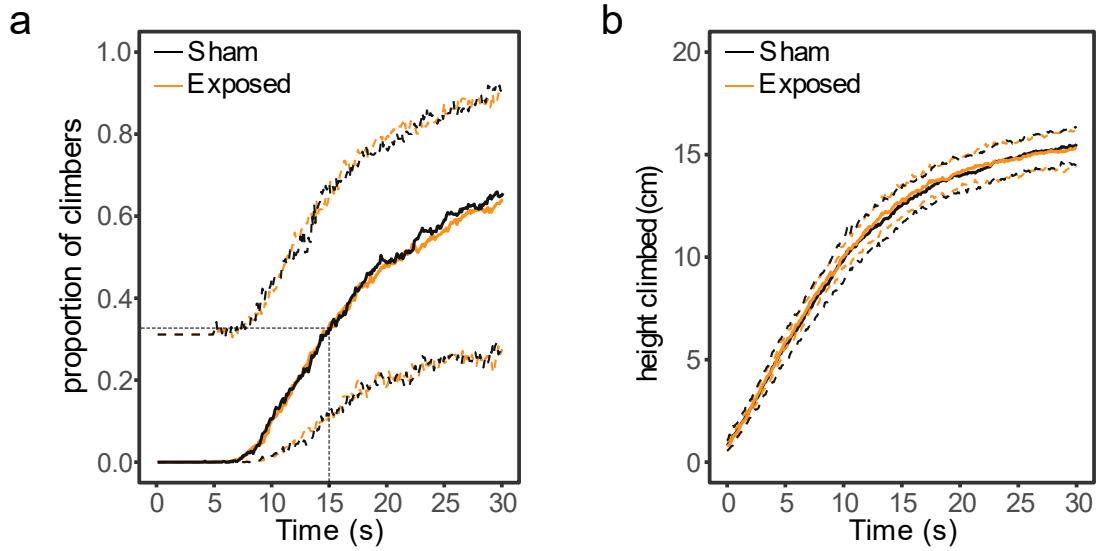


Figure 2.9. Climbing behaviour of CS-LE when exposed to a 300 µT field and blue light (410-490 nm). **a**. Temporal resolution of the proportion of flies able to reach 15 cm. Black line shows flies behaviour when exposed to a sham stimulus, orange line when exposed to a 300 µT field. In both conditions, flies were exposed to a blue light (410- 490 nm) stimulus. Data shown as mean ± confidence interval. The grey dotted line highlights the proportion of flies able to climb 15 cm in 15 s. At time point 15 s, there was no magnetic field response. Repeated Measure ANOVA, p = 0.827 (for details see Table 2.1). No magnetic field response was detected even when looking at the entire testing period. ANOVA of Generalized Linear Mixed Model, p = 0.824 (for details see Table 2.2). **b**. Average position of flies over time. Black line sham, orange line exposed to 300 µT field. Data shown as mean ± s.d. No difference between sham and exposed was detected. ANOVA of the Linear Mixed Effect Model, p = 0.6289 (for details see Table 2.3).

Repeated Measure ANOVA					
	DF	Sum Sq	Mean Sq	F-value	*p*-value
Exposure	1	0.0012	0.0012	0.049	0.827

Table 2.1. Repeated Measure ANOVA on the proportion of flies able to climb 15 cm in 15 s. There was no difference between flies exposed to a 300 μT magnetic field and a sham field in the presence of blue light.

Df = Degrees of Freedom; Sum Sq = sum of squares; Mean Sq = Mean Square error

ANOVA of the GLM				
	Estimate	Std. Error	z-value	*p*-value
Exposure	0.0285	0.12765	0.223	0.824

Table 2.2. ANOVA of Generalized Linear Mixed Model of the proportion of flies able to climb 15 cm over the entire testing period of 30 s. There was no difference between flies exposed to a 300 μT magnetic field and a sham field in the presence of blue light.

ANOVA of the LME						
	Sum Sq	Mean Sq	NumDF	DenDF	F-value	*p*-value
Exposure	0.3214	0.3214	1	28.001	0.2387	0.6289

Table 2.3. ANOVA of the Linear Mixed Effect Model of the average position of the flies over time (30 s). There was no difference between flies exposed to a 300 μT magnetic field and a sham field in the presence of blue light.

NumDF = Number of Denominator Degrees of Freedom; DenDF = Denominator Degrees of Freedom

Canton-S LE Blue light

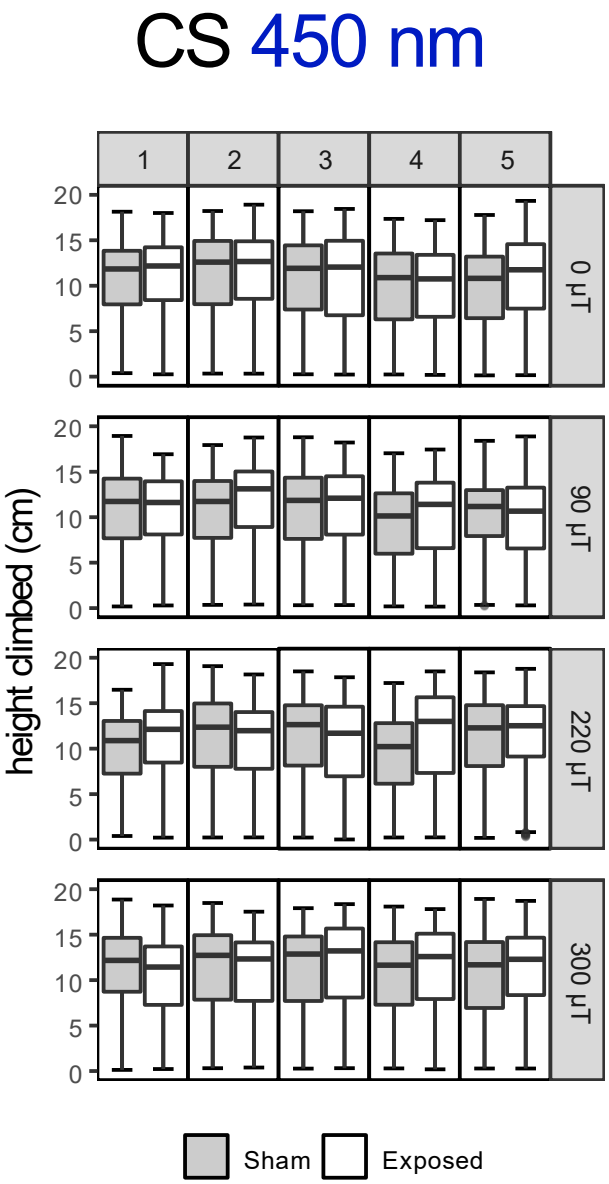


Figure 2.10. The data show the average position over time of the flies in three independent tubes over five trials. Flies belonging to the original Canton-S LE line were exposed to different magnetic stimuli (0 µT, 90 µT, 220 µT, 300 µT) in presence of blue light (410-490 nm). Each treatment (4 magnetic field condition + 4 sham) was tested independently five times giving the total sample size of 15 independent biological replicas per treatment, totalling 120 independent biological replicas. ANOVA output for Linear Mixed Effect Model analysis is summarised in Table 2.4.

Canton-S LE UV-blue light

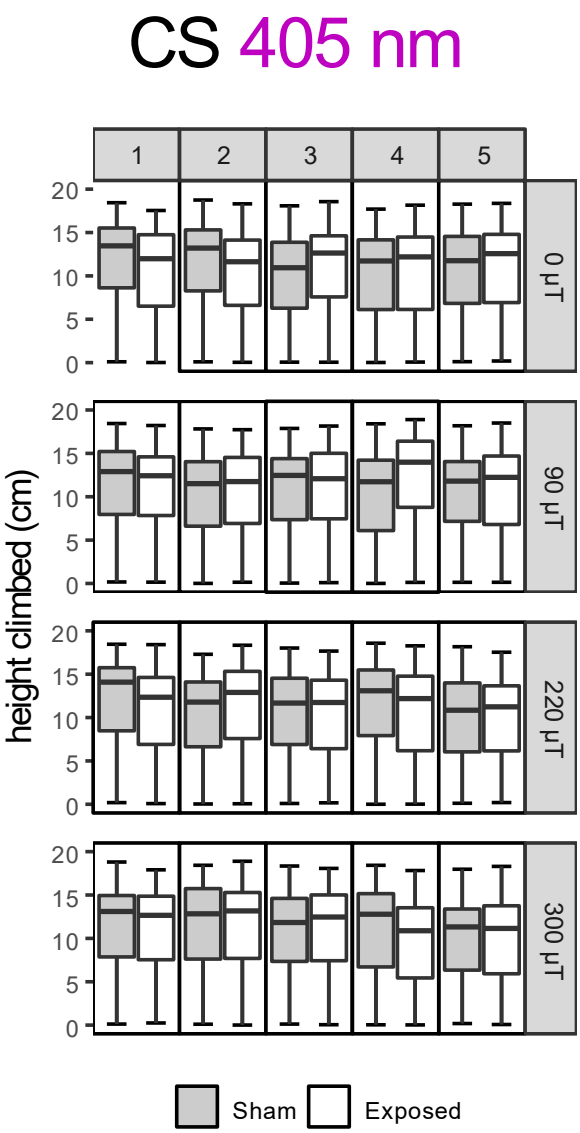


Figure 2.11. The data show the average position over time of the flies in three independent tubes over five trials. Flies belonging to the original Canton-S LE line were exposed to different magnetic stimuli (0, 90, 220, 300 µT) in presence of UV- blue light (380–450 nm). Each treatment (4 magnetic field condition + 4 sham) was tested independently five times giving the total sample size of 15 independent biological replicas per treatment, totalling 120 independent biological replicas. ANOVA output for Linear Mixed Effect Model analysis is summarised in Table 2.4.

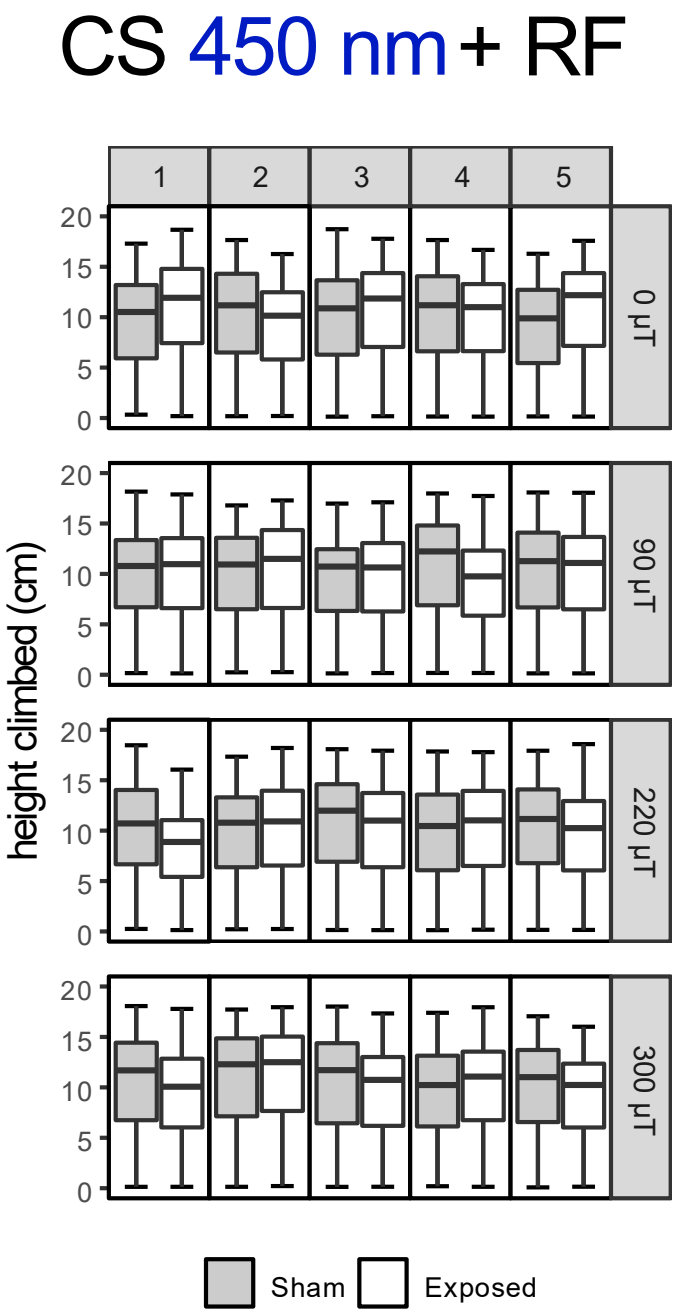


Figure 2.12. The data show the average position over time of the flies in three independent tubes over five trials. Flies belonging to the original Canton-S LE line were exposed to different magnetic stimuli (0, 90, 220, 300 µT), in presence of blue light (410-490 nm) and re-introduced time-dependent magnetic fields. Each treatment (4 magnetic field condition + 4 sham) was tested independently five times giving the total sample size of 15 independent biological replicas per treatment, totalling 120 independent biological replicas. ANOVA output for Linear Mixed Effect Model analysis is summarised in Table 2.4.

		CS LE 450 nm		CS LE 405 nm		CS LE 450 nm RF	
		F-value	*p*-value	F-value	*p*-value	F-value	*p*-value
Block 1	Exposure	0.0	0.986	7.8	0.013	1.2	0.289
	Condition	0.2	0.924	0.1	0.959	1.6	0.236
	Exposure:Condition	1.1	0.385	1.0	0.424	4.0	0.027
Block 2	Exposure	0.2	0.688	0.0	0.852	0.0	0.950
	Condition	0.4	0.754	1.5	0.247	4.2	0.022
	Exposure:Condition	1.9	0.171	2.2	0.122	1.6	0.221
Block 3	Exposure	0.2	0.703	1.1	0.311	0.5	0.494
	Condition	1.1	0.374	0.4	0.757	1.7	0.213
	Exposure:Condition	0.9	0.482	0.6	0.614	1.6	0.232
Block 4	Exposure	12.8	0.003	0.0	0.906	0.7	0.408
	Condition	5.8	0.007	3.9	0.028	0.1	0.948
	Exposure:Condition	3.0	0.061	8.8	0.001	1.9	0.163
Block 5	Exposure	2.2	0.160	0.2	0.644	0.0	0.914
	Condition	3.1	0.054	2.0	0.152	0.8	0.522
	Exposure:Condition	0.9	0.458	0.1	0.973	2.8	0.075

		F-value	*p*-value	F-value	*p*-value	F-value	*p*-value
All blocks	Exposure	3.7	0.058	0.1	0.807	1.3	0.260
	Condition	1.6	0.196	0.3	0.835	0.3	0.794
	Exposure:Condition	0.3	0.856	1.2	0.301	1.9	0.135

Table 2.4. Summary of the ANOVA of the Linear Mixed Effect Model of the experiments involving Canton-S LE strain. *p*-values below 0.05 are highlighted in yellow. The upper part of the table is divided into the three main experiments: blue light exposure (450 nm), UV-blue light exposure (405 nm) and blue light and radiofrequency exposure (450 nm RF). Each "Block" corresponds to three biological replicas per magnetic field exposure per magnetic field condition. "Exposure" is the factor describing the presence or absence of a magnetic field stimulus (Sham vs Exposed), while "Condition" is the factor describing the magnetic field intensity (0 µT, 90 µT, 220 µT or 300 µT). In the presence of blue light (450 nm), in one case out of five, there is an Exposure and Condition effect, but there is never an interaction between them. In the presence of UV-blue light (405 nm), in one case out of five, there is an Exposure effect, a Condition effect and an interaction between the two factors. In the presence of blue light and time-dependent electromagnetic fields (450 nm RF), in one case out of five there is a

Condition affect and an interaction between Condition and Exposure, but no Exposure effect. The lower part of the Table summarises all the experimental trials (i.e. considers all five "Blocks" altogether). Importantly, there is no factor (Exposure and Condition) or interaction between them, for which p is less than 0.05. In conclusion, we have found no effect of magnetic field intensity and exposure on *Drosophila* negative geotaxis.

CS- OX Blue light

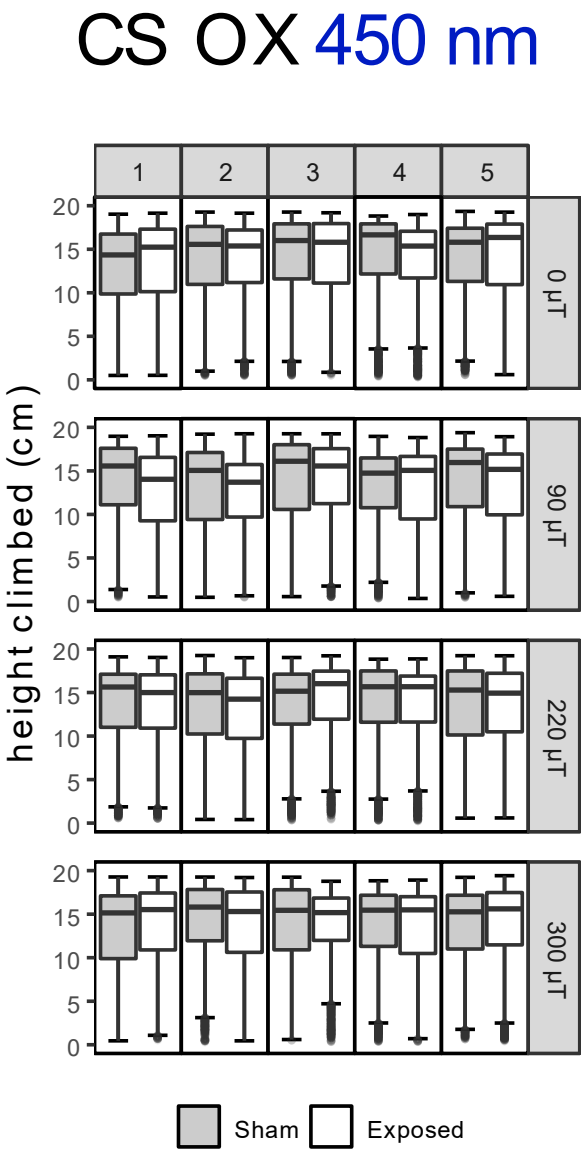


Figure 2.13. The data show the average position over time of the flies in three independent tubes over five trials. Flies belonging to the Canton-S OX line were exposed to different magnetic stimuli (0, 90, 220, 300 µT) in presence of blue light (410-490 nm). Each treatment (4 magnetic field condition + 4 sham) was tested independently five times giving the total sample size of 15 independent biological replicas per treatment, totalling 120 independent biological replicas. The dots represent outliers. ANOVA output for Linear Mixed Effect Model analysis is summarised in Table 2.5.

CS- OX UV-blue light

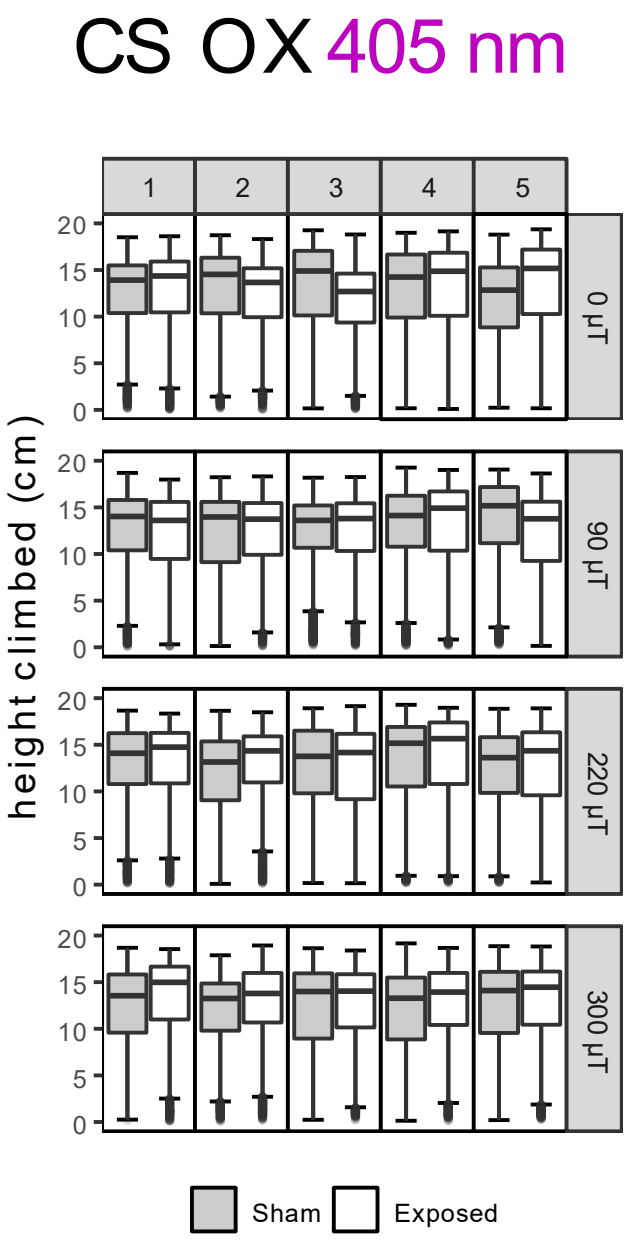


Figure 2.14. The data show the average position over time of the flies in three independent tubes over five trials. Flies belonging to the Canton-S OX line were exposed to different magnetic stimuli (0 µT, 90 µT, 220 µT, 300 µT) in presence of UV- blue light (380–450 nm). Each treatment (4 magnetic field condition + 4 sham) was tested independently five times giving the total sample size of 15 independent biological replicas per treatment, totalling 120 independent biological replicas. The dots represent outliers. ANOVA output for Linear Mixed Effect Model analysis is summarised in Table 2.5.

CS- OX UV-blue light

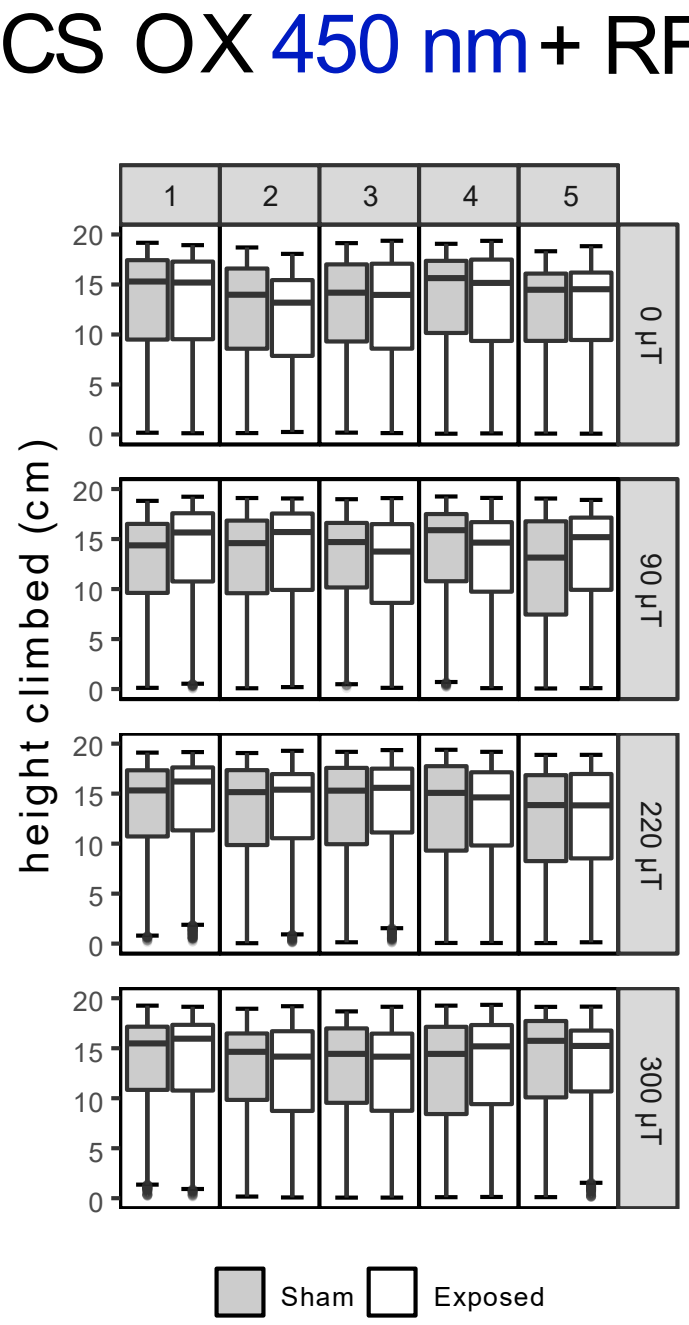


Figure 2.15. The data show the average position over time of the flies in three independent tubes over five trials. Flies belonging to the Canton-S OX line were exposed to different magnetic stimuli (0 µT, 90 µT, 220 µT, 300 µT), in presence of blue light (410-490 nm) and re-introduced time-dependent magnetic fields. Each treatment (4 magnetic field condition + 4 sham) was tested independently five times giving the total sample size of 15 independent biological replicas per treatment, totalling 120 independent biological replicas. The dots represent outliers. ANOVA output for Linear Mixed Effect Model analysis is summarised in Table 2.5.

		CS OX 450 nm		CS OX 405 nm		CS OX 450 nm RF	
		F-value	*p*-value	F-value	*p*-value	F-value	*p*-value
Block 1	Exposure	0.0	0.851	1.2	0.282	2.5	0.131
	Condition	0.5	0.704	0.8	0.514	1.3	0.301
	Exposure:Condition	1.9	0.163	1.5	0.263	0.8	0.505
Block 2	Exposure	3.1	0.099	1.0	0.336	0.1	0.742
	Condition	4.7	0.016	0.1	0.952	3.2	0.051
	Exposure:Condition	0.5	0.684	1.8	0.189	0.9	0.485
Block 3	Exposure	0.3	0.581	1.4	0.248	1.0	0.339
	Condition	0.1	0.936	0.2	0.920	3.3	0.048
	Exposure:Condition	0.6	0.618	2.3	0.119	0.7	0.567
Block 4	Exposure	1.3	0.274	2.3	0.147	0.6	0.440
	Condition	2.8	0.076	5.7	0.008	0.4	0.722
	Exposure:Condition	0.3	0.804	0.2	0.877	0.6	0.630
Block 5	Exposure	0.3	0.618	0.8	0.397	2.5	0.135
	Condition	1.3	0.311	0.3	0.851	4.8	0.014
	Exposure:Condition	1.3	0.314	5.6	0.008	2.9	0.069

		F-value	*p*-value	F-value	*p*-value	F-value	*p* -value
All blocks	Exposure	3.3	0.072	1.4	0.234	0.0	0.902
	Condition	3.3	0.022	1.0	0.411	2.2	0.094
	Exposure:Condition	1.0	0.405	2.4	0.070	0.8	0.518

Table 2.5. Summary of the ANOVA of the Linear Mixed Effect Model of the experiments involving Canton-S OX strain. *p*-values below 0.05 are highlighted in yellow. The upper part of the table is divided into the three main experiments: blue light exposure (450 nm), UV-blue light exposure (405 nm) and blue light and radiofrequency exposure (450 nm RF). Each "Block" corresponds to three biological replicas per magnetic field exposure per magnetic field condition. "Exposure" is the factor describing the presence or absence of a magnetic field stimulus (Sham vs Exposed), while "Condition" is the factor describing the magnetic field intensities (0 µT, 90 µT, 220 µT or 300 µT). In the presence of blue light (450 nm), in one case out of five, there is a Condition effect, but there is never an Exposure effect or an interaction between them. In presence of UV-blue light (405 nm), in one case out of five, there is a Condition effect, an interaction between Exposure and Condition but no Exposure effect. In

the presence of blue light and time-dependent electromagnetic fields (450 nm RF), in two cases out of five there is a Condition affect, but there is no Exposure effect and no interaction between Condition and Exposure. The lower part of the Table summarises all the experimental trials (i.e. considers all five "Blocks" altogether). In the presence of blue light (450 nm) there is a Condition effect, but no Exposure effect and no interaction between them. In the other two experiments, there is no factor (Exposure and Condition) or interaction between them, for which values are below the *p*-level of 0.05. In conclusion, we have found no effect of magnetic field intensity or exposure on *Drosophila* negative geotaxis.

2.3.2 FlyVac apparatus

Due to the lack of positive results while using the Gravity apparatus, we decided to switch to a single fly experiment using the FlyVac apparatus. As in the previous experiment, we looked at how different variables could influence *Drosophila* behaviour when exposed to an external magnetic field. The parameters we looked at were: different static magnetic field intensities (0 μT, 90 μT, 220 μT and 300 μT), different light conditions (UV-blue, blue and red light) and different *Drosophila* lines. Whichever variable was changed, we were not able to elicit a magnetic field response. In this section we show the summary of all the experiments and relevant statistical analysis. As a parameter to determine the flies behaviour we chose the average position of a single fly over time, averaged over five trials. We ran controls to check whether the flies were behaving as predicted when exposed to different light conditions (Figure 2.16 a) and when wild-type flies were compared to a genotype known to have a deficiency in negative geotaxis (Figure 2.16 b). As an example for magnetic exposure, we show the results of the experiment in which flies were exposed at 300 μT in presence of blue light (410-490 nm) (Figure 2.17).

The summary of all the experiments are showed from Figure 2.18 to Figure 2.20. The statistical analysis and corresponding *p*-values are collected from Table 2.6 to Table 2.14.

Light and genotype controls

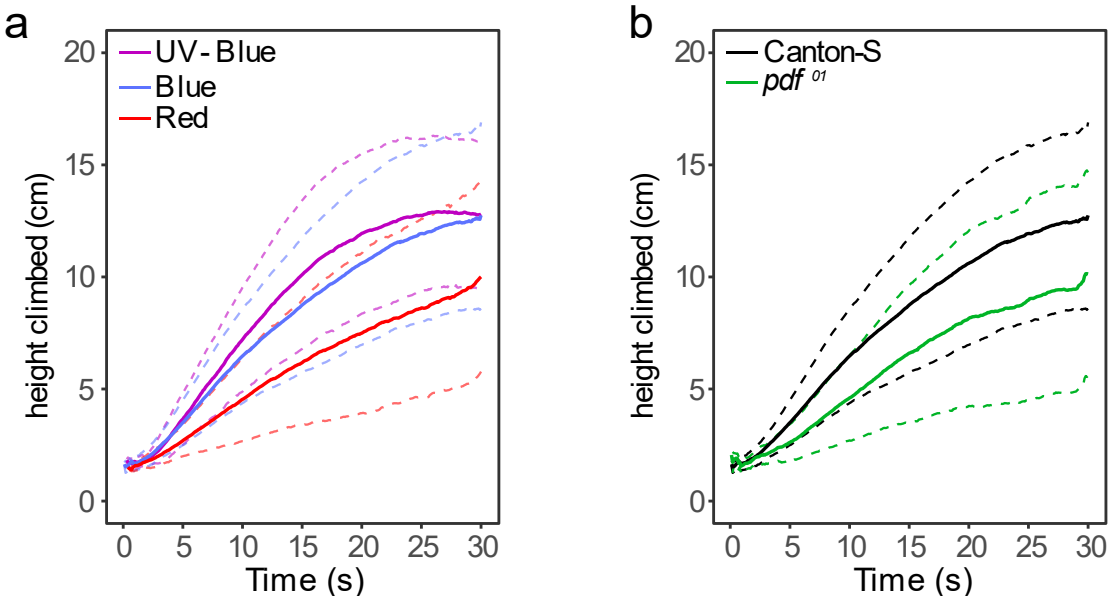


Figure 2.16 a. Positive control for light exposure. Purple line shows the average position of the flies over time over trials of 308 Canton-S flies when exposed to UV-blue light (380-450 nm), blue line when 208 Canton-S were exposed to blue light (410-490 nm) and red line when 199 Canton-S were exposed to red light (580–660 nm). Data shown as mean ± s.d. When flies are exposed to UV-blue and blue light, they perform better than when exposed to red light. ANOVA of the Linear Mixed Effect Model, $p < 0.0001$; Multiple comparisons of the means: Tukey contrast; UV-blue vs Red, $p < 0.0001$, Blue vs Red, $p < 0.0001$ (for details, see Table 2.6). **b**. Positive control for negative geotaxis. Black line shows the average position of the flies over time over trials of 208 Canton-S, green line shows average climbing behaviour of 82 *pdf* ^{01}. Data shown as mean ± s.d. When exposed to blue light (410-490 nm), Canton-S perform better than *pdf* ^{01}. ANOVA of the Linear Mixed Effect Model, $p < 0.0001$ (for details see Table 2.7).

ANOVA of the LME						
	Sum Sq	Mean Sq	NumDF	DenDF	F-value	*p*-value
Light	1308.4	654.19	2	711.89	91.61	< 2.2e-16
Multiple Comparisons of Means: Tukey Contrasts						
	Estimate	Std. Error	z -value	*p*-value		
Blue vs UV-blue	-0.923781	0.012627	-73.16	<2e-16		
Red vs UV-blue	-3.402175	0.012986	-261.99	<2e-16		
Red vs Blue	-2.478393	0.009423	-263.01	<2e-16		

Table 2.6. ANOVA of the LME indicates that there is a light effect. The multiple comparisons show a difference in the flies' behaviour when exposed to different light conditions. In UV-blue light *Drosophila* perform better than in blue and red lights and they perform worse in red light when compared to shorter wavelengths. *p*-values below 0.05 are highlighted in yellow.

ANOVA of the LME						
	Sum Sq	Mean Sq	NumDF	DenDF	F-value	*p*-value
Genotype	268.91	268.91	1	288.03	38.92	1.57 e-09

Table 2.7. ANOVA of the LME indicates that there is a genotype effect. As predicted, *pdf* ^{01} performed worse when compared to Canton-S. *p*-values below 0.05 are highlighted in yellow.

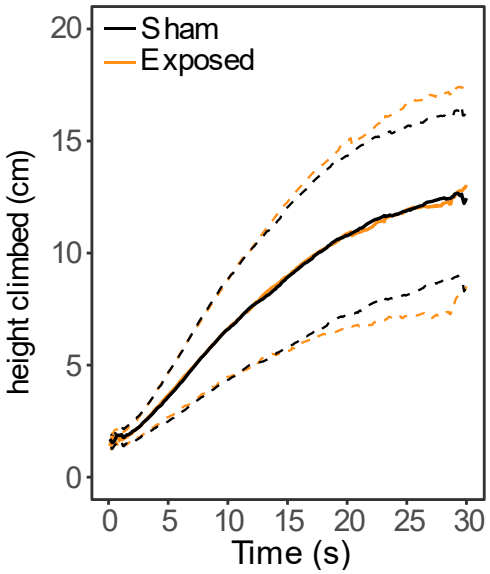


Figure 2.17. Climbing behaviour of CS-LE flies when exposed to a 300 µT field and corresponding sham in presence of blue light. Black line shows the average position of the flies over time in trials of 53 Canton-S flies when exposed to a 300 µT magnetic field, orange line when 49 flies were exposed to the relative sham exposure. Data shown as mean ± s.d. Noticeably, there was no difference in behaviour between flies exposed to a sham or to a 300 µT field in presence of blue light (410-490 nm). ANOVA of the Linear Mixed Effect Model $p = 0.9968$ (for details see Table 2.8).

ANOVA of the LME						
	Sum Sq	Mean Sq	NumDF	DenDF	F-value	*p*-value
Exposure	0.0001	0.00012	1	99.993	0	0.9968

Table 2.8. ANOVA of the LME to compare CS LE flies exposed to a magnetic stimulus of 300 µT and relative sham in presence of blue light. No magnetic field effect was detected.

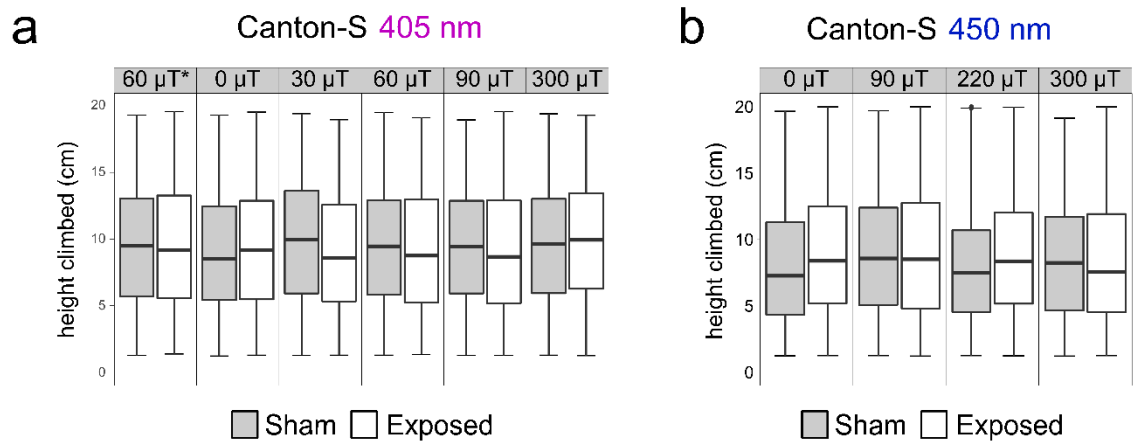


Figure 2.18. **a**. Average position of the flies over time over trials of a total of 617 individual Canton-S LE flies when exposed to UV-blue light (380-450 nm) and to different magnetic field intensities. The different magnetic field intensities applied were 60 µT *, 0 µT, 30 µT, 60 µT, 90 µT, 300 µT. Grey boxplots show a sham exposure, white a magnetic field exposure. Each boxplot represents the behaviour of ca. 50 individual *Drosophila*. No magnetic field effect was noticed. ANOVA of the Linear Mixed Effect Model, (Exp. p = 0.8079; Cond. p = 0.1864; Exp:Cond. p = 0.3944). **b**. Average position of the flies over time over trials of a total of 411 individual Canton-S LE flies when exposed to blue light (410-490 nm) and to different magnetic field intensities. The different magnetic field intensities applied were 0 µT, 90 µT, 220 µT and 300 µT. Grey boxplots show a sham exposure, white a magnetic field exposure. Each boxplot represents the behaviour of ca. 50 individual *Drosophila*. No magnetic field effect was noticed. ANOVA of the Linear Mixed Effect Model (Exp. p = 0.1365; Cond. p = 0.4055; Exp:Cond. p = 0.4905). For details see Table 2.9 and Table 2.10.

* The magnetic field was applied on the *z* axis but with the direction inverted (the field was pointing upwards)

ANOVA of the LME CS LE 405 nm						
	Sum Sq	Mean Sq	NumDF	DenDF	F-value	*p*-value
Exposure	0.4448	0.4448	1	299.95	0.0592	0.8079
Condition	25.369	12.6846	2	299.95	1.689	0.1864
Exposure:Condition	14.017	7.0082	2	299.95	0.9332	0.3944

Table 2.9. ANOVA of the LME to compare CS LE flies exposed to different magnetic stimuli (60 µT *, 0 µT, 30 µT, 60 µT, 90 µT, 300 µT) and relative shams in presence of UV-blue light. No magnetic field effect was detected.

* The magnetic field was applied on the *z* axis but with the direction inverted (the field was pointing upwards)

ANOVA of the LME CS LE 450 nm						
	Sum Sq	Mean Sq	NumDF	DenDF	F-value	*p*-value
Exposure	16.241	16.241	1	402.96	2.2262	0.1365
Condition	21.29	7.0965	3	402.96	0.9727	0.4055
Exposure:Condition	17.663	5.8876	3	402.96	0.807	0.4905

Table 2.10. ANOVA of the LME to compare CS LE flies exposed to different magnetic stimuli (0 µT, 90 µT, 220 µT and 300 µT) and relative shams in presence of blue light. No magnetic field effect was detected.

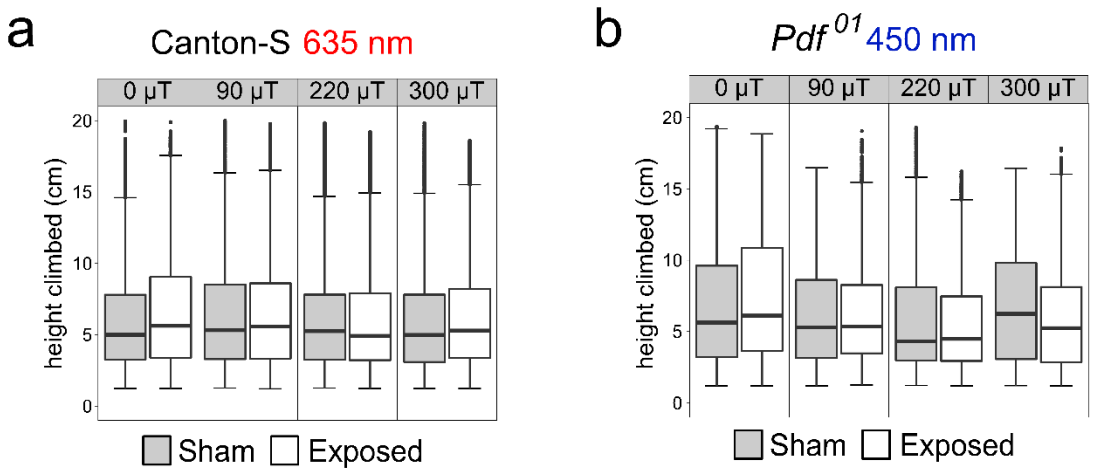


Figure 2.19. **a**. Average position of the flies over time over trials of a total of 412 individual Canton-S LE flies when exposed to red light (580–660 nm) and to different magnetic field intensities. The different magnetic field intensities applied were 0 µT, 90 µT, 220 µT, 300 µT. Grey boxplots show a sham exposure, white a magnetic field exposure. The dots represent outliers. Each boxplot represents the behaviour of ca. 50 individual *Drosophila*. No magnetic field effect was noticed. ANOVA of the Linear Mixed Effect Model, (Exp. $p = 0.4798$; Cond. $p = 0.7393$; Exp:Cond. $p = 0.6855$). **b**. Average position of the flies over time over trials of a total of 165 individual *pdf* ^{01} flies when exposed to blue light (410-490 nm) and to different magnetic field intensities. The different magnetic field intensities applied were 0 µT, 90 µT, 220 µT and 300 µT. Grey boxplots show a sham exposure, white a magnetic field exposure. The dots represent outliers. Each boxplot represents the behaviour of ca. 20 individual *Drosophila*. No magnetic field effect was noticed. ANOVA of the Linear Mixed Effect Model, (Exp. $p = 0.6439$; Cond. $p = 0.2206$; Exp:Cond. $p = 0.5394$). For details see Table 2.11 and Table 2.12.

ANOVA of the LME CS LE 635 nm						
	Sum Sq	Mean Sq	NumDF	DenDF	F-value	*p*-value
Exposure	2.8551	2.8551	1	403.99	0.5002	0.4798
Condition	7.1798	2.3933	3	403.99	0.4193	0.7393
Exposure:Condition	8.4875	2.8292	3	403.99	0.4956	0.6855

Table 2.11. ANOVA of the LME to compare CS LE flies exposed to different magnetic stimuli (0 μT, 90 μT, 220 μT and 300 μT) and relative shams in presence of red light. No magnetic field effect was detected.

ANOVA of the LME *pdf* ^{01} 450 nm						
	Sum Sq	Mean Sq	NumDF	DenDF	F-value	*p*-value
Exposure	1.4539	1.4539	1	156.97	0.2145	0.6439
Condition	30.212	10.0705	3	156.97	1.4854	0.2206
Exposure:Condition	14.715	4.9049	3	156.97	0.7235	0.5394

Table 2.12. ANOVA of the LME to compare *pdf* ^{01} flies exposed to different magnetic stimuli (0 μT, 90 μT, 220 μT and 300 μT) and relative shams in presence of blue light. No magnetic field effect was detected.

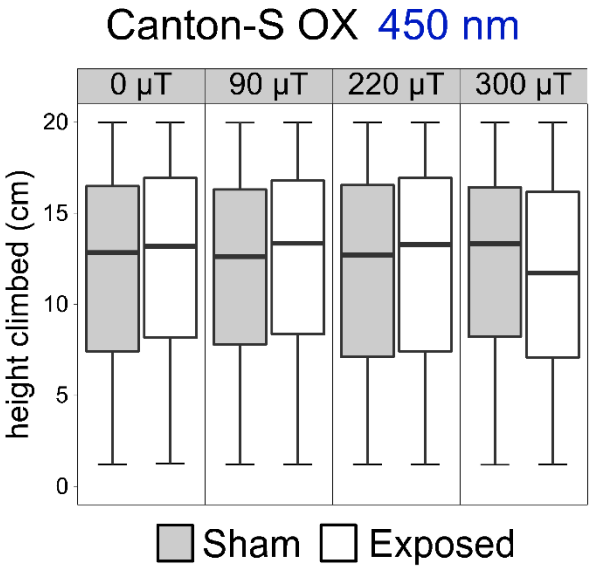


Figure 2.20. Average position of the flies over time over trials of a total of 355 individual Canton-S OX flies when exposed to blue light (410-490 nm) and to different magnetic field intensities. The different magnetic field intensities applied were 0 µT, 90 µT, 220 µT and 300 µT. Grey boxplots show a sham exposure, white a magnetic field exposure. Each boxplot represents the behaviour of ca. 50 individual *Drosophila*. No magnetic field effect was noticed. ANOVA of the Linear Mixed Effect Model, (Exp. $p = 0.5373$; Cond. $p = 0.7511$; Exp:Cond. $p = 0.1494$). For details see Table 2.13.

ANOVA of the LME CS OX 450 nm						
	Sum Sq	Mean Sq	NumDF	DenDF	F-value	*p*-value
Exposure	3.293	3.2933	1	346.99	0.3813	0.5373
Condition	10.435	3.4783	3	346.99	0.4027	0.7511
Exposure:Condition	46.293	15.4309	3	346.99	1.7866	0.1494

Table 2.13. ANOVA of the LME to compare CS OX flies exposed to different magnetic stimuli (0 µT, 90 µT, 220 µT and 300 µT) and relative shams in presence of blue light. No magnetic field effect was detected

	Exposure	Condition (μT)	*N* flies	ANOVA of the LME		
CS LE 405 nm	Exposed	60*	48		F-value	*p*-value
	Exposed	0	51	Exposure	0.0592	0.8079
	Exposed	30	50	Condition	1.689	0.1864
	Exposed	60	55	Exposure:Condition	0.9332	0.3944
	Exposed	90	54			
	Exposed	300	51			
	Sham	60*	55			
	Sham	0	49			
	Sham	30	52			
	Sham	60	51			
	Sham	90	52			
	Sham	300	49			
CS LE 450 nm	Exposed	0	51		F-value	*p*-value
	Exposed	90	49	Exposure	2.2262	0.1365
	Exposed	220	54	Condition	0.9727	0.4055
	Exposed	300	49	Exposure:Condition	0.807	0.4905
	Sham	0	51			
	Sham	90	51			
	Sham	220	53			
	Sham	300	53			
CS LE 635 nm	Exposed	0	56		F-value	*p*-value
	Exposed	90	53	Exposure	0.5002	0.4798
	Exposed	220	55	Condition	0.4193	0.7393
	Exposed	300	49	Exposure:Condition	0.4956	0.6855
	Sham	0	49			
	Sham	90	50			
	Sham	220	48			
	Sham	300	52			
***pdf*^{01} 450 nm**	Exposed	0	18		F-value	*p*-value
	Exposed	90	19	Exposure	0.2145	0.6439
	Exposed	220	20	Condition	1.4854	0.2206
	Exposed	300	26	Exposure:Condition	0.7235	0.5394
	Sham	0	19			
	Sham	90	20			
	Sham	220	24			
	Sham	300	19			
CS OX 450 nm	Exposed	0	41		F-value	*p*-value
	Exposed	90	49	Exposure	0.3813	0.5373
	Exposed	220	40	Condition	0.4027	0.7511
	Exposed	300	43	Exposure:Condition	1.7866	0.1494
	Sham	0	44			
	Sham	90	46			
	Sham	220	44			
	Sham	300	48			
		Total *N*	**1960**			

*The magnetic field was applied on the *z* axis but with the direction inverted (the field was pointing upwards)

Table 2.14. Summary of all the FlyVac experiments. The Exposure factor indicates the presence or the absence of an external magnetic field (Sham vs Exposed), the Condition factor indicates the intensity of the field to which the flies were exposed. After testing a total of 1960 single flies, independent of the light wavelength, the field intensity and the genotype of the flies tested, there is no factor, or interaction between them, that shows a *p*-value below the 0.05 *p*-level. In conclusion, *Drosophila* negative geotaxis is not disrupted by an external magnetic field.

2.4 Discussion

2.4.1 General discussion

As noticeable from the results reported in the summary Table 2.4, Table 2.5 and Table 2.14 we were not able to elicit a magnetic field effect response in *Drosophila* negative geotaxis. We tested our *Drosophilae* in two different set ups. The first one, the Gravity apparatus, resembled the original one[44], while the second one, the Fly-Vac, was built to greatly improve the original testing conditions. In the Gravity apparatus we first tested the same *Drosophila* line as in the original study, under the same light condition (same wavelength and intensity) but we saw no magnetic field effect, (ANOVA of the LME: Exp. $p = 0.058$; Cond. $p = 0.196$; Exp:Cond. $p = 0.856$). Then, since other studies have reported magnetic field effects in *Drosophila* when exposed to shorter wavelengths[7,47], we tested our flies in UV-blue light (380–450 nm). Again, we saw no magnetic field effect (ANOVA of the LME: Exp. $p = 0.807$; Cond. $p = 0.835$; Exp:Cond. $p = 0.301$). Wondering whether the *absence* of radiofrequency fields (which were shielded by the chamber in which the experiments were run) might have played a role, we reintroduced broadband electromagnetic fields in order to recreate the environment of the laboratories at the University of Leicester in which the original experiments had been performed. Again, we saw no magnetic field effects (ANOVA of the LME: Exp. $p = 0.260$; Cond. $p = 0.794$; Exp:Cond. $p = 0.135$). Finally, we tested all these conditions using another Canton-S line, to check that it was not a genotype-dependent problem. Once more, no magnetic field was detected (ANOVA of the LME: blue light - Exp. $p = 0.072$; Cond. $p = 0.022$; Exp:Cond. $p = 0.405$; UV-blue light - Exp. $p = 0.234$; Cond. $p = 0.411$; Exp:Cond. $p = 0.070$; blue light and RF - Exp. $p = 0.902$; Cond. $p = 0.094$; Exp:Cond. $p = 0.518$). For details, see Tables 2.4 and 2.5.

Importantly, when looking at the overall experiments in the presence of blue light (CS LE 450 nm and CS OX 450 nm), the *p*-values associated with the “exposure” factor are for both

CS LE and CS OX not too far from significance (p = 0.058 and p = 0.072, respectively; for details see Tables 2.15 and 2.16). This could indicate that the presence of an external magnetic field could influence *Drosophila* negative geotaxis. However, as depicted in Figure 2.21, the two *Drosophila* lines present opposite "effects". In the case of CS LE, the magnetic field increased the ability to ascend a tube, while in the case of CS OX it decreased it. Not only is there no real explanation for such contradictory effects, but also the "magnetic field effect" on CS LE is in the opposite direction to that reported in Fedele *et al.*[44]. To summarise, even though the *p*-values associated with the "exposure" factor were close to significance, this did not result in a clear effect on the flies' behaviour. Therefore, we were not able to demonstrate a magnetic field effect on *Drosophila* negative geotaxis while using our Gravity apparatus.

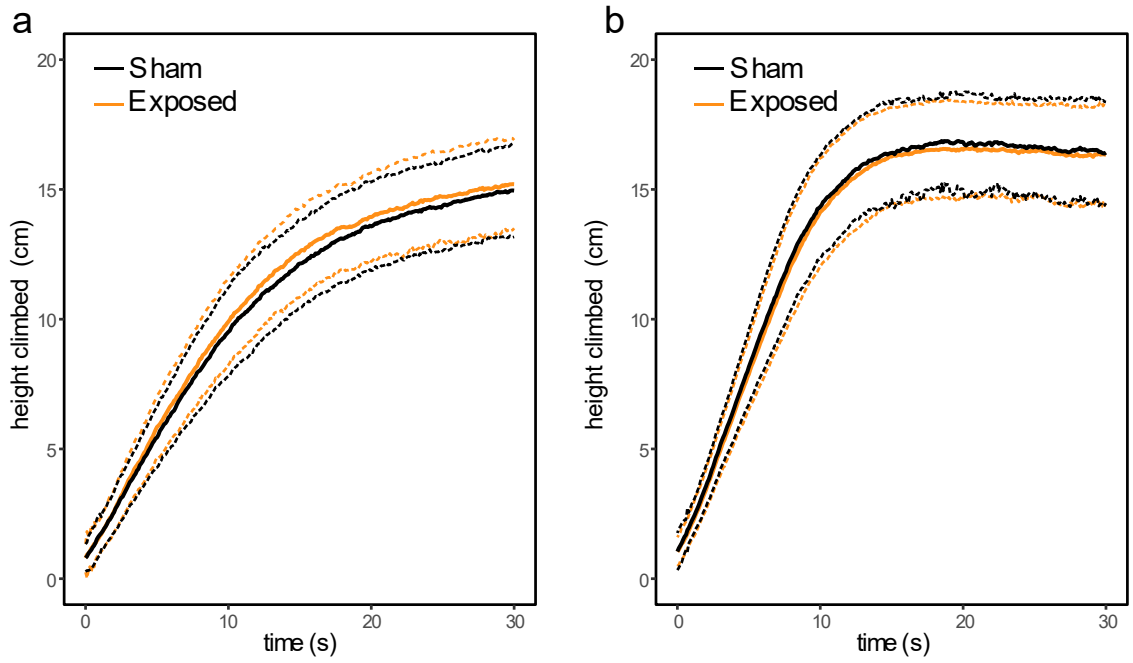


Figure 2.21 Summary of all the Gravity apparatus experiments involving CS LE and CS OX in presence of blue light. **a**. Average position of the CS LE flies over time when exposed to magnetic and sham stimuli. The data represents the flies' behaviour in 120 biological replicas. When considering the overall experiments, the *p*-value associated with the magnetic exposure tantalised close to significance (p = 0.058). However, the supposed magnetic field effect is opposite to the one reported in Fedele *et al*[44]. **b.** Average position of the CS OX flies over time when exposed to magnetic and sham stimuli. The data represents the flies' behaviour in 120 biological replicas. When considering the overall experiments, the *p*-value associated with the magnetic exposure is not too far from significance (p = 0.072). In this scenario, the supposed magnetic field effect is the same as the one reported in literature.

ANOVA of the LME CS LE 450 nm						
	Sum Sq	Mean Sq	NumDF	DenDF	F-value	*p*-value
Exposure	5.711	5.711	1	111.98	3.655	0.058
Condition	7.442	2.481	3	111.98	1.587	0.196
Exposure:Condition	1.208	0.403	3	111.98	0.258	0.856

Table 2.15 Summary of the ANOVA of the LME of the experiments involving Canton-S LE strain in the presence of blue light.

ANOVA of the LME CS OX 450 nm						
	Sum Sq	Mean Sq	NumDF	DenDF	F-value	*p*-value
Exposure	6.332	6.332	1	111.95	3.306	0.072
Condition	19.178	6.393	3	111.95	3.337	0.022
Exposure:Condition	5.630	1.877	3	111.95	0.980	0.405

Table 2.16. Summary of the ANOVA of the LME of the experiments involving Canton-S OX strain in the presence of blue light.

Switching to a single fly experiment did not reveal a magnetic field effect either. Independent of the wavelength, the magnetic field intensity and the genotype used, we were not able to interfere with *Drosophila's* ability to ascend a tube (see Table 2.14). However, we reported strong positive results. As seen in Figure 2.16 a. flies responded differently when exposed to different light spectra. In fact, when exposed to blue (410-490 nm) and UV-blue (380–450 nm) *Drosophilae* climbed faster than when exposed to red light (580–660 nm) (ANOVA of the LME, $p < 0.0001$). This resembles the result reported in Figure 2a in Fedele *et al* [44]. Moreover, as a positive control we compared wild type flies to pdf^{01}, a mutant known to have a negative geotaxis deficiency [104,160]. Again, the positive control gave the expected results, with pdf^{01} climbing less well than the wild type (Figure 2.16 b, ANOVA of the LME, $p < 0.0001$).

Unfortunately, the replication of magnetic field effects has always been challenging in the magnetoreception field. For example, Wiltschko *et al.* [178] claimed that the magnetic compass

of European robins is located in the birds' right eye, while Hein *et al.*[56] reported that birds can perceive magnetic fields using both eyes. What had been thought to be magnetite particles in the upper beak of homing pigeons necessary for their magnetic map [42,45], was later revealed to be clusters of iron-rich macrophages[162]. *Arabidopsis thaliana* hypocotyl growth has been reported to be inhibited when the plant was exposed to a 500 μT static magnetic field[3]. However, when this experiment was replicated independently in a more controlled fashion, no magnetic field effect was reported [54]. The reasons behind this lack of ability of independent replication is somehow difficult to explain without being purely speculative. As humans, we do not perceive magnetic fields (even though some authors claim that we can do it passively [165], or in a gender-blue light-chocolate-dependent manner [20]), so it is hard (if not impossible) to imagine how external cues can affect the perception of such stimuli. While it is relatively easy for us to understand how, for example, light is perceived by an animal, this is not the case with magnetic fields. Therefore, without this previous experience-based knowledge it is hard to build a set-up that is free from artefacts. What might be unimportant to us, might be fundamental for animal perception. An example of that is the presence of broadband time-dependent electromagnetic fields. What for us is nothing more than a tool to propagate a signal and does not affect our daily life, is profoundly disturbing for European robins during their migratory season, causing them to be disoriented[40]. Even though we took maximum care into making our two different set ups as artefact-free as possible, we cannot exclude that we might have introduced some involuntarily. However, we consider this highly unlikely, and we will discuss in the following paragraphs why we think we have performed our experiments in the most optimal way.

2.4.2 Considerations on the set-ups

The Gravity apparatus was built to mimic as closely as possible the original one[44]. Not only that, but we built an improved version compared to the one described in Fedele *et al.*[44]. To produce the magnetic stimuli, instead of using two double-wrapped coils, we used a ca. 2 m × 2 m × 2 m double-wrapped three-dimensional Merritt four-coil system, which provided a much more homogeneous magnetic field[83]. Our experiments were run inside chambers with attenuation factors of 10^5 at 10 kHz and $>10^6$ at frequencies above 150 kHz. This allowed to block time-dependent fields that are known to disrupt bird's orientation, but at the same time allowed the geomagnetic field to penetrate the aluminium shielding without distortion[152]. The

original study[44] does not state that the person running the experiment was unaware of the testing condition. Therefore, it is legitimate to assume that those experiments were run in an unblinded fashion. To overcome the possibility of dealing with unwanted biases we made sure that the experimenter not only was running eight different testing conditions (0 µT, 90 µT, 220 µT, 300 µT and corresponding sham exposures) but that the order in which these were run was randomised by a MATLAB script.

After not being able to replicate the original experiment with a similar set up we decided to improve the testing condition. Therefore, we switched to a single fly experiment which has the advantage of providing robust climbing data that cannot be confused by group effects. To further improve the testing conditions, we fully automated the set-up. In this way the human interaction was reduced to a minimum. Finally, in the original study[44], the only parameter taken in consideration to assess negative geotaxis was dividing the *Drosophilae* in two separate categories (climbers vs non-climbers) based on an arbitrary cut off. Instead we looked at the entire experimental time and analysed the data in different manner. The statistical consideration of Fedele *et al*.[44] is discussed below.

2.4.3 Statistical considerations on Fedele *et al.*[44]

Using the advantage of the video recording and tracking of the flies during the trials (see paragraph 2.7.1 "Video analysis"), we could enhance both the time and the spatial resolution of the climbing behaviour. If animals showed a robust and continuous response to the magnetic stimuli, we would have been able to detect a difference between sham and exposed groups. At the same time this would have avoided unnecessary and artificial categorization of the behavioural response (climbers vs. non-climbers) based on somewhat arbitrary cut-off criteria (minimum height of 15 cm, maximum time of 15 s) that might lead have led to possible pitfalls.

In the previous work, the continuous behaviour response (position of flies) was binarized into two mutually exclusive categories (e.g. flies that climbed above 15 cm in 15 s vs. flies that climbed less than 15 cm in 15 s). Importantly, such a procedure requires bimodally distributed responses to produce robust categories. However, when we looked at the distribution of the flies' position in the tubes at the 15 s time point, we observed no clear bimodality neither in the control group, nor when the flies were exposed to magnetic field (Figure 2.22).

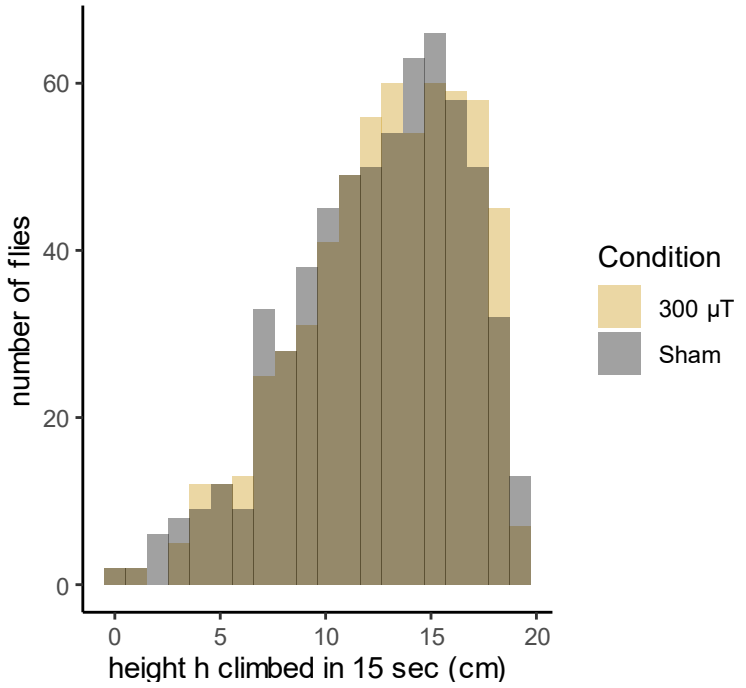


Figure 2.22. The distribution of flies in the tubes at the 15 s time point, when exposed to a "sham" (grey bars) or to a magnetic field stimulus of 300 µT (beige bars). As clearly shown, the distribution is not bimodal, hence there is no justification for a binary division of the data based on climbers vs non-climbers. The histogram is based on the behaviour of 150 flies per condition (Sham and 300 µT) per 5 repeats.

By treating this type of data as proportions one could easily overestimate the actual difference. If ten flies from an experimental group at time point 15 s have climbed (14.6, 15.0, 13.5, 14.5, 16.5, 16.2, 15.4, 14.6, 14.9, 14.4) cm, while another ten flies from a sham group climbed (15.0, 15.9, 15.3, 13.4, 15.9, 15.3, 13.8, 15.2, 15.1, 15.1) cm, in the experimental group we would have 30% of the flies that climbed above 15 cm, while in the sham group it would be 70%. At the same time the average position of the flies in these two groups is virtually the same (mean ± sd: 15.0 ± 0.9 vs 15.0 ± 0.8 in the experimental and sham group respectively).

To overcome this problem one could either increase the number of tested flies per tube, thus minimizing the within-group variance or perform the negative geotaxis experiments with a single fly per tube. The latter has several advantages: it excludes the possible group effect and allows one to precisely track and analyse individual climbing behaviour over time. The FlyVac

set-up was built exactly for this purpose, but still we were not able to see any magnetic field effect. Therefore, we estimated the Fly Vac "sensitivity", by modelling what would have been the minimum detectable difference in the flies' behaviour that was also statistically significant.

To do so, we modelled the climbing curves for the flies assuming that the magnetic field exposure would reduce the climbing speed of the flies as reported in the original study[44]. For each fly, in every trial of the control condition (blue light, "Sham" exposure, Canton-S LE line; total $N = 208$ flies) we calculated the average climbing speed (v) as the difference between its highest and lowest detected position (in cm) divided by 30 s (the duration of one trial). The average speed ± s.d. of the control group resulted to be $v = 0.396 \pm 0.173$ cm/s. To model the effect of the magnetic field, we subtracted either 0.5 cm or 1.0 cm from the highest climbing point for each fly and calculated the adjusted climbing speed. This corresponded to a difference in the speed of 0.016 cm/s (4% of the average speed) and 0.033 cm/s (8% of the average speed), for 0.5 cm and 1.0 cm respectively. According to the adjusted climbing speed we then modelled the climbing curve for each fly and compared the control and the modelled groups using the Linear Mixed Effect model (LME). After the adjustment by 1.0 cm (but not by 0.5 cm), the two groups resulted significantly different from each other (ANOVA of LME: $p = 0.045$). Therefore, if animals showed a robust and continuous response to the magnetic stimuli, we would have been able to detect a difference down to ca. 8% of the average climbing speed between sham and exposed groups (Figure 2.23). This high sensitivity would have allowed us to detect magnetic field effects smaller than the ones originally reported[44].

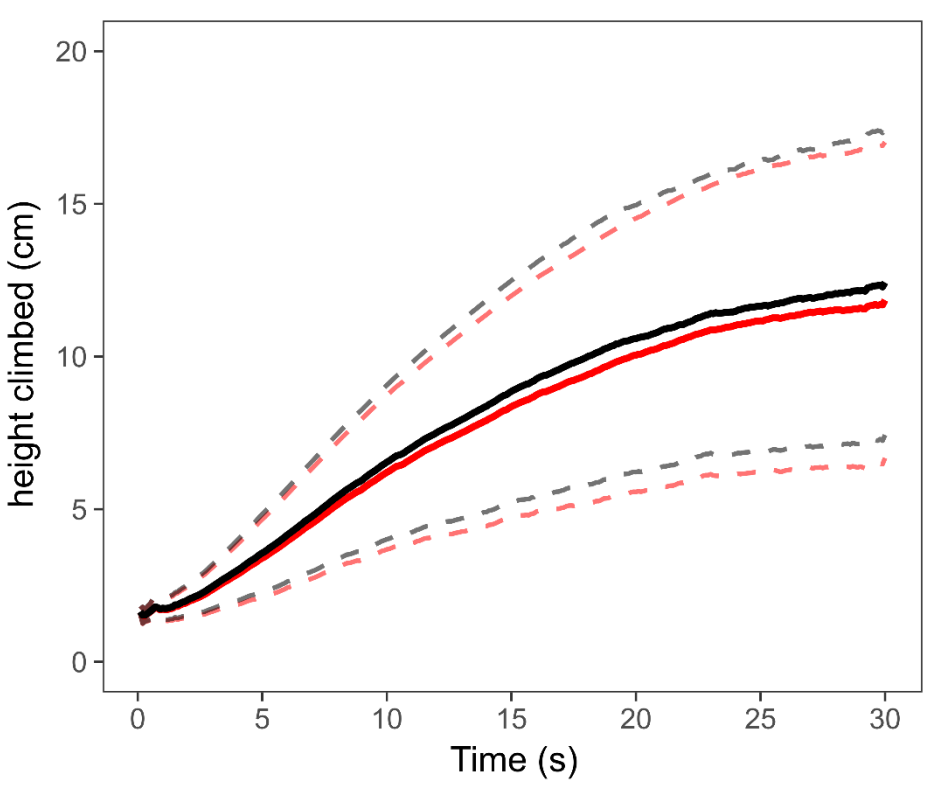


Figure 2.23 Minimal detectable difference between groups in the FlyVac set-up. The black line shows the average climbing speed of 208 Canton-S LE flies tested in blue light in presence of a "sham" stimulus. The red line models what is the minimum detectable difference if a magnetic field would have reduced the ability of the flies to ascend a tube as originally reported[44]. These two groups are significantly different from each other (ANOVA of LME: $p = 0.045$). The actual minimum detectable difference is evaluated as 8% of the average climbing speed. The data are shown as mean ± s.d.

2.4.4 Possible explanations for the lack of positive results

Even though we tried to run our experiments in the most careful and controlled way, there is still the chance that we might have overlooked some possible sources of interferences.

One could argue that we were not able to elicit a magnetic field effect because of the way in which the magnetic stimuli were applied. Due to technical reasons, we were able to produce only a field as high as 300 µT, while using the double-wrapped three-dimensional Merritt four-coil system. In order to produce a field with an intensity of 500 µT it would have been necessary to increase the voltage running though the coils and thus risk serious damage to the set-up. At first glance, this could be an issue. However, the effect of a weak magnetic field on a radical pair should be between linearly and quadratically dependent on the strength of the field. Thus,

the effect of a 300 μT field should be 36-60% of the effect of a 500 μT field, making it unlikely that we would have missed the magnetic sensitivity by using a weaker field. Given that Fedele *et al.*[44] saw a 25% effect at 500 μT, we would have expected a 9-15% effect at 300 μT, an effect we should have been able to detect using our set-up.

Moreover, if we look in the published literature, we can see that there is no "dose-response" relationship between magnetic field intensity and magnetic field effects on different behaviours in *Drosophila*. Bae *et al.*[7] saw an effect on negative geotaxis when fields of 0 μT, 71 μT and 85 μT were applied. Yoshii *et al.*[185] and Fedele *et al.*[43] reported a magnetic field effect on the *Drosophila* circadian rhythm at 300 μT, while Gegear *et al.*[46–48] reported that they were able to train flies to associate a 500 μT magnetic stimulus with a sucrose reward. Wu *et al.*[182] required 1 mT to see an effect on *Drosophila* courtship, while both Marley *et al.*[103] and Giacchello *et al.*[49] needed 100 mT to see an effect on seizure in larvae and to create a magnetically dependent neuronal firing, respectively.

Another difference between our Gravity apparatus experiments and the ones described in Fedele *et al*.[44] is the number of testing replications. In the original work[44], the authors tested the flies every 30 s, five times in a row, waited 15 min and then tested the same individuals another five times. Each *Drosophila* line was tested at least three times independently. On the other hand, while we also tested our flies every 30 s, five times in a row, we omitted the second replication of the experiment after 15 min, and we tested each condition independently 15 times. Thus, we decreased the number of testing repeats on the same individuals (from ten to five), but we increased the overall number of tested individuals (from at least three groups of ten flies, to fifteen groups of ten flies per condition). Increasing the number of tested individuals should not invalidate a testing paradigm. On the contrary, it should result in more statistically relevant datasets.

Moreover, while the authors of the original study[44] tested their flies immediately after switching on the coils and the lights (personal communication, Prof. Charalambos Kyriacou, University of Leicester), we pre-exposed the flies for two minutes to the testing conditions (magnetic field and light exposure). This was done for pragmatic reasons. Since the power supplies of the coils were outside the testing chambers, some time was needed to enter the testing chamber, start the recording of the video and reach the set-up inside the Merritt coils.

In hindsight, however, we might have overlooked a positive control in the Gravity apparatus. We did not validate the testing paradigm using a *Drosophila* line that is known to show an attenuated or increased geotactic response, as we did for the FlyVac set-up. Therefore, without such a control we cannot be absolutely certain that the Gravity apparatus is artefact-free and, ideally, we should repeat these control experiments using pdf^{01}. One could also argue that a better positive control to test for an attenuated geotactic response is a *cry-null* strain. In fact, pdf^{01} flies lack the ability of producing Protein Dispersing Factor (PDF), a neuropeptide that is crucial for the proper functioning of the circadian clock. This means that pdf^{01} flies present an anomalous inner clock which results in arrhythmia[141]. This would not be the case in *cry-null* flies, since, even though they do not express Cryptochrome, they maintain a functional circadian phenotype[33]. Therefore, the use of *cry-null* would be preferred, since one would not have to take in account also the circadian component when dealing with geotaxis experiments.

However, it is important to note that while both the *pdf* and *cry* genes are involved in circadian rhythms and geotaxis, several authors have failed to find circadian variations in the geotaxis score of a Y-maze when testing both wild type *Drosophila* and strains selected for geotaxis[6,24,160]. Therefore, *pdf* and *cry* are pleiotropic genes that regulates circadian clocks and geotaxis, however the relationship between these two different behaviours has still to be determined.

To summarise, while there are differences between our testing paradigm and that employed by Fedele *et al.*[44], these should not have affected the overall final result. Importantly, it was not possible for us to determine exactly what was the cause of the lack of positive results. Even assuming we introduced an artefact in the Gravity apparatus, we should have been able to see a magnetic field effect when the flies were tested singularly in the FlyVac, given its high sensitivity.

Unfortunately, our results are even more at odds when considering that another laboratory[7,125], independently supported and extended the results presented in Fedele *et al.*[44]. In fact, first Bae *et al.*[7] and later Oh *et al.*[125] reported that *Drosophila* negative geotaxis is affected when an external magnetic field is applied and that this behaviour is light and cryptochrome dependent[7]. Moreover, the authors offered an ecological and behavioural explanation for why flies should be able to perceive the geomagnetic field in a natural environment. According to them, flies might get imprinted on the Earth's magnetic field present at birth, and this helps them to recognize locations that are favourable for foraging and reproduction[125]. Importantly, the

Earth's magnetic field increases by ~ 4 nT per km as one moves towards one of the magnetic poles and it has a 25-50 nT diurnal variation. Therefore, the error in geographic location using a magnetic intensity sensor could be as large as 12 km, depending on the time of day. Thus, it could be argued that the flies could get imprinted on a distance scale of 12 km or more. Interestingly, it has been reported that *Drosophila pseudoobscura* can travel up to 10 km across desert terrain in a single night[26,73]. Therefore, the travelling distances reported in *Drosophila* are close to the theoretical maximal geographical error calculated for a magnetic intensity sensor. Thus, the hypothesis formulated by Oh *et al.*[125] on magnetic imprinting in *Drosophila* could be plausible.

Nonetheless, it is interesting to note that the studies performed by Bae *et al.*[7] and Oh *et al.*[125] came to the same conclusions as Fedele *et al.*[44], even though the testing conditions used by the two research groups present major differences. To start with, the testing paradigm used by the Bae *et al.*[7] and Oh *et al.*[125] was different from the one used in Fedele *et al*[44]. In the original study[44], ten flies were tapped to the bottom of a tube and their ability to climb 15 cm in 15 s was evaluated. In the following studies[7,125], ~50 flies were filmed for several minutes and their geotactic positioning inside a tube was measured. The geotactic positioning was estimated by dividing the tube into five imaginary sections and the number of flies in the lowest four sections was divided by the total amount of flies per 100%[7]. Moreover, the original authors[44] only tested male flies (in accordance with the results presented in Phillips & Sayeed[134]), while afterwards, both sexes were used[7,125]. The magnetic field intensities used as stimuli were dramatically different (500 μT[44] and 0 μT – 85 μT[7]) as well as the coils used to produce them (a single pair of Helmholtz coils[44] and 3-axis Helmholtz coils[7]). Finally, the light used as stimulus was different in both spectrum (blue[44] and full spectrum[7]) and intensity (dim, ~0.25 μW/cm^2 [44], and bright, 500 lux[7]). To summarise, our testing conditions (even though not identical) were more similar to those of Fedele *et al.*[44], than the original study was to Bae *et al*[7]. Despite of that, we were not able to determine why we did not manage to see a magnetic field effect. We can conclude by saying that it would be interesting to replicate the testing conditions of Bae *et al.*[7] in the future, and see whether we are able to see a magnetic field effect on *Drosophila* geotaxis.

Finally, another result supporting *Drosophila*'s ability to perceive magnetic fields comes from spectroscopic measurements on purified *Drosophila* cryptochrome. However, even though millitesla magnetic field effects have been observed *in vitro*[153], this is not sufficient proof for

the existence of magnetic sensing in the whole organism. A reproducible behavioural essay in which flies can be affected by external magnetic fields is necessary as well.

In conclusion, we were not able to reproduce the magnetic fields effects on *Drosophila* negative geotaxis that have been reported in the published literature[7,44,125]. Unfortunately, the exact cause of our negative results remains unclear. However, we cannot exclude the possibility that the lack of positive results is that our experiments were much more carefully controlled than those we set out to replicate.

2.5 Conclusions

The inability to elicit a magnetically dependent response in *Drosophila* has been disappointing for us. Originally, we were looking for a broadly reproducible behavioural paradigm to test for radio frequency effect on *Drosophila*, that would have greatly facilitated the search for the exact mechanisms, sensory molecules, genetic basis, and neuronal responses to a magnetic stimulus. The reason behind that is that the same level of knowledge and insight using only night-migratory songbirds would be much more difficult to achieve. In fact, techniques such as gene knock-in and knock-out, RNA interference or CRISPR-Cas9, which are commonly used on *Drosophila*, are not currently possible in any night migratory species, due to the impossibility of breeding such birds in captivity. Initially we choose negative geotaxis as a testing paradigm because this behaviour is an innate one (flies will always tend to go towards the top of a vial) and because the magnetic field effect reported on this behaviour was as high as 25-30% (Fedele *et al*. Figure 2a[44]). Unfortunately, we were not able to see any magnetic field effect on *Drosophila* negative geotaxis even though we took maximum care into building and optimising the two different set-ups, we ran the experiments in a blinded fashion in a meticulously controlled environment, we applied strong statistical tests on a large-scale dataset, and we saw positive results in the control experiments.

Chapter 3

AVIAN CRY1S AS PUTATIVE MAGNETORECEPTORS

3.1 Introduction

For many years, the major challenge in measuring magnetic field effects on avian cryptochromes was due to the difficulty of purifying isolated proteins with a bound cofactor. In fact, without bound FAD, the proteins cannot be light-activated and therefore cannot form magnetically sensitive long-lived radical pairs. Kutta *et al.*[90] argued that vertebrate cryptochromes 1 and 2 have lost their ability to bind a chromophore, raising doubts on whether these proteins can be the actual magnetoreceptors, and thus explaining why it has always been difficult to purify such proteins with an incorporated FAD.

However, Cry1s for years seemed to be the ideal magnetoreceptor candidates (see 1.5.3), and even though one study reported that *Sb*Cry1 was purified with a bound a chromophore, this was never independently repeated[95]. Therefore, we decided to try to express and purify *Er*Cry1a and *Er*Cry1b using a system that has been successful in producing avian Cry4s with bound FAD[140]. Once we had the two purified isoforms, we tested their affinity for FAD using two titration methods: Isothermal Titration Calorimetry (ITC) and Surface Plasmon Resonance (SPR) spectroscopy.

3.1.1 Isothermal Titration Calorimetry (ITC)

ITC is a physical technique that is commonly used to study the binding properties of two compounds, by determining their thermodynamic parameters. An ITC calorimeter is composed by an adiabatic jacket containing two identical cells made of highly conductive and chemically inert material. One cell is filled with buffer or water and acts as a reference cell, while the other is the sample cell containing the tested macromolecules. During an experiment, a ligand is titrated into the sample cell in precisely known quantities by the means of a syringe, causing heat to be released or absorbed (depending on the nature of the reaction). Thermosensitive circuits will detect these changes in heat, and by means of a feedback circuit, the temperature in the reference cell is maintained equal to that in the sample cell[18,23] (Figure 3.1 a).

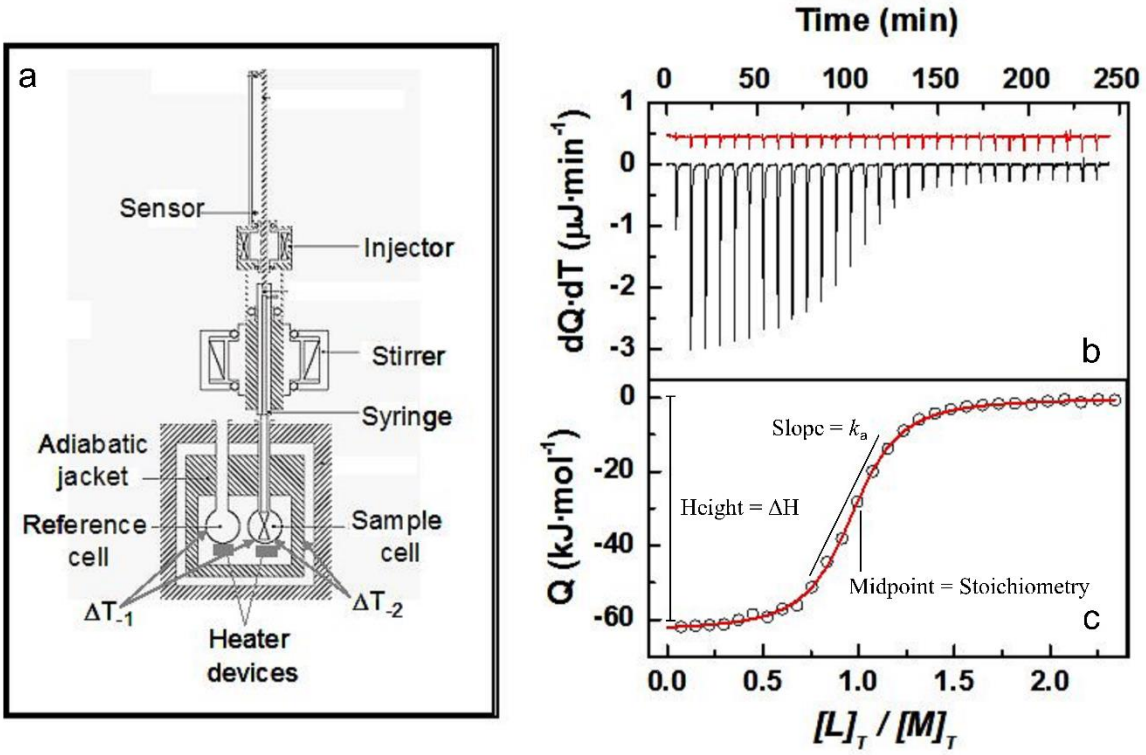


Figure 3.1. ITC calorimeter and data representation. **a**. Schematic of an ITC calorimeter. **b**. The data are plotted as the power needed to maintain the reference and the sample cell at the same temperature over time. Therefore, the raw experimental data look like a series of spikes of heat (with each spike corresponding to one injection of the ligand) over time. Thus, one can calculate the total heat exchanged per injection. **c**. The enthalpy changes (ΔH), binding affinity (k_a), and binding stoichiometry (n) of the reaction under study can be obtained from the heat exchanges as a function of the molar ratio [ligand]/[macromolecule]. Modified from Martinez *et al.*, (2013).

3.1.2 Surface Plasmon Resonance (SPR) spectroscopy

Another technique to measure the affinity between two compounds is SPR spectroscopy. In this technique, a protein of interest is immobilized on the dextran matrix of a sensor chip. The sensor chip is connected to a flow cell that allows buffers and ligands to be injected over the dextran matrix, and thus interact with the immobilised protein. These interactions are monitored via an optical detection unit that can be seen in a sensorgram as an increase or decrease of resonance units (RU) over time (sec), (Figure 3.2).

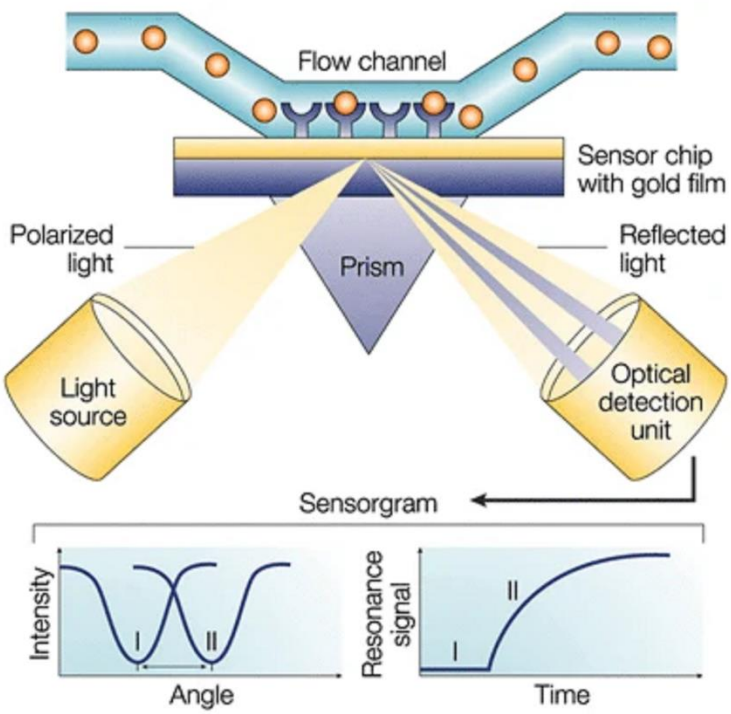


Figure 3.2. Principles of an SPR spectrophotometer. A light source shines polarized monochromatic light through a prism onto a sensor chip. The chip is made of a glass plate, covered with a gold layer which is connected to a dextran matrix. When hitting the glass and gold surfaces the light is reflected, resulting in an excitation of the surface plasmons when the light angle is in resonance with them. The resonance phenomenon is dependent on the refractive index of the medium and it results in a weaker total reflection and a dip in the intensity (I). The refractive index changes and shifts the light angle when there is an interaction between the immobilized protein and a ligand or another protein, resulting in a second intensity dip (II). These dips are reported in a sensorgram as a change of the relative resonance signal. Adapted from Cooper (2002)[25].

3.2 Material and Methods

3.2.1 Cloning procedure

The full-length sequences of *Erithacus rubecula* (European robin) cryptochromes 1a and 1b[15] were cloned from p-Turbo vectors containing the desired sequences. The p-turbo vectors were made previously by Anja Gunther (University of Oldenburg). To clone the inserts in the new vector we followed a standard cloning procedure. The cloning was performed using the Thermo Scientific Phusion High-Fidelity DNA Polymerase kit (Thermo Scientific, MAN0012393), according to the producer guidelines (for details see Table 6.1 and Table 6.2 in the Appendix),

using a Vapo Protect Mastercycler Pro (Eppendorf) thermocycler. The primers' annealing temperature T_m was calculated using the Thermo Fisher T_m calculator. The cloned product was inserted into a reconstructed *p-cold* vector (TAKARA), containing an N-terminus 10× His tag, a multiple cloning site, ampicillin resistance and a *lac* operator. The vector was generously provided by Professor Can Xie (Peking University) and was previously used to successfully express and purify *Columba livia* cryptochrome 4 in *E. coli*[140]. The inserts were sequenced (LGC Genomics) to check for possible mutations. Whether a mutation was present or was added intentionally, the Q5 Site-Directed Mutagenesis Kit (New England Biolabs) was used, as indicated by the producer. This cloning procedure was identical for *Gallus gallus* (chicken) cryptochrome 4[53,105,127], and *Taeniopygia guttata* (zebra finch) cryptochrome 4 (see Chapter 4). A full list of primers used with relative restriction site is given in Table 6.3.

3.2.2 Expression and purification

The general protocol involved the amplification of *E. coli* expressing a recombinant protein, the collection of the *E. coli* cells, their lysis, the purification of the lysate via immobilized metal ion affinity chromatography first and anion exchange chromatography afterwards. For each studied protein there were minor changes in the general protocol. Those changes were due to a trial and error approach that aimed to achieve proteins as pure and with the highest yield as possible.

Recombinant proteins expression in E. coli

The expression and purification of the proteins were done as follows. 50–100 ng of recombinant plasmid was mixed into 50 µL of BL21 *E. coli* cells and let rest for 30 min on ice. A 45 s heat shock at 42 °C and 2 min rest on ice followed. 300 µL LB medium were added to the cells which were then incubated for 45 min at 37 °C and 220 rpm. 100-150 µL of the cell culture were added to an agarose plate containing 100 µg/mL ampicillin. The plate was incubated overnight at 37 °C.

A single colony was picked from the overnight plate and amplified in 30 mL LB medium containing 100 µg/mL ampicillin for 6-7 h at 37 °C and 220 rpm. The *E. coli* culture was transferred into 700 mL LB medium (containing 100 µg/mL ampicillin) and incubated at 37 °C and 200 rpm for 1-1.5 h into an Innova 40 (New Brunswick) incubator. As soon as the OD600

reached ~0.5 the temperature needed to be cooled down to 15 °C and the speed reduced to 160 rpm. The OD600 was measured using a BioPhotometer Plus (Eppendorf) spectrophotometer. After 25-30 min the OD600 would have reached ~0.9–1.0. When this parameter was reached, an extra 500 µL 100 µg/mL ampicillin per 700 mL LB medium was added. Then, we induced the protein expression using IPTG (isopropyl β-D-1-thiogalactopyranoside) at a final working concentration that varied depending on which protein was expressed. Table 6.4 summarises the different IPTG concentrations used. The *E. coli* culture was kept at 15 °C and 160 rpm for 20-24 h.

The cells were harvested using an Avanti J-e (Beckman Coulter) centrifuge (Rotor JLA-10.5) at 7000 rpm for 7 min. The supernatant was discarded, and the pellet was resuspended in 15-20 mL Binding buffer (20 mM Tris, 150 mM NaCl, 5 mM Imidazole, pH 8.0) for 700 mL of cell culture. The suspension was centrifuged into a Centrifuge 5804 R (Eppendorf) at 7000 rpm and 4 °C for 10 min. The supernatant was discarded, and the pellet was stored at –20 °C until further purification.

Affinity chromatography

The frozen pellet was thawed into room temperature water until it was completely defrosted. The pellet was resuspended in 10 mL Binding buffer, per 700 mL cell culture. One protease cocktail inhibitor tablet (cOmplete™, Mini, EDTA-free Protease Inhibitor Cocktail, Roche) was dissolved into 2100 mL cell culture. The solution was poured into a metal container which was placed into a mixture of ice and water. The cells were lysed via sonication (Hielscher UP 200 Ht), using the following parameters: power 170 W, amplitude 75%, 7 mm sonotrode, 40-50 cycles (with 4-s sonication, 8-s break) per 700 mL cell culture. The resulting solution was centrifuged (Avanti J-e, Beckman Coulter) using a JLA-25.5 rotor at 17,000 rpm and 4 °C for 40 min.

The lysate was loaded onto a nickel affinity chromatography column that allowed the separation of the proteins based on the affinity between the His-tag and nickel ions. Before adding the lysate, the Ni-NTA agarose column (Qiagen) was placed at 4 °C and was equilibrated with 12-15 CV of Binding buffer (1 CV = 1 Column Volume = 2.5 mL). The lysate flowed through the column by gravity. The agarose column was then washed with 50-60 CV of Washing Buffer (20 mM Tris, 150 mM NaCl, 20 mM Imidazole, pH 8.0), until it was not possible to quantify the protein concentration of the elute by the means of a spectrophotometer

(BioDrop Duo, SERVA). The final elution was achieved by adding 3-4 CV of Elution Buffer (20 mM Tris, 150 mM NaCl, 300 mM Imidazole, pH 8.0). On average around 3-4 mg of protein mixture was eluted per 700 mL of initial cell culture. The elution fraction was preserved and used for the next purification steps.

These expression and purification steps were common to all studied cryptochromes. The next steps varied between proteins.

ErCry1a and ErCry1b anion exchange chromatography

The elution fraction from the affinity chromatography was concentrated using a spin column (Amicon Ultra 30 kDa, Merck) to a final volume of 2 mL. The solution was loaded into a desalting column (PD-10 Desalting Column, GE Healthcare) and eluted using 3.5 mL of Buffer A (20 mM Tris, 50 mM NaCl, pH 9.1). The buffer exchange steps were done at 4 °C. The protein was further concentrated with a spin column to 2 mL and then centrifuged at 13,000 rpm and 4 °C for 10 min. The supernatant was collected with the help of a syringe and loaded into the Fast Protein Liquid Chromatography instrument (Akta Pure, GE Healthcare).

The proteins were loaded via a syringe into a 5 mm loop that was previously equilibrated using 10 mL of Buffer A. The proteins were then loaded into a HiTrap Q HP 5 mL column that was previously equilibrated using 50 mL of Buffer A. The proteins were eluted following a 20 CV (1 CV = 5 mL) linear gradient up to 500 mM NaCl. Both *Er*Cry 1a and 1b were eluted in the first elution peak (Figure 6.1 and 6.2). Table 6.5 summarises all the buffers used.

3.2.3 SDS – PAGE and Western Blot

The samples were run on SDS PAGE and on Western Blot. The SDS PAGE was run on a 12% acrylamide gel to check the purity of the samples and to validate the results. For each step of the expression and purification procedure, fractions were collected and loaded into a 5× Loading Dye. The samples were heated at 95 °C for 5 min and then centrifuged at 13,000 rpm for 5 min. The fractions were loaded into the gel which was run at 190 V for 50-60 min. The gel was stained with Coomassie Blue overnight and washed with a de-staining solution the next morning.

The Western Blot was run using a standard protocol. The SDS PAGE gel was run as described above. The proteins were transferred onto a nitrocellulose membrane (GE Healthcare). The transfer was done by applying a 350 mA current for 60 min at room temperature. To check the success of the transfer the membrane was soaked into Ponceau S for a few minutes. The membrane was then washed with TBS-T (1× TBS with 0.1% Tween 20) until Ponceau S was completely washed away. The membrane was blocked with a 5% milk TBS-T solution for at least 30 min at room temperature. The primary antibody used was diluted into a 5% milk TBS-T solution and applied to the membrane for an overnight incubation at 4 °C. After the overnight incubation the primary antibody was removed via three 15-min TBS-T washes. Afterwards, the secondary antibody (diluted in a 5% milk TBS-T solution) was applied to the membrane and incubated for 1 h at room temperature. The secondary antibody was washed by three 5-min TBS-T washes. The signal was obtained by chemiluminescence (SuperSignal West Pico PLUS Chemiluminescent, ThermoFisher) and analysed by the means of a I Bright CL 1000 (Invitrogen) imaging system.

For more details regarding the composition of the acrylamide gel, buffers and antibodies used, see Tables 6.7 and 6.8.

3.2.4 UV-Vis and Circular Dichroism (CD) spectroscopy

To check the proteins' absorption, we measured it on a Cary60 UV-Vis (Agilent Technologies) UV-Vis spectrometer. The proteins were loaded into a 1 cm path length quartz cuvette. For each measurement a zero/baseline was calculated, and the proteins were blanked against their own buffer. The secondary structure of *Er*Cry1a and 1b was checked via CD spectroscopy. These measurements were run in the Chemistry Research Laboratory at the University of Oxford.

3.2.5 Isothermal Titration Calorimetry (ITC)

ITC experiments on *Er*Cry 1a and 1b were performed on a VP-ITC microcalorimeter (MicroCal Northampton). To avoid a possible buffer mismatch, *Er*Cry1a and 1b and FAD were diluted in the same buffer (20 mM HEPES, 150 mM NaCl, pH 7.4). The buffer was filtered (0.22 μm) and degassed twice before use. The buffer exchange was achieved by means of a

PD-10 desalting column. The proteins were titrated at a concentration of 10 µM (which was estimated via a Bradford assay) against 5 µL injection of 100 µM FAD, at 25 °C. In total 50 injections were made. The experiment was run three times independently. A reference titration was performed between FAD and the buffer and it was subtracted from each experiment to correct for the heat of dilution. Each titration was analysed by a one-site binding model implemented by Origin (MicroCal).

3.2.6 Surface Plasmon Resonance spectroscopy (SPR)

Experiments were run on a Biacore3000 surface plasmon resonance instrument (GE Healthcare). The proteins (*Er*Cry1a and 1b) were immobilised on a CM5 sensor chip (GE Healthcare) in a two-step process. First, a commercially available anti-His tag antibody was immobilised on the chip via an amine coupling, a process that allows the N-terminus and each lysine residue to be bound to the dextran matrix. Then, *Er*Cry1a or 1b was immobilised on the antibody via a His-tag present at the N-terminus of the proteins. The amine coupling was achieved by injecting the flow cell at a flow rate of 5 µL/min with a solution containing equal parts of 50 mM *N*-hydroxysuccinimide (NHS) and 200 mM *N*-ethyl-*N*'-(dimethylaminopropyl)-carbodiimide (EDC) for a total volume of 35 µL. This allowed to activate the carboxy groups at the sensor chip surface. Then the anti-His tag antibody (at the concentration of 10 µg/mL) was injected over the flow cell at a flow rate of 5 µL/min. The surface of the chip was blocked to deactivate the remaining activated carboxy groups by an injection of 50 µL of 10 mM ethanolamine hydrochloride-NaOH pH 8.5, in order to avoid further unspecific binding to the sensor chip (Figure 3.3). After that, *Er*Cry 1a and 1b were injected into separate flow cells at a concentration of 10 µg/mL and with a flow rate of 5 µL/min (Figure 3.4). For every experiment, a control flow cell was prepared, by activating the surface and deactivating it without immobilizing any protein. The signal from the control flow cell was subtracted from the sample flow cell to avoid unspecific binding signals and an effect of the buffer. As in the ITC experiment, the two *Er*Cry1 isoforms and FAD were dissolved into 20 mM HEPES, 150 mM NaCl, pH 7.4. The proteins were titrated against 15 injections of FAD at increasing concentrations (1 nM, 30 nM, 100 nM, 500 nM, 1 µM, 3 µM, 7.5, µM, 10 µM, 16 µM, 30 µM, 50 µM, 100 µM, 500 µM, 1 mM, 2 mM).

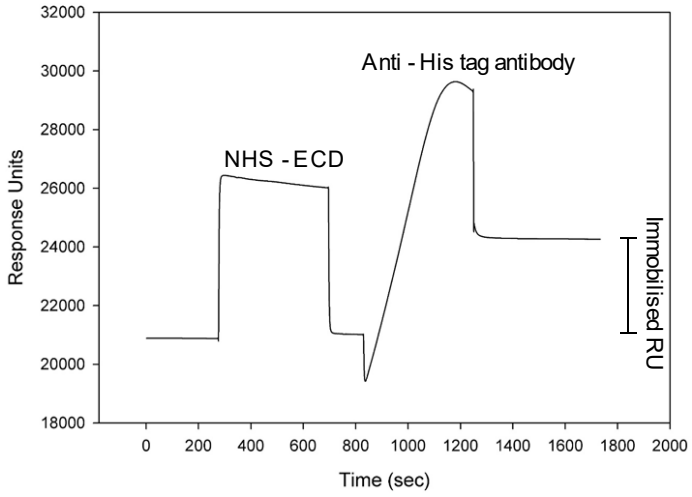


Figure 3.3. Amine coupling of the anti-His tag antibody onto the CM5 SPR chip. The amine coupling was recorded on a sensogram with the relative response signal (RU) as a function of time (s). The first peak shows the activation of the chip via a 1:1 mixture of NHS (*N*-hydroxysuccinimide) and ECD (*N*-ethyl-*N*'-(dimethylaminopropyl)-carbodiimide). The second peak shows the binding of the commercially available anti-His tag antibody. The difference between the two peaks (Immobilised RU) gives and estimation of how much protein was successfully bound to the sensor chip (an increase 1000 RU equals to 1 ng/mm^2 of protein that was immobilised to the sensor chip[25]).

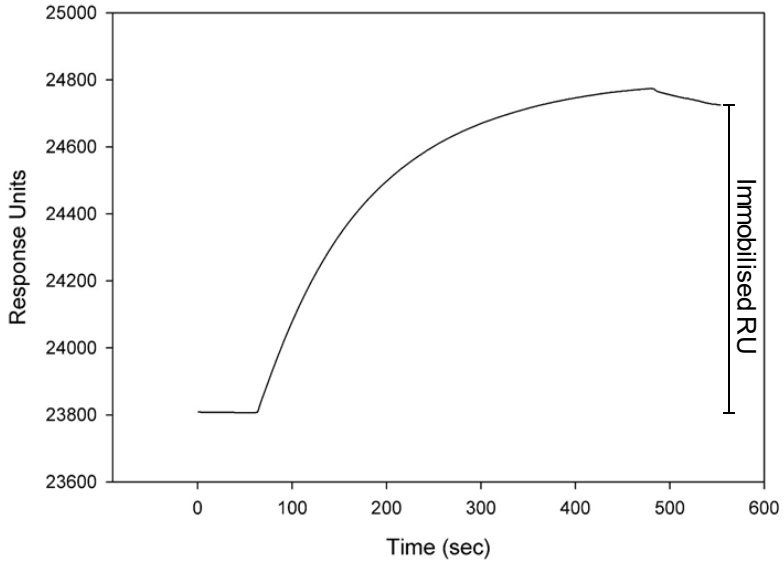


Figure 3.4. *ErCry*1a coupling with the anti-His tag antibody. The signal was recorded on a sensorgram with the relative response signal (RU) as a function of time (s).

3.3 Results

3.3.1 *Er*Cry1a - Characterisation of the protein

The protein was characterised both via SDS PAGE and Western blot (Figure 3.5). Interestingly, the protein was present in two forms, the full one and one that has a truncation of the C-terminus. This truncation is somehow hard to explain since a protease inhibitor cocktail tablet was added during the purification steps.

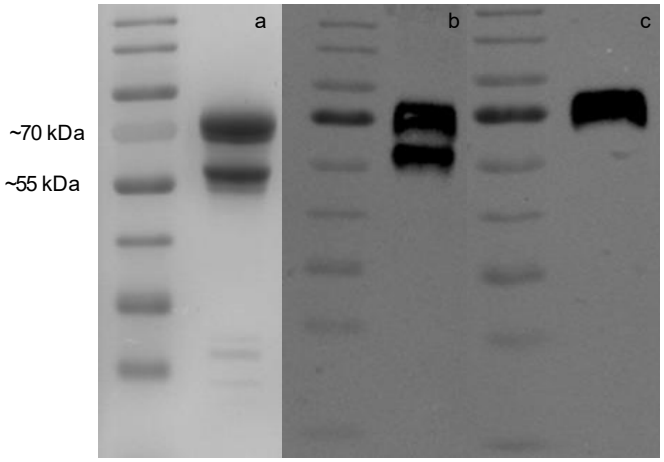


Figure 3.5. Coomassie-stained 10% SDS PAGE gel of *Er*Cry1a and Western Blots **a**. The two forms in which *Er*Cry 1a is present after the purification. The upper band at ~70 kDa is the expected one (theoretical MW = 72,018.77 Da), the lower one at ~60 kDa indicates that there has been a truncation of the C-terminus. **b** and **c**. Western Blot against the N-terminus (b) and the C-terminus of the proteins (c). The epitopes of the antibodies recognised amino acids 179-191 and amino acids 600-619, respectively.

When *Er*Cry1a was concentrated using a spin column (Amicon Ultra 30 kDa, Merck), the result was colourless, a clear indication that no chromophore was bound. This was confirmed by checking the protein absorption via UV-Vis spectroscopy. As clearly seen from Figure 3.6, *Er*Cry1a did not show the classic FAD spectrum in the visible range. Further CD spectroscopy measurement in the UV range showed an expected spectrum, indicating that the protein was well-folded.

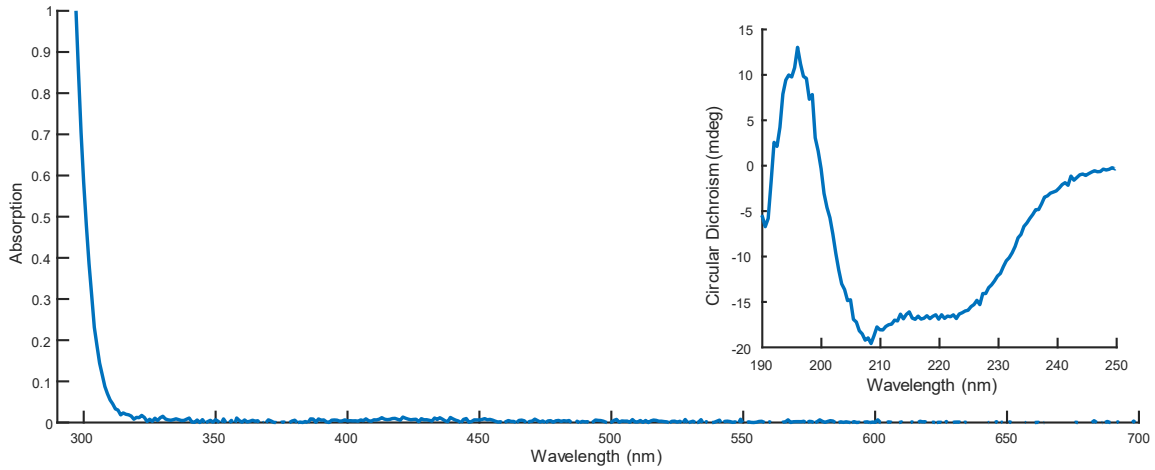


Figure 3.6. UV-Vis and circular dichroism absorption of *Er*Cry1a. The UV-visible absorption spectrum (main panel) shows no absorption in the visible range, indicating the lack of a bound chromophore. The protein was in a 20 mM Tris, 80 mM NaCl, 20% glycerol pH 9.1 buffer. The CD spectrum (inset) indicates that the secondary structure of the protein is correctly folded. For the CD spectroscopy, the protein was in a 10 mM phosphate buffer, pH 8.0.

3.3.2 *Er*Cry1a - Isothermal Titration Calorimetry

We tested the binding affinity of *ErCry*1a and FAD using ITC. The protein was titrated at a concentration of 10 µM against 5 µL injection of 100 µM FAD, at 25 °C. In total 50 injections were made. Figure 3.7 shows that no titration curve was calculated, indicating a low to null affinity between *ErCry* 1a and FAD.

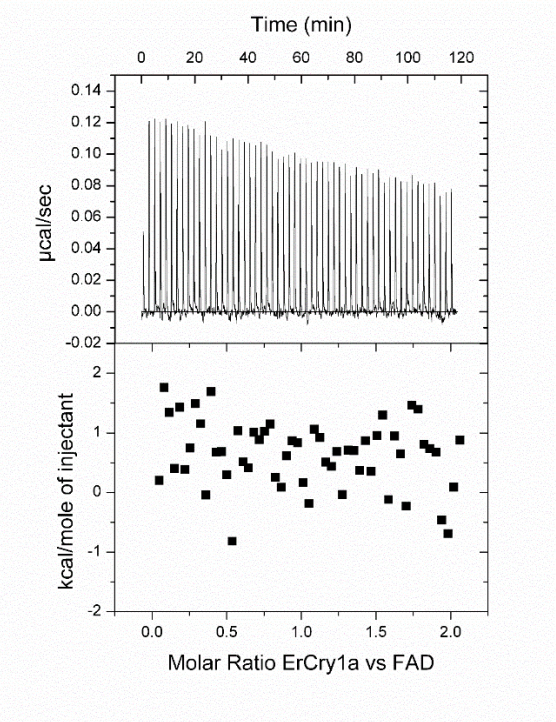


Figure 3.7. ITC results on the titration of FAD against *Er*Cry1a. The upper plot shows the heat absorption over time per injection. Each peak show one injection of 5 µL of 100 µM FAD. The lower graph plots the amount of energy released per molar ratio of *Er*Cry1a against FAD. As noticeable, no titration curve was calculated. The heat signal decreases over time because the samples get more diluted with each injection. The data were subtracted from a control experiment (FAD against the buffer).

3.3.3 *Er*Cry1a - Surface Plasmon Resonance

To confirm the ITC results, we titrated *Er*Cry1a against 15 injections of FAD at increasing concentrations (1 nM, 30 nM, 100 nM, 500 nM, 1 µM, 3 µM, 7.5, µM, 10 µM, 16 µM, 30 µM, 50 µM, 100 µM, 500 µM, 1 mM, 2 mM) using SPR. Again, as shown in Figure 3.8 no binding curve was calculated, again indicating little to no affinity between the protein and the chromophore.

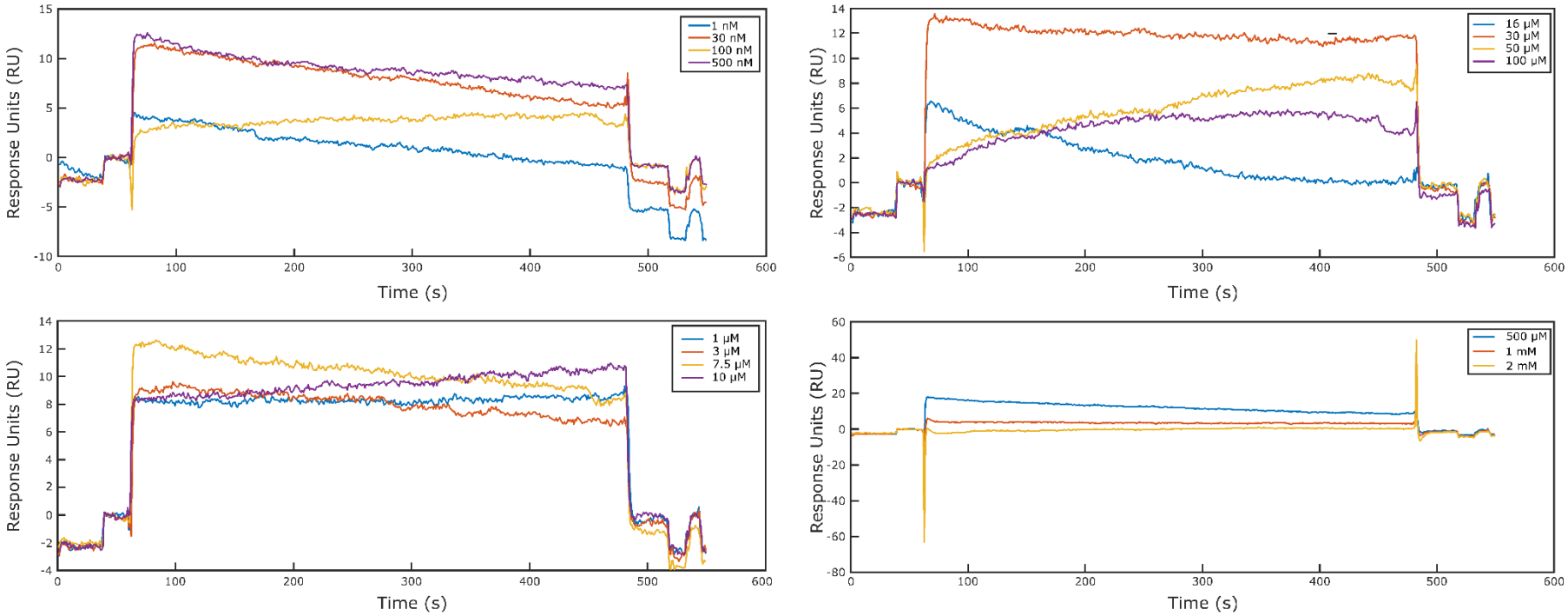


Figure 3.8. SPR results for the titration of FAD against *Er*Cry1a. The signal was recorded on a sensorgram with the relative response signal (RU) as a function of time (s). The four graphs show the responses of the 15 injections with increasing concentration of FAD. Noticeably the RU responses are minimal (most likely due to the small size of FAD) and none of them show any binding to the protein. If there were any binding

between the protein and FAD, we would have expected a curve similar to the one in Figure 3.4. The signal was subtracted from a control cell in which FAD was titrated against the buffer.

3.3.4 *Er*Cry1b - Characterisation of the protein

The same procedure was done for *ErCry*1b. The protein was first characterised both via SDS PAGE and Western blot (Figure 3.9).

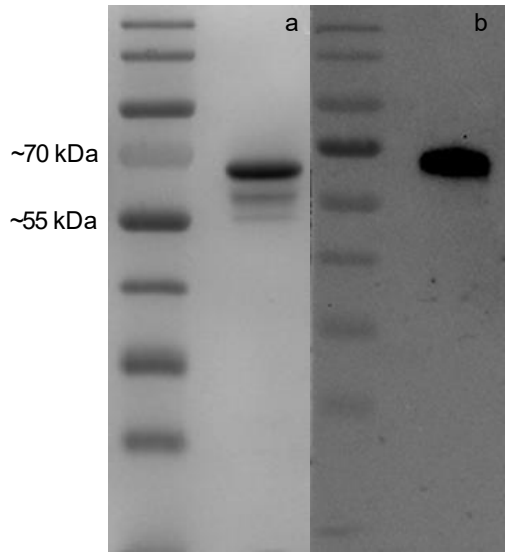


Figure 3.9. a. Coomassie-stained 10% SDS page gel of *Er*Cry1b. The band appears at the expected size (theoretical MW 68,437.07 Da). **b**. Identification of the protein via Western Blot. The antibody recognised the amino acid in positions 570-587.

Once more, after being concentrated, the protein was colourless, a clear indication that no chromophore was bound. Again, the protein absorbance was checked both via UV-Vis and CD spectroscopy (Figure 3.10). As expected, the protein did not absorb in the visible range and thus the presence of bound FAD was excluded. The CD spectroscopy did not reveal any anomalies in the secondary structure of the protein indicating that *ErCry*1b appeared to be well-folded.

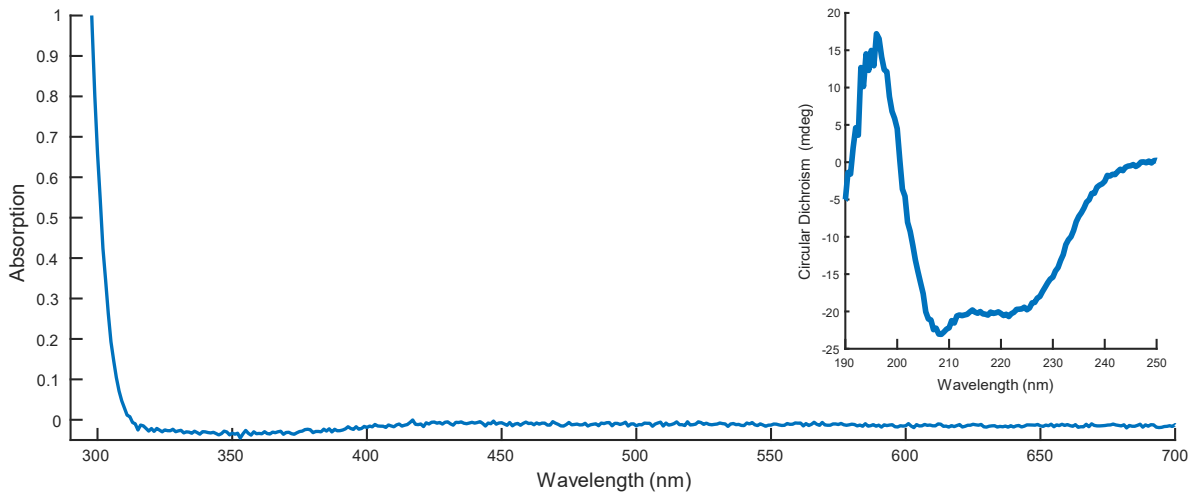


Figure 3.10. UV-Vis and circular dichroism absorption of *Er*Cry1b. The UV-visible absorption spectrum shows no absorption in the visible range, indicating the lack of a bound chromophore. The protein was in a 20 mM Tris, 80 mM NaCl, 20% glycerol pH 9.1 buffer. The CD spectrum indicates that the secondary structure of the protein should be correctly folded. For the CD spectroscopy, the protein was in a 10 mM phosphate buffer, pH 8.0.

3.3.5 *Er*Cry1b - Isothermal Titration Calorimetry

Identical titration experiments were done to test whether there is any binding affinity between *Er*Cry1b and FAD. Once more, no titration curve was calculated, indicating no binding affinity between the protein and the chromophore (Figure 3.11).

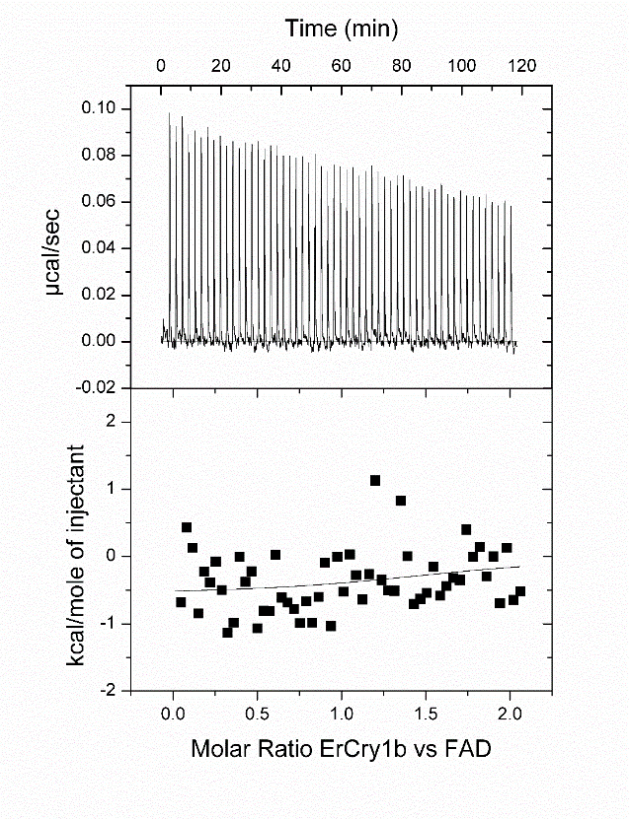


Figure 3.11. ITC results for the titration of FAD against *Er*Cry1b. The upper plot shows the heat absorption over time per injection. Each peak show one injection of 5 µL of 100 µM FAD. The lower graph plots the amount of energy release per molar ratio of *Er*Cry1b against FAD. As noticeable, no titration curve was calculated. The heat signal decreases over time because the samples get more diluted with each injection. The data were subtracted from a control experiment (FAD against the buffer).

3.3.6 *Er*Cry1b - Surface Plasmon Resonance

To confirm our previous findings, we also tested the binding affinity between *Er*Cry1b and FAD. The experiment was identical to the one on *ErCry*1a. The results followed as expected: once more, no binding curve was calculated (Figure 3.12).

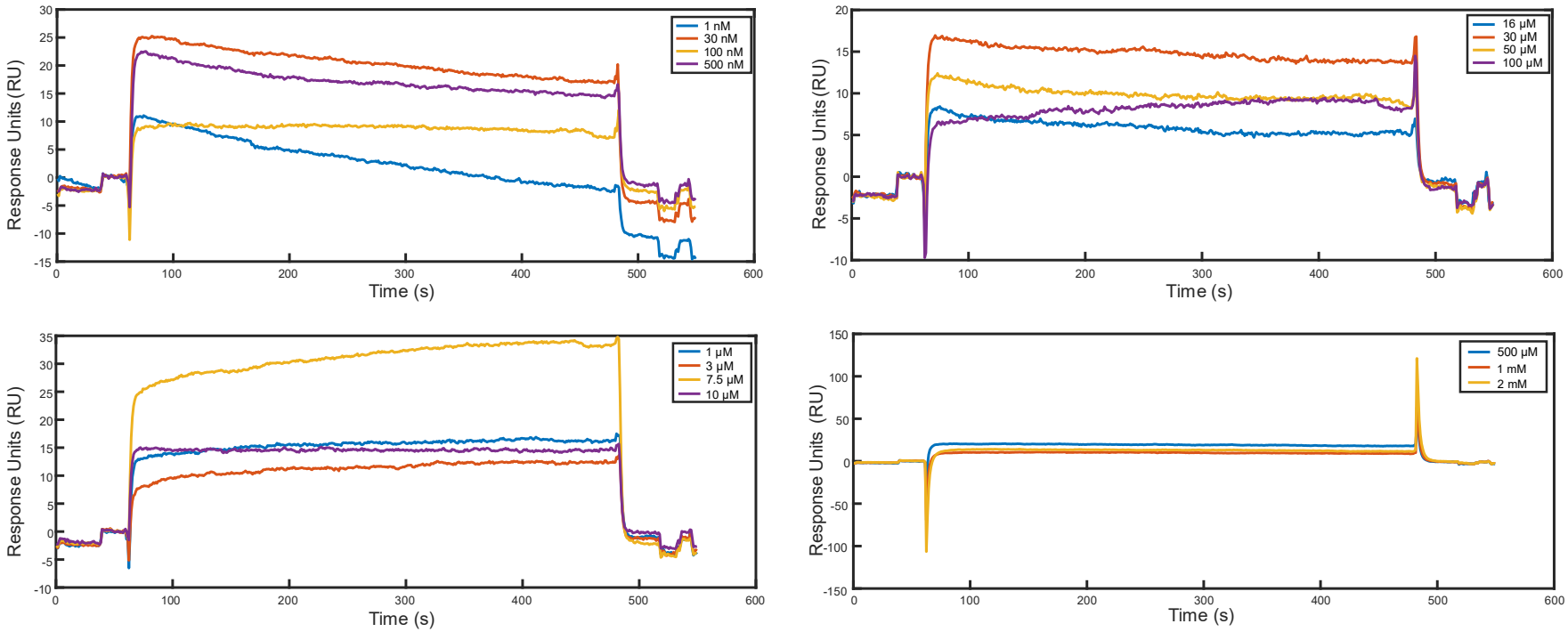


Figure 3.12. Titration of FAD against *Er*Cry1b. The signal was recorded on a sensorgram with the relative response signal (RU) as a function of time (s). The four graphs show the responses of the 15 injections with increasing concentration of FAD. Noticeably the RU responses are minimal (most likely due to the small size of FAD) and none of them show any binding to the protein. The signal was subtracted from a control cell in which FAD was titrated against the buffer.

3.4 Discussion

For many years vertebrate cryptochromes 1 and 2 have been described as difficult to express and isolate with bound FAD[28,95,126]. A possible explanation for this phenomenon was given by Kutta *et al.*[90]. In their study, they proposed that these proteins can be considered to be vestigial flavoproteins which have lost the ability to bind FAD, due to amino acid changes in the PHR domain[90] (for details see Chapter 1.5.1). One of the major consequences of this study in the magnetoreception field was that proteins that have been proposed for years to be "the putative magnetoreceptor[15,95]" (namely Cry 1a and 1b) could have not been. In fact, a *condicio sine qua non* for a protein to be considered as a candidate protein compass is the ability to bind a chromophore that can be light activated. Without the photoexcitation, the protein cannot form magnetically sensitive radical pairs[67]. However, Cry1a was considered for years as the ideal candidate because it was expressed only in the UV cones of chicken and European robins[119]. The localisation of the protein in that region of the retina would have matched the light-dependent magnetic orientation reported in behavioural experiments (birds orient well only when exposed to wavelengths in the range 400-565 nm[171,177]). On the other hand, Cry1b is mainly expressed in the ganglion cell layer[15,121]. Moreover, immunohistochemical studies of the birds' retina, reported a light-driven conformational change in *Gg*Cry1a[120,122,170]. This would suggest that Cry1s would bind FAD *in vivo* and that the lack of a bound chromophore in isolated proteins, would be due to a purification artefact (i.e. protein misfolding). This idea is supported by a study reporting that human Cry1 undergoes flavin reduction *in vivo* when expressed in insect cells[65]. Furthermore, one study reported that *Sylvia borin* Cry1a was successfully purified with bound FAD and when photoexcited could form FAD-Trp radicals with millisecond lifetimes[95]. Another study also reported successful expression and purification of *Columba livia* Cry1a with bound FAD[186].

Our results agree with the thesis proposed by Kutta *et al.*[90] and reject the hypothesis that *Er*Cry1a and 1b are putative magnetoreceptors. We expressed, isolated and characterised both protein isoforms and showed that they do not bind a chromophore. CD spectroscopy in the UV region showed normal spectra and this is an indication of a well-folded protein. Two different titration methods (ITC and SPR) gave the same result, indicating low to null affinity between Cry1s and FAD. Moreover, with our expression and purification protocol, we managed to successfully purify avian cryptochrome 4s with bound FAD from different species (*Er*Cry4, *Cl*Cry4[140], *Gg*Cry4, *Tg*Cry4, see Chapter 4). Therefore, the lack of a Cry1 with bound FAD

cannot be due to our expression and purification protocols. However, it has been proposed that Cry1s can bind FAD *in vivo* due to the presence of a binding partner that can increase the affinity between the protein and the chromophore[65]. Unfortunately, the authors did not clarify how such a mechanism would exactly work and did not indicate a candidate interaction partner that could support their hypothesis. With our current knowledge it is not possible to confirm or refute this hypothesis.

Independent replication from Yogarany Chelliah (UT Southwestern Medical Centre, Joseph Takashi's lab) seemed to confirm our results. The protein crystals showed that the FAD binding pocket is lacking in *ErCry*1a and 1b, making it impossible for these isoforms to bind FAD (personal communication). Moreover, molecular dynamics simulations run by Emil Sjulstok Rasmussen (University of Southern Denmark, Ilia Solov'yov's lab) showed that both *mm*Cry1 (*Mus musculus*, the house mouse) and *Er*Cry1 have a lower ability to bind FAD compared to cryptochromes that are known to be flavoproteins such as *At*Cry1, *Dm*Cry and *Er*Cry4 (personal communication).

Taking these results together, we highly doubt that Cry1s are the possible magnetoreceptors. The function of these proteins remains unknown; however, we can speculate that they might participate in the light-independent regulation of the avian circadian clock, since the proteins have a circadian expression pattern[53] and this is the function of the other known vertebrate Cry1s[158].

3.4.1 Considerations on the published results on Cry1s

As stated before, for a long time avian Cry1s have been considered as the number one candidate magnetoreceptor. However, all the evidence supporting this thesis is circumstantial (such as their expression in the UV cones[119]), or not independently replicated (such as the immunohistochemical results[120,122,123]), or both. Even though two studies reported that avian Cry1s can be purified with a bound chromophore[95,186], they both present major critical problems. The study reporting that *Cl*Cry1a can bind FAD unfortunately lacks hard supporting evidence. The authors only presented a photograph of a bright yellow Eppendorf tube as proof of being able to express the protein with a bound chromophore (Figure 3.13). This is not compelling evidence and without further spectroscopic measurements (such as UV-Vis) that can show the actual binding of the chromophore, it is not possible to determine whether the

yellow colour of the solution was due to free FAD present in the solution or if the *Cl*Cry1a indeed was purified with a bound chromophore.

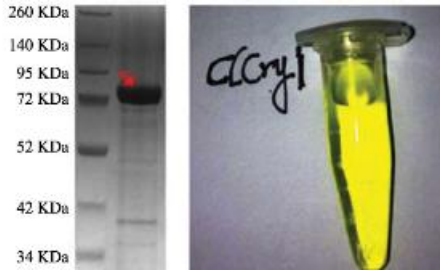


Figure 3.13. Online image preview of "Efficient expression and purification of Cryptochrome1 from *Columbia livia* in *E. coli*" [186]. While the Eppendorf tube presents a bright yellow colour typical of fully oxidised FAD, this is no proof that the chromophore is bound to the protein. The same colour can be obtained by having free FAD present in the solution.

On the other hand, Liedvogel *et al.*[95] reported that they were able to express and isolate *Sylvia borin* Cry1a with bound FAD. The reported absorption spectrum of the protein did not show the characteristic vibrational fine structure around 450 nm, making *Sb*Cry1 a unique protein among all known FAD-binding cryptochromes. In fact, the shape of the spectra resembled more that of free FAD compared to the one of bound FAD (Figure 3.14)

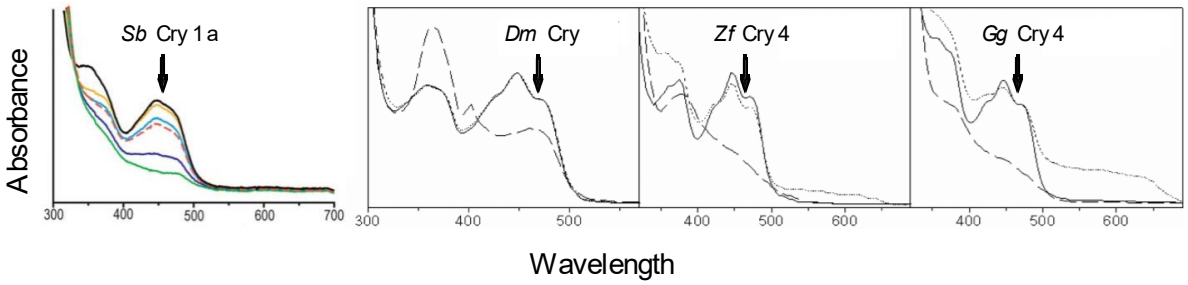


Figure 3.14. Published absorption spectra of different cryptochromes. *Sb*Cry1a is the only cryptochrome that does not show the pronounced shoulder of the vibrational fine structure at 450 nm, which is present in both invertebrate Cry1 (*Drosophila melanogaster*) and vertebrate Cry4 (zebra fish and *Gallus gallus*). Even though a hint of a shoulder at 450 nm is present, the shape of *SbCry*1a resembles more that of a non-specific interaction between FAD and Cry, rather than the shape of a bound chromophore. Images adapted from Liedvogel *et al.*[95] and Otzurk *et al.*[127]

The authors stated that the NMR measurement run on the sample did not reveal any free flavin, meaning that FAD was bound to the protein. However, how was it possible that FAD was

bound to *Sb*Cry1 without showing a very pronounced vibrational fine structures at 450 nm? The explanation for such an odd phenomenon might rely on the purification protocol. The protein was tagged with a 6× His tag and loaded into an IMAC column. It was denatured by a linear gradient (0 M to 6 M) of urea in 20 mM HEPES buffer containing 50 µM FAD. The protein was then renatured by an opposite linear gradient from 6 M to 0 M urea in the same buffer, and finally eluted by increasing imidazole concentration[95]. Given the high concentration of FAD used, (the intracellular concentration of free FAD present in human *HeLa* cells is estimated to be between 100 nM and 3 µM[183]), there might have been the chance that some FAD could have been "trapped" inside the refolded protein. This speculation is motivated by the fact that the main author of the study was able to produce only a single sample and never obtained the protein with bound FAD again (personal communication, Prof. Henrik Mouritsen).

Moreover, a private company (Planet Biotechnology, https://www.planetbiotechnology.com/) tried to replicate the purification method, but they failed to do so (personal communication, Prof. Peter Hore). We can speculate that, for (un)lucky reasons that are unrepeatable, the protein could have been in a thermodynamically unfavourable situation in which the FAD would have appeared to be bound. This would both explain why it was never repeated by the original author of the study (personal communication, Prof. Henrik Mouritsen), and why the absorption spectrum showed a not very pronounced spectrum instead of the classic vibrational fine structures at 450 nm.

3.5 Conclusions

In conclusion, we were not able to purify either of the *Er*Cry1 isoforms with bound FAD. The spectroscopic measurements showed that no chromophore was present and that the proteins seemed to be correctly folded. Two different titration methods showed no binding affinity between the folded proteins and FAD. These results support the idea that avian Cry1s are not flavoproteins and therefore cannot be considered putative magnetoreceptors. This contradicts the previous results that reported a light-induced conformational change in Cry1s present in the avian retina. Although our results cannot exclude a possible light activation of Cry1s *in vivo*, we would strongly suggest that the studies reporting such results[65,120,122,123] need to be independently replicated.

Chapter 4

MAGNETIC FIELD EFFECTS ON AVIAN CRYPTOCHROME 4S

4.1 Introduction

Based on the results presented in Chapter 3, we concluded that avian Cry1s are unlikely candidate magnetoreceptors. Therefore, we decided to switch our attention towards Cry4s which are the only avian cryptochromes that have been successfully and independently expressed and purified with a bound chromophore in physiological conditions[105,127,140]. If these proteins are indeed the magnetoreceptor molecules, we can expect that they should be able to form magnetically sensitive radical pairs upon light excitation and that there should be differences in the spectroscopic properties of proteins belonging to migratory and non-migratory birds. In "Cryptochrome 4 from a night-migratory songbird has the magnetic properties required of a light-dependent magnetoreceptor", Xu *et al.* (submitted)[184], showed that avian Cryptochrome 4s belonging to non-migratory and migratory birds indeed possess completely different spectroscopic properties. In particular, the magnetic sensitivity of *Er*Cry4 is highly enhanced compared to that of *Gg*Cry4 and *Cl*Cry4 (Figure 4.6). This is an indirect indication that the Cryptochrome belonging to the night-migratory songbird might have evolved to possess such properties. The work described in this chapter will try to explain from which amino acidic residues these differences in avian Cryptochromes might arise.

To do so, we run a sequence alignment between the known avian Cry4s to check whether there are obvious amino acid changes that could explain such dramatic differences. While the protein N- and C-termini are variable, the PHR domains are highly conserved. However, we were able to find a few interesting sequence differences, specifically in positions 317 and 320 (Figure 4.1). These two amino acids are interesting in particular because of their location. In *Er*Cry4 the Cys in position 317 is in between TrpC and TrpD, while Lys 320 is at the surface of the binding pocket (Figure 4.2). Therefore, we decided to compare the properties of *Er*Cry4, *Gg*Cry4, and *Tg*Cry4 proteins from, respectively, a night-migratory passerine (the European robin), a distantly related bird species (the common chicken) and an non-migratory passerine (zebra finch). In addition to that, we mutated the amino acids in positions 317 and 320 of

*Gg*Cry4 and *Tg*Cry4 to see whether these two amino acids might be the cause of the striking difference between the different avian Cryptochromes.

To test this hypothesis, we used Broadband Cavity-Enhanced Absorption Spectroscopy (BBCEAS). This technique detects the change in the optical absorbance of photo-induced radicals when the proteins are exposed to a 30 mT magnetic field and continuous illumination at 450 nm. This experiment was done in collaboration with Marcin Konowalczyk and Patrick Murton, in Prof. Christiane Timmel's lab at the University of Oxford. BBCEAS was designed and built by Marcin Konowalczyk during his DPhil and he and Patrick Murton ran all the experiments. In chapter 4.2.4 we summarise the main features of the spectrometer.

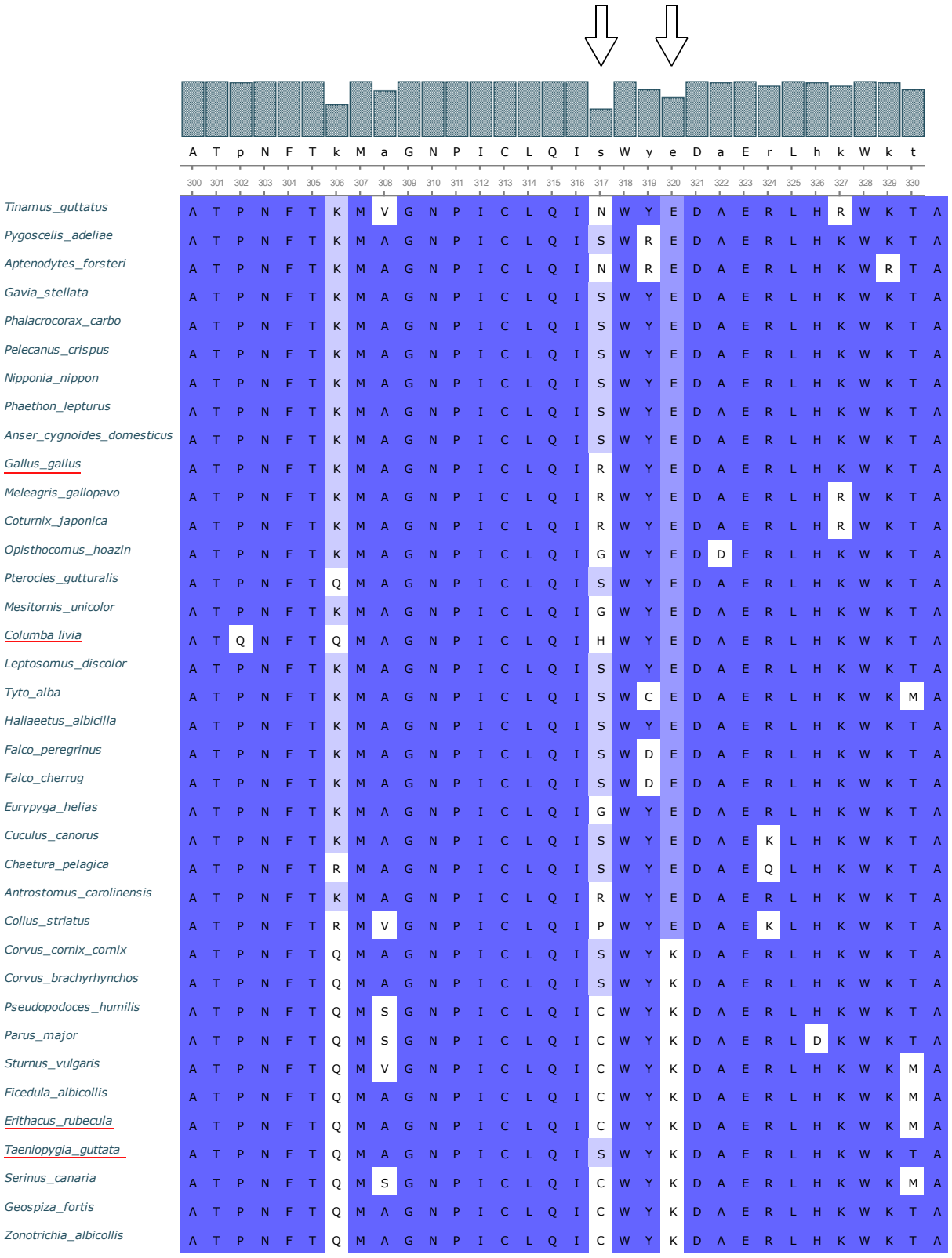


Figure 4.1. Sequence alignment of various avian Cry4s. Despite being highly conserved, the PHR domain presents two highly variable sites in positions 317 and 320. In those positions *Er*Cry4 presents a Cys and a Lys, while *Gg*Cry4 and *Tg*Cry4 present respectively an Arg and Ser in position 317 and a Glu and Lys in position 320. The sequences reported here are the ones *predicted* by a whole genome alignment algorithm found in the NCBI database. The

colour coding is determined by shades of blue. Dark blue indicates 100% identity, while white indicates no identity. The species names underlined in red are chicken, pigeon, robin and zebra finch (from top to bottom) which cryptochrome 4s have been already expressed and purified. The only night migratory songbird present in the sequence alignment is European robin. The full alignment can be found in Chapter 6.1.

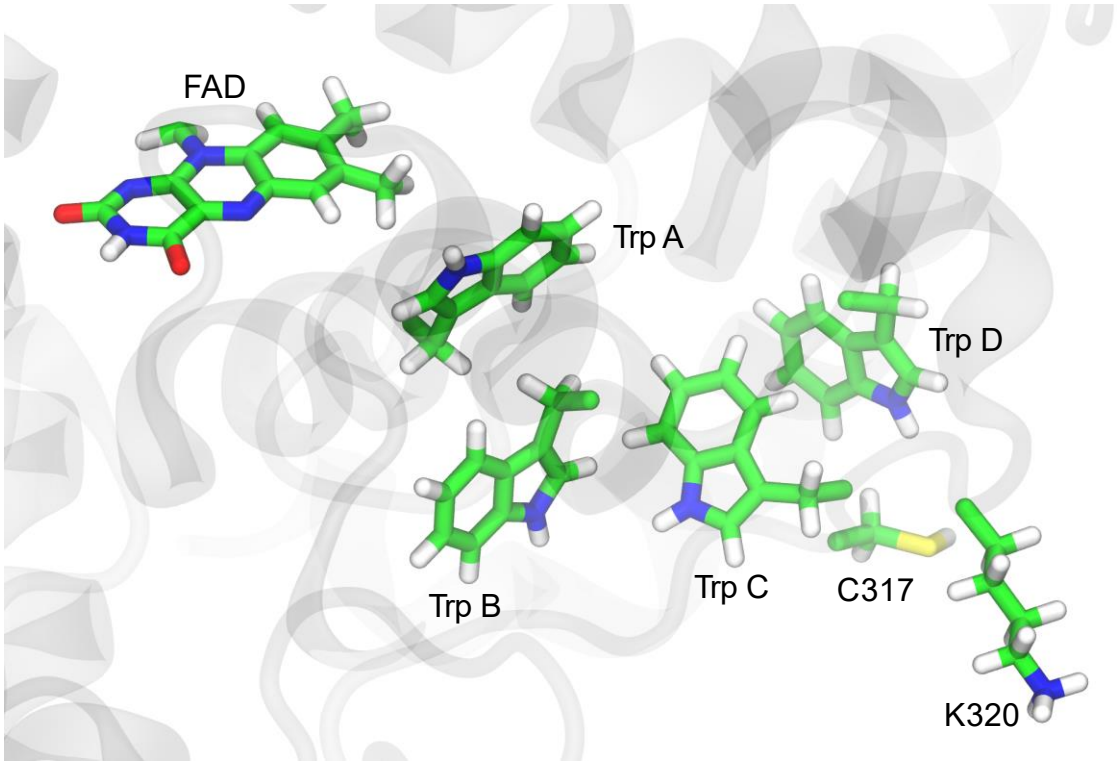


Figure 4.2. The FAD binding pocket of *Er*Cry4. The image shows the position of the four Trp forming the Trp-tetrad in respect to FAD and Cys317 and Lys320. This homology model is based on the crystal structure of *Cl*Cry4[190]. At the moment, this is the only avian Cry4 crystal structure available.

4.2 Material and Methods

4.2.1 Cloning, expression and purification of Cry4s

The sequences cloning, the expression and affinity chromatography of the tested proteins were identical to the procedures described in Chapter 3.2.1. However, the anion exchange chromatography was performed as described below.

GgCry4 WT, GgCry4 R317C, TgCry4 WT and TgCry4 S317C anion exchange chromatography purification

The elution fraction from the affinity chromatography was concentrated using a spin column (Amicon Ultra 30 kDa, Merck) to a final volume of 1 mL. The solution was diluted 1:1 using a Dilution Buffer (20 mM Tris, pH 8.0). The protein was centrifuged at 13,000 rpm and 4 °C for 10 min. The supernatant was collected with the help of a syringe and loaded into the Fast Protein Liquid Chromatography instrument (Akta Pure, GE Healthcare).

The protein was loaded via a syringe into a 5 mm loop that was previously equilibrated using 10 mL of Buffer A (20 mM Tris, 75 mM NaCl, pH 8.0). The proteins were then loaded into a HiTrap Q HP 5 mL column that that was previously equilibrated using 50 mL of Buffer A. The proteins were eluted following a 24 CV linear gradient up to 500 mM NaCl. All proteins were eluted in the first elution peak (Figures 6.3-6.6). Table 6.6 summarises all the buffers used.

GgCry4 R317C- E320K and GgCry4 E320K anion exchange chromatography purification

The elution fraction from the affinity chromatography was concentrated using a spin column (Amicon Ultra 30 kDa, Merck) to a final volume of 2 mL. The solution was diluted 1:1 using a Dilution Buffer (20 mM Tris, pH 8.0). The concentration and dilution steps were repeated. The protein was centrifuged at 13,000 rpm and 4 °C for 10 min. The supernatant was collected with the help of a syringe and loaded into the Fast Protein Liquid Chromatography instrument (Akta Pure, GE Healthcare).

The protein was loaded via a syringe into a 5 mm loop that was previously equilibrated using 10 mL of Buffer A (20 mM Tris, 37.5 mM NaCl, pH 8.0). The proteins were then loaded into a HiTrap Q HP 5 mL column that that was previously equilibrated using 50 mL of Buffer A. The proteins were eluted following a 24 CV linear gradient up to 500 mM NaCl. All proteins

were eluted in the first elution peak (Figures 6.7 and 6.8). Table 6.6 summarises all the buffers used.

4.2.2 Broadband Cavity-Enhanced Spectroscopy (BBCEAS)

Set-up

The set-up was based on that described in Neil *et al*[117]. A supercontinuum laser injected white light into the optical cavity composed by two highly reflective mirrors. The cavity had at its centre a temperature-controlled quartz sample cell, containing the tested protein. A spectrograph measured the cavity output by means of a CCD camera. The 450 nm pump beam, responsible for the sample photoexcitation, was guided onto the sample by two turning mirrors. A set of water-cooled Helmholtz coils produced the magnetic field (Figure 4.3). The changes in the absorbance of photo-induced radicals was measured as $\Delta\Delta A$, defined as the difference in the sample absorbance when a 30 mT magnetic field was present compared to when no field was applied.

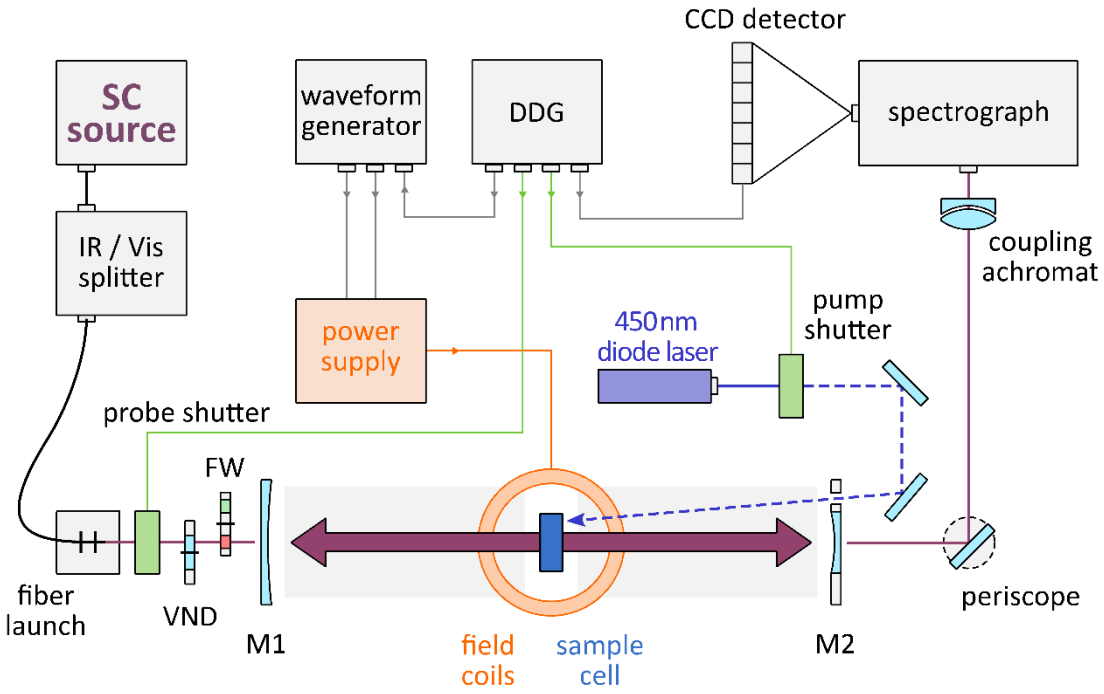


Figure 4.3. Schematic representation of the BBCEAS spectrophotometer. A supercontinuum (SC) source injects white light into the cavity made between the two mirrors M1 and M2. The output of the cavity is coupled with a spectrograph and dispersed onto a charge-coupled device (CCD) detector. The sample inside the cavity is photoexcited by a 450 nm diode laser. The opening and closing of the shutters, the triggering of the magnetic coils and the CCD were controlled by a digital delay generator (DDG). The image was kindly provided by Marcin Konowalczyk.

Experimental procedure

Before being measured, all the samples were dialysed into a 100 mM Tris, 200 mM NaCl, 20% glycerol, pH 8.0 buffer. The quality of the sample was assessed via UV-Vis spectroscopy. If needed, the samples were re-oxidized by a 2 h centrifugation at 5 °C in the presence of 5 mM $K_3Fe(CN)_6$ (ferricyanide). This step allowed the proteins to be in a fully oxidized ground state. Figure 4.5b shows an example of the spectrum of a fully oxidized Cry4. Noticeably the signal of the $FADH^{\bullet}$, which absorbs at > 500 nm, has disappeared. The concentration of the samples during the measurements was set to be 10 µM. The concentration was estimated via UV-Vis measurement. Based on previous studies an absorption of 0.7 OD at the 450 nm peak (oxidised ground state) corresponds to a protein concentration of 60 µM. The samples were then concentrated or diluted accordingly.

During the experiment each sample was tested at 5°C with 5 mM $K_3Fe(CN)_6$ to help with re-oxidation of the sample after the proteins had been photoexcited. Each sample was measured for around 10 s and then allowed to recover and re-oxidise for 20 min. The sample was initially measured for 200 ms under only white light emitting from the supercontinuum source in order to measure the sample in the ground state. This was followed by ca. 9 s of continuous photoexcitation by a diode laser at 450 nm. The light-induced change in the sample absorbance (ΔA) was simultaneously measured by the white light. During the 9 s blue illumination, measurement steps with a period of 400 ms were performed in which the magnetic field was either present in a range of constant values (up to 30 mT) or the magnetic field was switched off (with 50% duty cycle). The field switching times were calibrated and measured, so that at any time point it was known whether a magnetic field was applied or not. The last 50 ms of each measuring step were considered for the data analysis. The magnetic field effect ($\Delta\Delta A$) was determined as the interpolated difference in the sample absorbance between the magnetic field on and magnetic field off measurement steps. This experimental step was repeated for each magnetic field strength value and, as a reference, for the zero field (twice). The experiment was repeated consecutively multiple times (ca. 17) over a period of 3 days.

4.3 Results

4.3.1 Proteins characterisation

We characterised each of the expressed and purified proteins via SDS-PAGE and UV-Vis absorption (Figures 4.4 and 4.5). A Western Blot analysis was deemed not necessary since the proteins appear in a characteristic bright yellow colour.

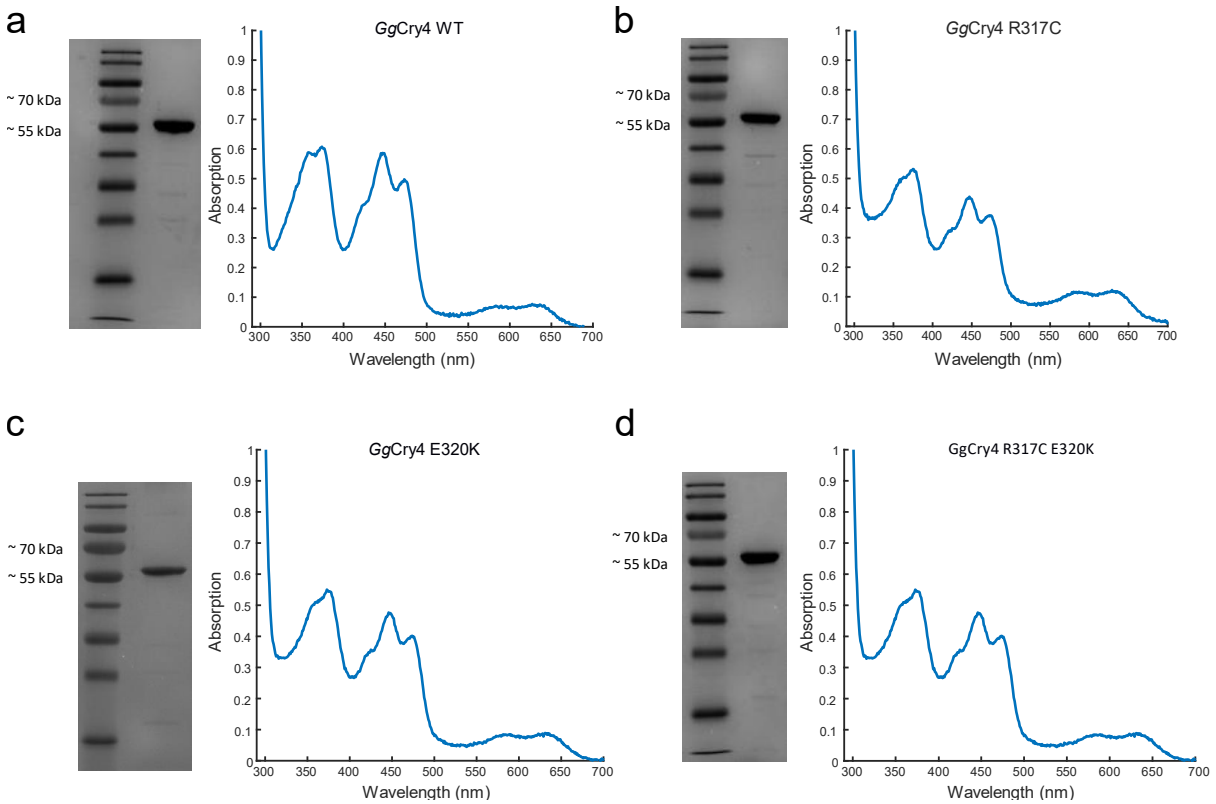


Figure 4.4. Coomassie stained 10% SDS-PAGE and UV-Vis characterisation of *Gg*Cry4 and its different mutants. All the proteins show the characteristic visible spectrum that is a clear indication of a bound FAD. **a.** *Gg*Cry4 WT; **b.** *Gg*Cry4 R317C; **c.** *Gg*Cry4 E320K; **d**. *Gg*Cry4 R317C E320K. The theoretical molecular weight of the proteins is ~ 62.5 kDa. The samples did not contain any ferricyanide. The samples were in a semi-reduced state, thus absorbing at wavelengths > 500 nm.

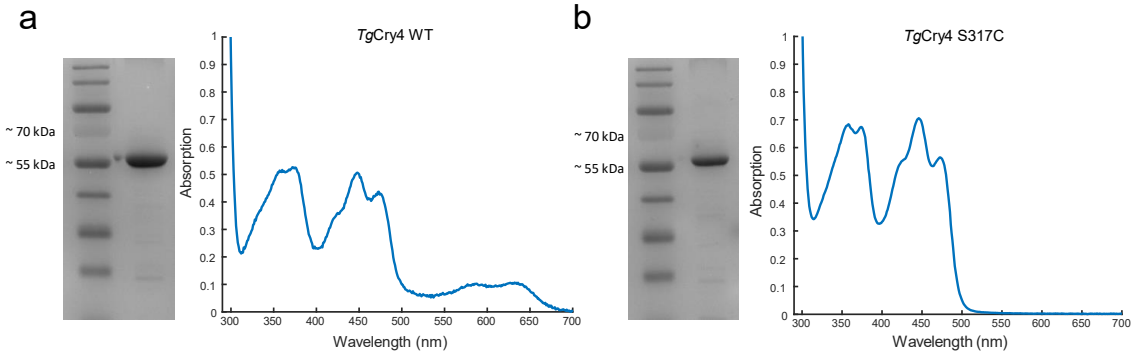


Figure 4.5. Coomassie stained 10% SDS-PAGE and UV-Vis characterisation of *Tg*Cry4 and its mutant. All the proteins show the characteristic visible spectrum that is a clear indication of a bound FAD. **a.** *Tg*Cry4 WT; **b.** *Tg*Cry4 S317C. The theoretical molecular weight of the proteins is ~ 62.5 kDa. The *Tg*Cry4 S317C sample was re oxidised with ferricyanide.

4.3.2 BBCEAS measurements

The results of the measurements are reported in Figures 4.6-4.8. The data are shown as the changes in the absorption of the protein due to its photoexcitation at 450 nm in a presence of a magnetic field ($\Delta\Delta A$) as a function of wavelength. The data do not show the absorbance below 500 nm due to the presence of $K_3Fe(CN)_6$ in the sample. The potassium salt strongly absorbs in the 420 nm region, obscuring most of the ground-state absorption of the flavin. The MARY curve (Figure 4.6b) indicates the Magnetically Altered Reaction Yield and it refers to the change of the absorbance as a function of the applied magnetic field. The parameter $B_{1/2}$ indicates the magnetic field that produces 50% of the effect at high field. The smaller this parameter is, the more sensitive is a sample to smaller field intensities.

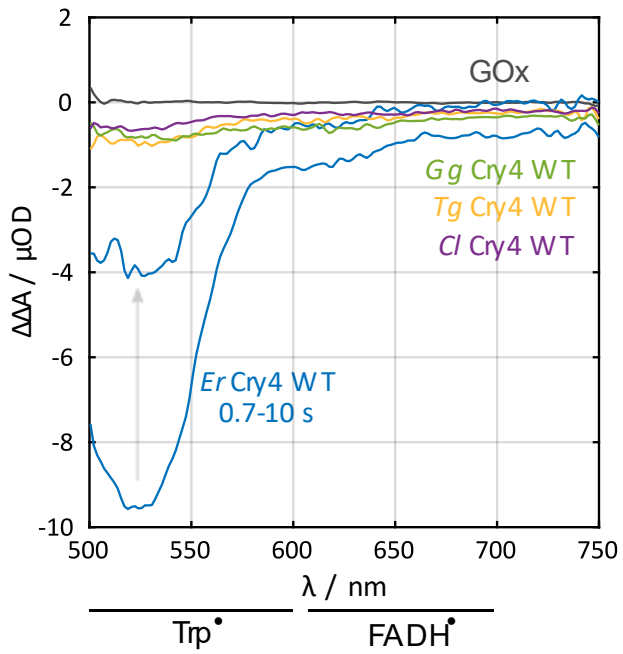


Figure 4.6. BBCEAS measurements of the photo- induced changes in the optical absorbance of four different avian Cryptochrome 4s caused by a 30 mT magnetic field. The avian cryptochromes tested belonged to robin (*Er*Cry4), chicken (*Gg*Cry4), pigeon (*Cl*Cry4) and zebra finch (*Tg*Cry4). GOx (glucose oxidase) is a flavoprotein from *Aspergillus niger* (the fungus causing black mould) which does not have any residues that can support an electron transfer, and therefore cannot form a magnetically sensitive radical pair. For these reasons it was chosen as a blank. All the Cry4 spectra show a reduction in the yield of $Trp^{\bullet}$ radical (which absorbs in the 500-600 nm range), while the signals > 600 nm represent the magnetic field effects on the formation of $FADH^{\bullet}$. Importantly, *Er*Cry4 shows a clear time-dependence in the reduction yield of the $Trp^{\bullet}$ that does not appear in the other proteins. Therefore, *Er*Cry4 spectra

have been reported for the times at 0.7 s and 10 s. Since the other proteins did not show any of these time components their spectra was averaged over the 10 s measurement. *Er*Cry4 and *Cl*Cry4 were expressed and purified by Jingjing Xu (University of Oldenburg). Some of these data were included in "Cryptochrome 4 from a night-migratory songbird has the magnetic properties required of a light-dependent magnetoreceptor", Xu *et al.* (submitted)[184].

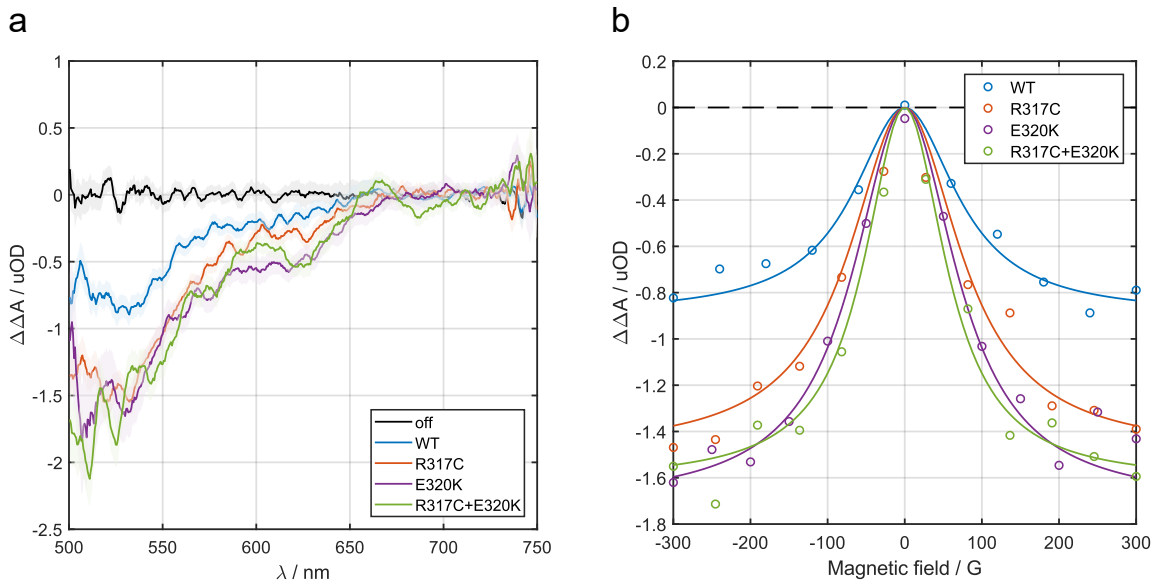


Figure 4.7. BBCEAS measurements of the four different *Gg*Cry4 constructs. **a**. Photo-induced changes in the optical absorbance caused by a 30 mT magnetic field. Noticeably, the magnetic field effect is doubled by either mutation (or both). The shadows represent the standard deviation. **b**. MARY curve of the measurements. There is a striking difference between the wild type protein and its mutants, indicating a change in the protein magnetic sensitivity. The results are summarised in Table 4.1.

Construct	ΔΔ*A*/μOD	$B_{1/2}$/G
*Gg*Cry4 WT	0.9 ± 0.1	79.8 ± 6.6
*Gg*Cry4 R317C	1.5 ± 0.1	82.8 ± 11
*Gg*Cry4 E320K	1.7 ± 0.2	80.5 ± 3.4
*Gg*Cry4 R317C E320K	1.6 ± 0.1	64.8 ± 6.7

Table 4.1. Summary of the BBCEAS results of the *Gg*Cry4 constructs. The single mutations do not seem to affect the $B_{1/2}$ of the reaction, which seems to be comparable with the wild type one. It is possible that the R317C decreases the $B_{1/2}$, but due to the high standard deviation, every conclusion would be merely speculative. The presence of both R317C E320K mutations,

however, seem to decrease the $B_{1/2}$, making the protein more sensitive to magnetic fields with a lower intensity.

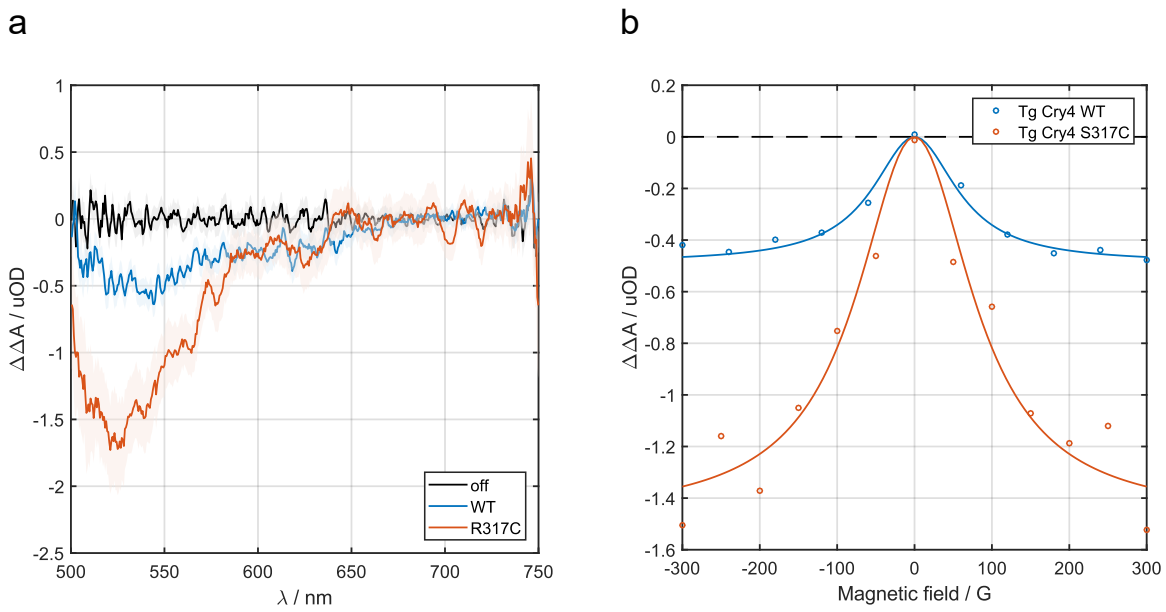


Figure 4.8. BBCEAS measurements of the two different *Tg*Cry4 constructs. **a**. photo-induced changes in the optical absorbance caused by a 30 mT magnetic field. Noticeably, the magnetic field effect is doubled by the Cys 317 mutation. The shadows represent the standard deviation **b**. MARY curve of the measurements. The Cys 317 mutation effectively changes the magnetic properties of the protein. The results are summarised in Table 4.2.

Construct	ΔΔ*A*/μOD	$B_{1/2}$/G
*Tg*Cry4 WT	0.5 ± 0.1	65.4 ± 5.3
*Tg*Cry4 S317C	1.85 ± 0.1	89.8 ± 13.9

Table 4.2. Summary of the BBCEAS results of the *Tg*Cry4 constructs. While the ΔΔ*A*/μOD is tripled in the S317C mutant compared to the WT, the $B_{1/2}$ seems to increase. However, given the high value of the standard deviation, it would be better to repeat the measurement to be sure about this result.

4.4 Discussion

The results reported in Figure 4.6 show the striking differences between avian Cry4s belonging to different species. Importantly, *Er*Cry4 has properties that are unique when compared to *Cl*Cry4, *Gg*Cry4 and *Tg*Cry4. Not only *Er*Cry4 presents the strongest magnetic field effect, but it also shows a time-dependent component that is not present in any of the other studied avian Cryptochromes. This is even more relevant if we considered that the European Robin is the only animal among these four that has been shown to be able to use a magnetic compass in multiple independent studies[40,174,187]. There have been reports of magnetic orientation in pigeons[106], chickens[176] and zebra finches[138]. However, not only none of these studies were ever independently repeated, but none of these birds are a migratory. The difference in the photochemistry of the avian Cryptochromes is even more striking when we compare the percentage of amino acid identity between these proteins. In fact, *Gg*Cry4, *Cl*Cry4 and *Tg*Cry4 share the 88.8%, the 88.4% and 94.1% of their sequence with *Er*Cry4. Most of these differences are present in the N- and C-terminus region, while the PHR domains are mostly identical. It is also important to notice that all the four tryptophans forming the Trp-tetrad necessary for the electron transfer to FAD, are in conserved positions (Figure 4.7).

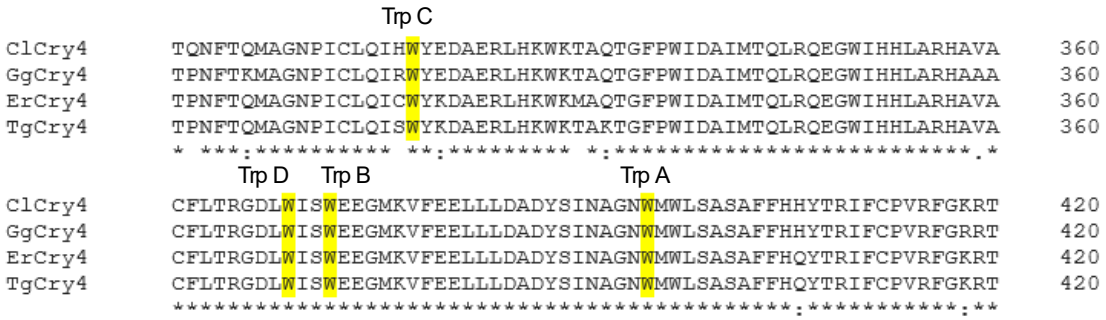


Figure 4.7. Trp-tetrad in different avian Cryptochromes. The Trp-tetrad is highly conserved among avian Cryptochromes. The Trp are named in alphabetical order starting from the closest (Trp_A) to the furthest (Trp_D) to the FAD. The Trp are conserved in position 395 (Trp_A), 372 (Trp_B), 318 (Trp_C), 369 (Trp_D). In the alignment, a star at the bottom of the sequences indicates 100% identity. Noticeably, the sequences are highly conserved.

Therefore, the main difference between the Cryptochromes cannot be due to different electron transfer pathways along the Trp-chain. Consequently, we decided to do a multiple alignment of all the avian Cry4s sequences available on the NCBI database, looking for amino acid

residues that could affect the environment surrounding the Trp-tetrad (Figure 4.2). It is important to stress that the majority of the sequences present in the database are *predicted* by a whole genome alignment algorithm, and not yet published. Therefore, it is not impossible to exclude the presence of mistakes in the sequences. Unfortunately, no other data are available to the public. Based on the data available, we deemed interesting the residues in position 317 and 320. Table 4.3 summarises the amino acidic differences among the studied Cryptochromes.

Protein	Species	Amino acid in position 317	Amino acid in position 320
*Er*Cry4	European Robin	Cys (C)	Lys (K)
*Tg*Cry4	Zebra finch	Ser (S)	Lys (K)
*Cl*Cry4	Pigeon	His (H)	Glu (E)
*Gg*Cry4	Chicken	Arg (R)	Glu (E)

Table 4.3. Amino acid changes in positions 317 and 320 in the studied avian Cryptochromes.

We then decided to substitute the amino acids in *Gg*Cry4 and *Tg*Cry4 with the one present in *Er*Cry4 to see whether we were able to rescue the spectroscopic characteristic of the Robin Cryptochrome 4. Interestingly, in *Gg*Cry4 both the R317C and E320K mutations seem to have a major effect on the magnetic properties of the protein. Since Arg is positively charged and Glu is negatively charged, there is the chance of them forming a salt bridge. The substitution of one of the two amino acids, might lead to the breaking of such a bond. It is important to notice that the Arg is substituted with a Cys (which is not charged) and the Glu with a Lys (which is positively charged). This dramatic change in the overall charge distribution might affect the surroundings of Trp_C and Trp_D, and this might increase the magnetic sensitivity of the protein as a side effect. In *Tg*Cry4 the S317C mutation increases the magnetic field effect measured on the protein. In this case, however, the mutation is less drastic since there is no overall change of the charge distribution. It is important to notice that *Tg*Cry4 WT already presents a Lys in position 320 and this mutation alone seems to have no real effect. In fact, the $\Delta\Delta A$ of *Gg*Cry4 WT and *Tg*Cry4 WT are very similar. However, the S317C mutation might cause the formation of a bond between Cys317 and Trp_D, stabilizing it. If this were the case,

Trp_D would move less in respect to Trp_C allowing the formation of a more stable radical pair (Prof. Ilia Solov'yov, personal communication).

To summarise, while the role of Lys320 is not completely clear, it appears that Cys317 is playing a major role in the magnetic sensitivity of avian Cryptochromes. It is important to notice that none of these mutations has fully rescued the magnetic field effect on *Er*Cry4. Therefore, other amino acids, probably not in the PHR domain, might have an effect on the magnetic sensitivity of Robin Cry4. We could speculate that the protein might undergo a conformational change upon light excitation that could increase the magnetic sensitivity of the protein. This overall change of the protein structure has already been shown in *Dm*Cry. In fact, *Dm*Cry in its fully oxidized state is present in U-shape form, and the C-terminus act as a "lid" over the FAD binding region[128]. Once photoexcited, the C-terminus opens, drastically changing the protein structure. We could imagine that something similar might happen in *Er*Cry4, which, however, does not happen in the other studied avian Cryptochromes. What exactly is causing these differences has still to be determined.

4.5 Conclusions

In conclusion, we found striking differences between cryptochrome 4s from migratory and non-migratory birds, thus supporting the idea that Cry4s might be the magnetoreceptor molecule. The difference between these Cryptochromes could also be due to the presence of a Cys in position 317, which can enhance the magnetic sensitivity of the proteins. However, the mutation of this single amino acid in both *Gg*Cry4 and *Tg*Cry4 does not completely restore the spectroscopic characteristics of *Er*Cry4, indicating that other residues must be involved in this mechanism.

Therefore, these can be considered as promising preliminary data that can help understand where the differences between the avian cryptochromes come from. Hopefully, these data can open possibilities for future experiments, such as different spectroscopic measurements, molecular dynamics simulations and a comparative phylogenetic study.

As for the spectroscopic measurements, it is important to highlight that BBCEAS is a technique that can only resolve the long timescales of a photochemical reaction. For early timescale resolution, other techniques can be used, such as picosecond Transient Absorption

spectroscopy (psTA)[101] and Cavity-Ring Down Spectroscopy (CRDS)[117]. Therefore, it would be useful to combine the data from these three spectroscopic techniques to have a better understanding of these photochemical reactions.

On the other hand, molecular dynamics simulations can help understand what exactly the role of Cys317 is (and possibly Lys320), and how these and other residues can interact with each other and affect the formation and the lifetime of the radical pairs.

Finally, it is interesting to note that, based on the data in our possession, Cys317 is only present in the most recent branch of the passerines, to which all night-migratory songbirds belong. Therefore, it seems that the Cys317 mutation initially appeared as a neutral one in the passerine order. Therefore, we can speculate that this mutation was the base from which the evolution of a magneto-sensitive protein could have started. At the moment, unfortunately, we have no proof to sustain this hypothesis. As a future work, it would be interesting to run a phylogenetic study to check when the Cys317 mutation appeared and whether some other amino acids were positively selected in night-migratory passerines. If this were the case, it would be interesting to test whether these residues play a role on the magnetic properties of the avian cryptochromes. Another interesting test would be to reconstruct the primitive avian Cry4 sequence and to express this protein to be used as a baseline to test avian Cry4s magnetic properties.

Chapter 5

CONCLUSIONS AND FUTURE WORK

Validation and independent replication of published results are a core feature of science. Without them, it is not possible to distinguish between true data variation and unknown experimental artefacts. For these reasons, most of the work presented in this thesis is focussed on trying (and failing) to replicate already published material. However, exact replications are not always easy or possible. This is especially true regarding biological experiments, since a 100% identical replication is *de facto* impossible. Moreover, replicating experiments requires a high investment of time and money, resources that most laboratories are not easily willing to spare, and, in case of negative results, such experiments are a major source of frustration for the experimenter.

Nevertheless, negative results are important datasets that can help understanding better a phenomenon and as such, their importance should not be underestimated. This has proven to be true especially in the field of magnetoreception, in which replication has always been challenging. For example, originally it was thought that robins' magnetic compass was located only in their right eye[178], but later it was found out that there was no eye lateralization[56]. What had been thought to be magnetite particles in the upper beak of homing pigeons necessary for their magnetic map [42,45], was later revealed to be clusters of iron-rich macrophages[162]. *Arabidopsis thaliana* hypocotyl growth has been reported to be inhibited when the plant was exposed to a 500 μT static magnetic field[3]. However, when this experiment was repeated in more stringent conditions, no magnetic field effects were found[54]. Night-migratory songbirds were reported to be disoriented when exposed to electromagnetic fields oscillating at the Larmor frequency[142], but once more, these results were not replicated when birds were tested in a more controlled environment[152]. And the list could go on.

Therefore, in hindsight, it might not be surprising that we were unable to replicate the results presented in Fedele *et al*[44] and Bae *et al*[7]. Unfortunately, it was not possible to determine the cause of this discrepancy. We can, however, state that we tried to run our experiments in the best possible way according to our possibilities. In fact, we built and optimised two different set-ups, we ran the experiments in a blinded fashion in a meticulously controlled environment, we applied strong statistical tests on a large-scale dataset, and we saw positive results in the

control experiments. Despite our efforts, we were unable to see any magnetic field effect on *Drosophila* negative geotaxis.

The search for the magnetoreceptor molecule in night-migratory songbirds has kept researchers busy for quite a long time. For roughly ten years, attention was focussed on Cry1, mostly because of its ideal location in the UV cones of the retina. Over the years, a variety of evidence was collected indicating that Cry1s were indeed the magnetoreceptor molecule. However, none of these studies was independently replicated[65,120,122], or, as in the case of Liedvogel *et al.*[95], were only replicated by the main author. Importantly, all these studies assumed that Cry1s were photosensitive flavoproteins, but we were not able to find evidence supporting this idea. In fact, our results show that Cry1s cannot bind (or have any affinity for) FAD when the protein is been expressed and purified *in vitro*. This contradicts the results from Liedvogel *et al.*[95] and Yuan *et al.*[186]. However, even though our results cannot completely exclude that Cry1s can be light-activated *in vivo*, we do not consider it to be likely. Therefore, it would be interesting to try to replicate the studies of Hoang. *et al.*[65] and Nießner *et al.*[120,121].

On the other hand, avian Cry4s have been successfully expressed and purified with a bound chromophore in physiological conditions in a series of independent studies[105,127,140,184]. Thus, they are now considered to be the most likely candidate magnetoreceptor. This is also supported by our results showing that there are striking differences in the magnetic and spectroscopic properties of avian Cry 4s belonging to migratory and non-migratory birds. Based on the data that we collected, these differences might also arise from the presence of a Cys in position 317. The presence of this residue, however, only partially explains the differences in the spectroscopic properties of avian Cry4s, indicating that other amino acids, which at the moment are unknown, might play a central role. Therefore, these results open the possibilities for future studies involving different spectroscopic measurements, molecular dynamics simulations and a comparative phylogeny, which can help better understanding how the magnetoreceptor molecules have evolved in night-migratory songbirds.

APPENDIX

Reagent	Amount
5× Phusion HF buffer	10 µL
10 mM dNTPs	1 µL
Forward Primer 0.5 µM	1 µL
Reverse primer 0.5 µM	1 µL
Template DNA from vector	100-150 ng
Phusion DNA polymerase	0.5 µL
H_2O	Up to 50 µL

Table 6.1. Components of a standard polymerase chain reaction (PCR) according to the producer guidelines.

Cycle step	Temperature	Time	
Initial denaturation	98 °C	30 s	
Denaturation	98 °C	10 s	25 cycles
Annealing	X °C	30 s	
Extension	72 °C	45 s	
Final extension	72 °C	7 min	

Table 6.2. Standard PCR cycle according to the producer guidelines. The annealing temperature T_m was varied depending on the primers used and was calculated using the ThermoFisher T_m Calculator.

Insert	Primer	Direction	Restriction Site
*Er*Cry1a	TGACGACTAGTATGGGGGTGAACGCCGTG	F	SpeI
	GCCAATGGATCCTTAATTTGTGCTCTGTCGCTG	R	Bam HI
*Er*Cry1b	TGACGACTAGTATGGGGGTGAACGCCGTG	F	SpeI
	GCCAGTGGATCCCTATTTTGATGTTTTGTCTGG	R	Bam HI
*Gg*Cry4	TATCGACTAGTATGCGGCACCGCACCATCC	F	SpeI
	GTACCTCTAGACTAGGTTGGCTCTGTCATCCTGG	R	Xba I
*Gg*Cry4 R317C	CCTCCAGATCTGTTGGTATGAGGATG	F	/
	CAGATGGGGTTCCCGGCC	R	
*Gg*Cry4 E320K	CCGTTGGTATAAGGATGCTGAGAG	F	/
	ATCTGGAGGCAGATGGGG	R	
*Gg*Cry4 R317C E320K	TATAAGGATGCTGAGAGGCTCCAC	F	/
	CCAACAGATCTGGAGGCAGATGGG	R	
Tg Cry4	TGACGACTAGTATGCTGCATCGCACCATTCACC	F	SpeI
	TGACGAAGCTTTTATTCTGTCGTTCGGGCC	R	Hind III
Tg Cry4 S317C	CCTCCAGATTTGCTGGTACAAGGATGCAGAGAG	F	/
	ATCTGGAGGCAGATGGGG	R	

Table 6.3. List of all the primers used.

Insert	IPTG Concentration
*Er*Cry1a	10 µM
*Er*Cry1b	10 µM
*Gg*Cry4	10 µM
*Gg*Cry4 R317C	5 µM
*Gg*Cry4 E320K	5 µM
*Gg*Cry4 R317C K320E	5 µM
*Tg*Cry4	10 µM
*Tg*Cry4 S317C	10 µM

Table 6.4. Final working ITPG concentration for each construct.

	Tris	NaCl	Imidazole	pH
Binding Buffer	20 mM	150 mM	5 mM	8.0
Washing Buffer	20 mM	150 mM	20 mM	8.0
Elution Buffer	20 mM	150 mM	300 mM	8.0
Buffer A	20 mM	50 mM	/	9.1
Buffer B	20 mM	1 M	/	9.1

Table 6.5. List of buffers used in the purification of *Er*Cry1a and 1b. In each buffer 700 µL/L of β-mercaptoethanol were added to the buffer to improve the binding of the proteins to the Ni-NTA agarose column and to prevent the formation of dimers.

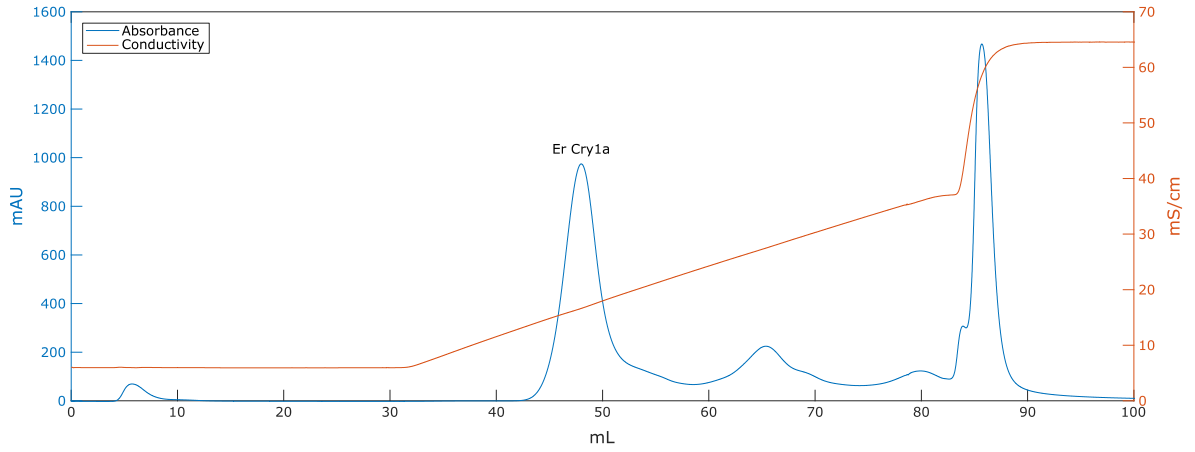


Figure 6.1. Purification of *Er*Cry1a via anion exchange chromatography. The fractions forming the first peak contained the desired protein.

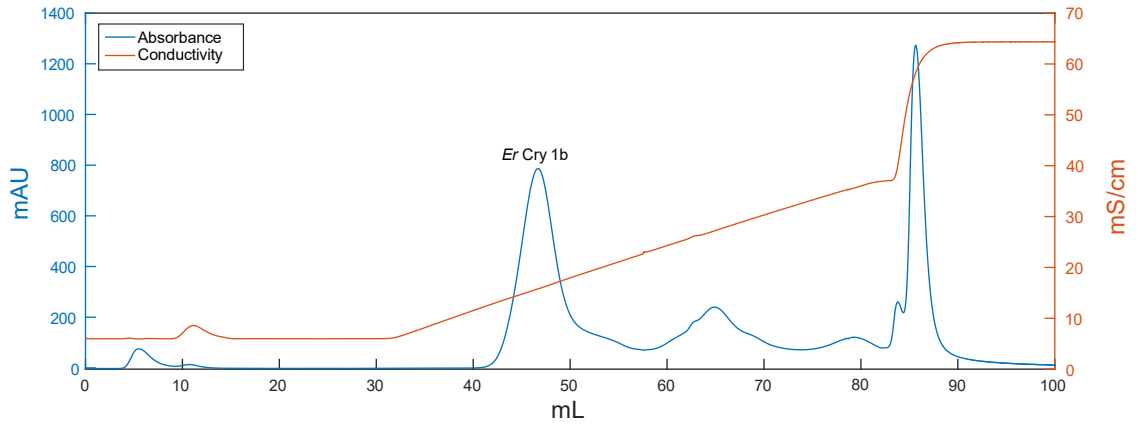


Figure 6.2. Purification of *Er*Cry1b via anion exchange chromatography. The fractions forming the first peak contained the desired protein.

	Tris	NaCl	Imidazole	pH
Binding Buffer	20 mM	150 mM	5 mM	8.0
Washing Buffer	20 mM	150 mM	20 mM	8.0
Elution Buffer	20 mM	150 mM	300 mM	8.0
Dilution Buffer	20 mM	/	/	8.0
Buffer A	20 mM	75 mM	/	8.0
Buffer B	20 mM	1 M	/	8.0

Table 6.6. List of buffers used in the purification of *Gg*Cry4, *Gg*Cry4 R317C, *Tg*Cry4 and *Tg*Cry4 S317C. In each buffer 700 µL/L of β-mercaptoethanol were added to the buffer to improve the binding of the proteins to the Ni-NTA agarose column and to prevent the formation of dimers.

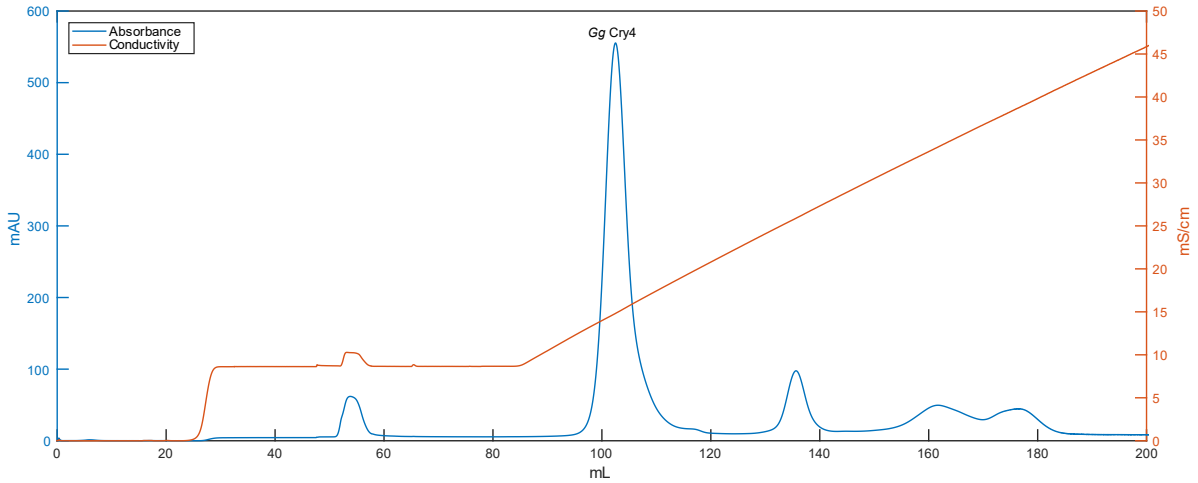


Figure 6.3. Purification of *Gg*Cry4 via anion exchange chromatography. The fractions forming the first peak contained the desired protein.

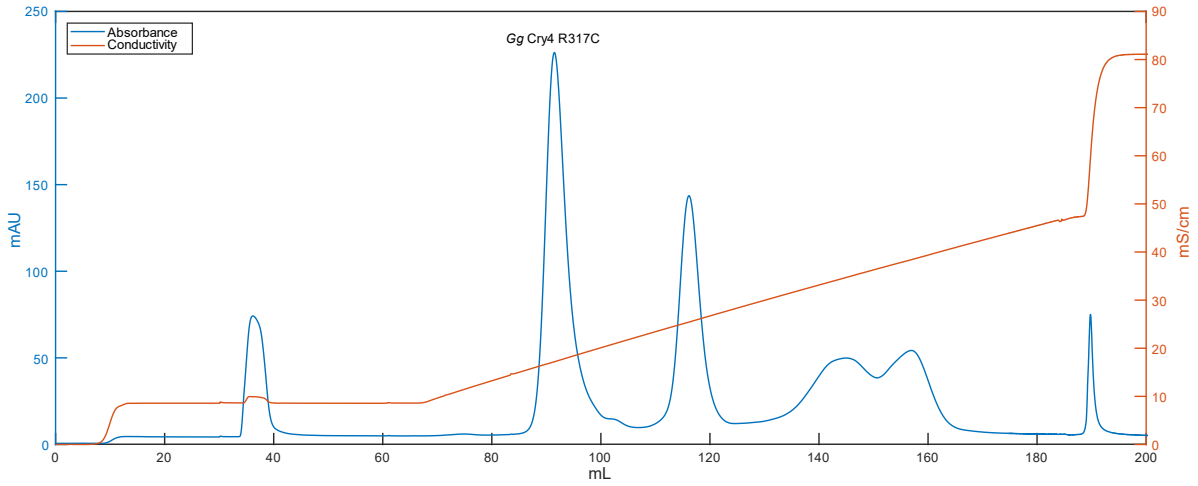


Figure 6.4. Purification of *Gg*Cry4 R317C via anion exchange chromatography. The fractions forming the first peak contained the desired protein.

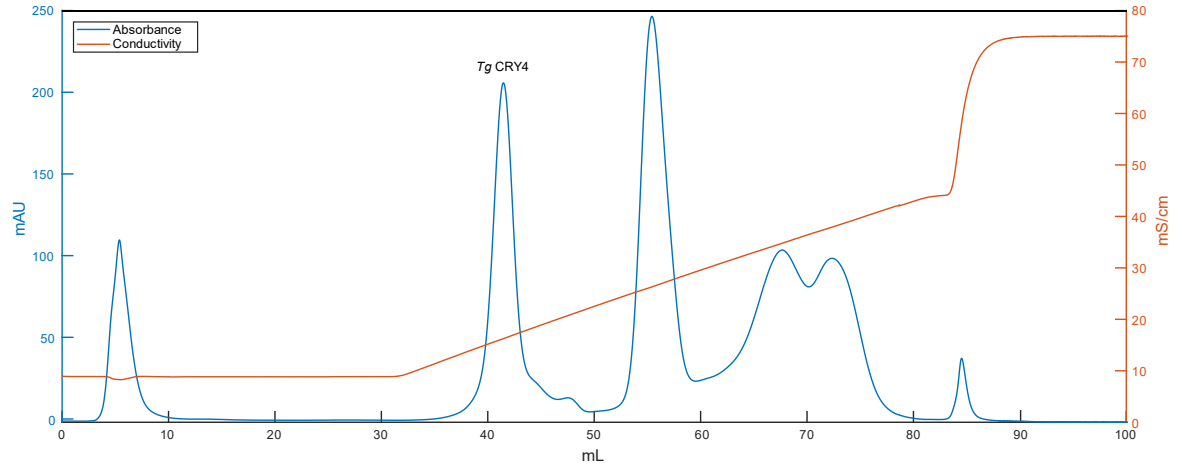


Figure 6.5. Purification of *Tg*Cry4 via anion exchange chromatography. The fractions forming the first peak contained the desired protein.

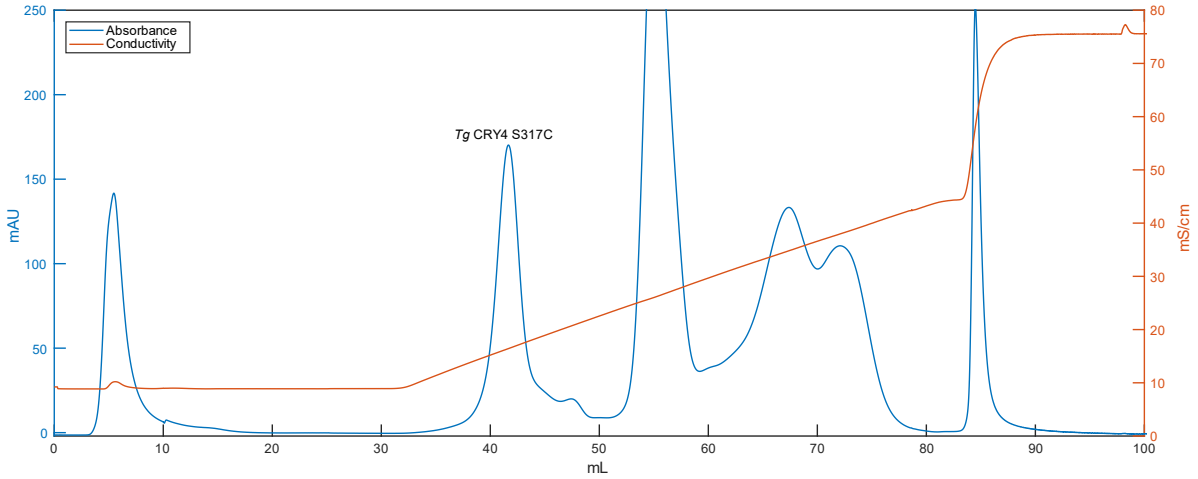


Figure 6.6. Purification of *Tg*Cry4 S317C via anion exchange chromatography. The fractions forming the first peak contained the desired protein.

	Tris	NaCl	Imidazole	pH
Binding Buffer	20 mM	150 mM	5 mM	8.0
Washing Buffer	20 mM	150 mM	20 mM	8.0
Elution Buffer	20 mM	150 mM	300 mM	8.0
Dilution Buffer	20 mM	/	/	8.0
Buffer A	20 mM	37.5 mM	/	8.0
Buffer B	20 mM	1 M	/	8.0

Table 6.7. List of buffers used in the purification of *Gg*Cry 4 R317C- E320K and *Gg*Cry 4 E320K. In each buffer 700 µL/L of β-mercaptoethanol were added to the buffer to improve the binding of the proteins to the Ni-NTA agarose column and to prevent the formation of dimers.

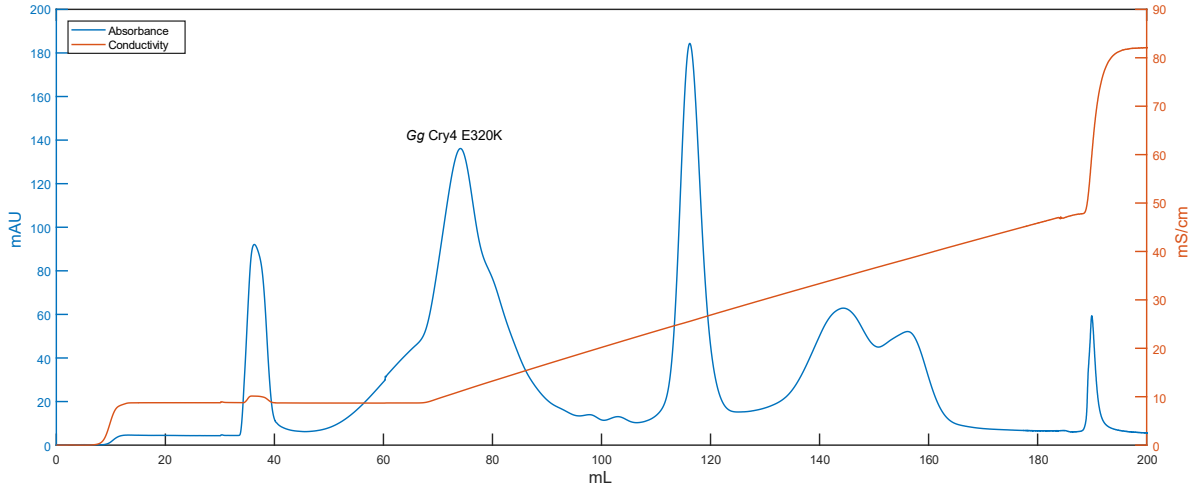


Figure 6.7. Purification of *Gg*Cry4 E320K via anion exchange chromatography. The fractions forming the first peak contained the desired protein.

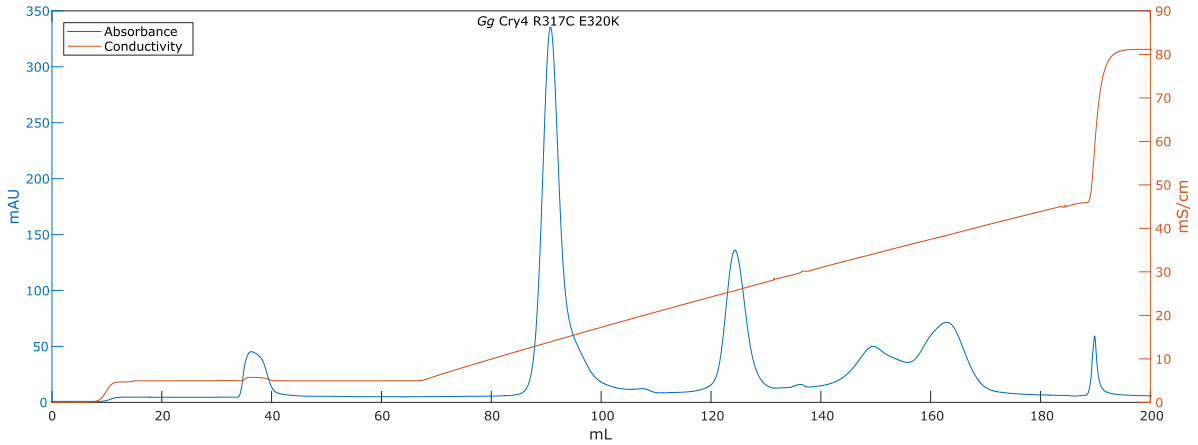


Figure 6.8. Purification of *Gg*Cry4 R317C E320K via anion exchange chromatography. The fractions forming the first peak contained the desired protein.

	Concentration	10%	12%
2× Separating Gel	dd H_2O	2.8 mL	2.3 mL
	1.5 M Tris pH 8.8	1.75 mL	1.75 mL
	30% Acr/Bis	2.3 mL	2.8 mL
	10% SDS	70 µL	70 µL
	10% APS	70 µL	70 µL
	TEMED	7 µL	7 µL
	Concentration	**6%**	
2× Stacking Gel	dd H_2O	2.1 mL	
	0.5 M Tris pH 6.8	1 mL	
	30% Acr/Bis	0.8 mL	
	10% SDS	40 µL	
	10%APS	40 µL	
	TEMED	4 µL	
Gel Stain Dye (1 L)	Coomassie R250	1 g	
	Ethanol	500 mL	
	Acetic Acid	100 mL	
	dd H_20	350 mL	
Destainer (1 L)	Ethanol	450 mL	
	Acetic Acid	100 mL	
	dd H_20	450 mL	
5× Running Buffer	Tris	15.1 g/L	
	Glycine	72 g/L	
	SDS	5 g/l	
1× Transfer Buffer	Tris	3 g	
	Glycine	14.4 g	
	20% Methanol	150 mL	
	dd H_2O	Up to 1 L	
10× TBS pH 7.5	Tris	24.2 g	
	NaCl	87.6 g	
	1 M Tris-HCl pH 6.8	12.5 mL	
5× SDS-PAGE Loading Buffer*	SDS	5 g	
	Bromophenol Blue	0.25 g	
	Glycerol	25 mL	
	dd H_20	Up to 50 mL	

Table 6.8. Various buffers used for the SDS-page and Western Blot analysis. *50 µL in 1000 µL aliquot β-mercaptoethanol were added before use.

Protein	Epitope	Clone name	Host	Dilution
ErCry1a	RPNPEEETQSVGPKVQRQST	3E12	Rat	1:3000
ErCry1b	CRGSPNACNYGKPDKTSK	17B11	Rat	1:3000
ErCry1a and b	TTPVSDDHDEKYG	17A2	Rat	1:3000

Table 6.9. List of antibodies used. The secondary antibody used was HRP goat anti-rat, with a 1:3000 dilution.

6.1 Sequences alignments



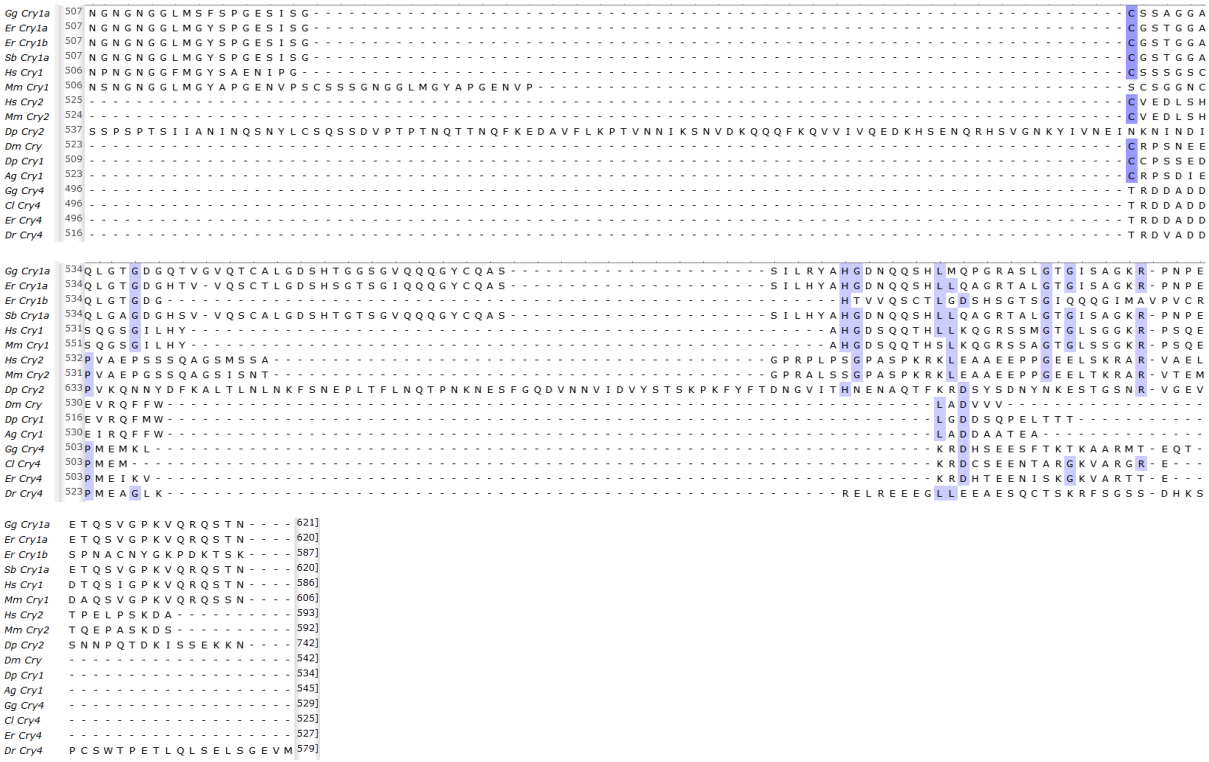
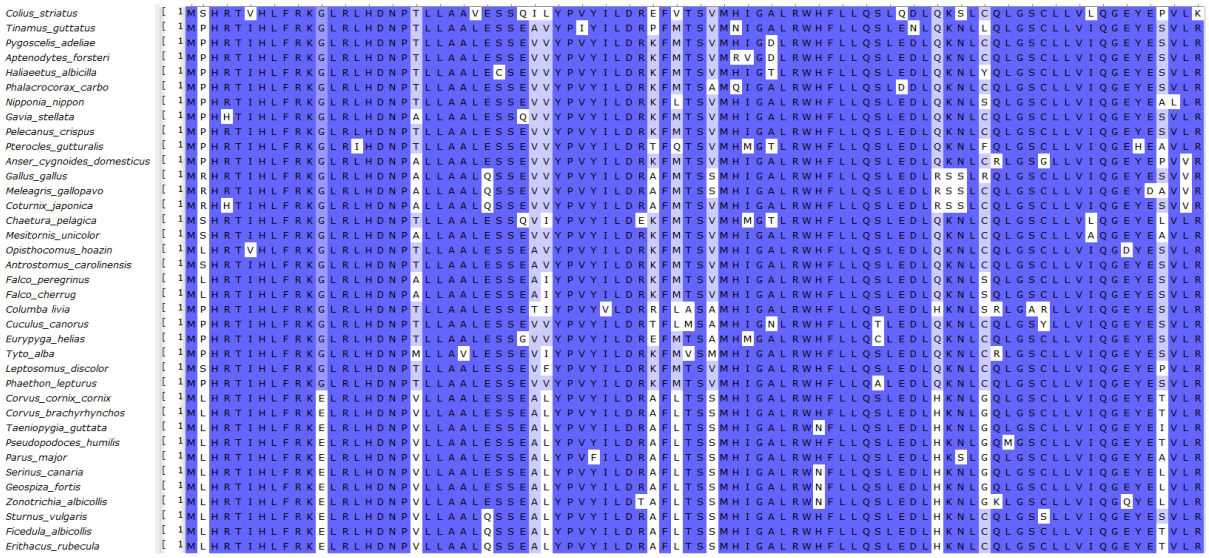
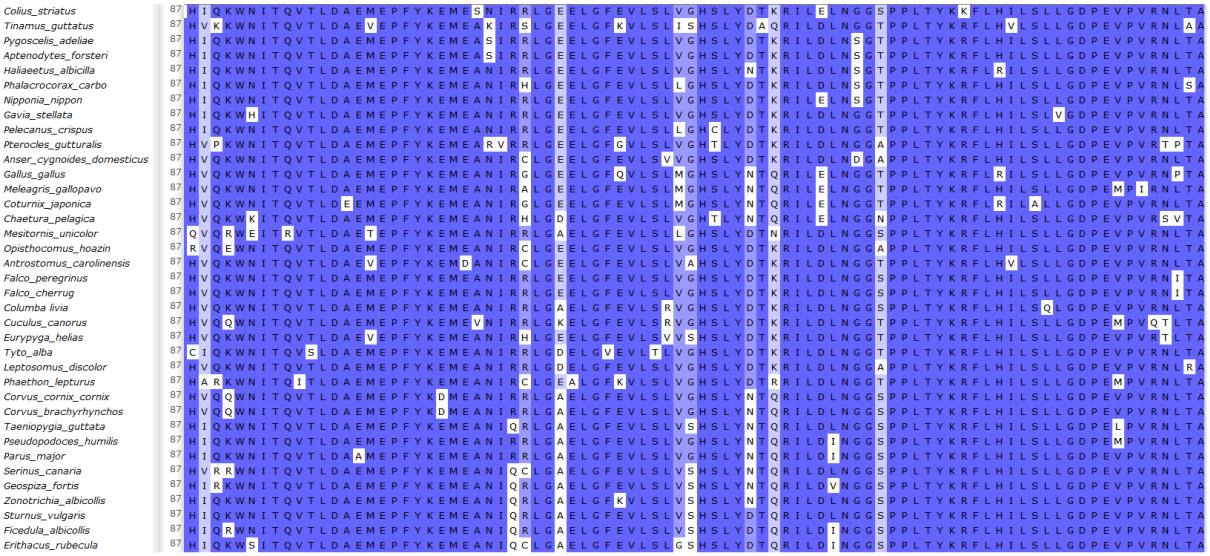
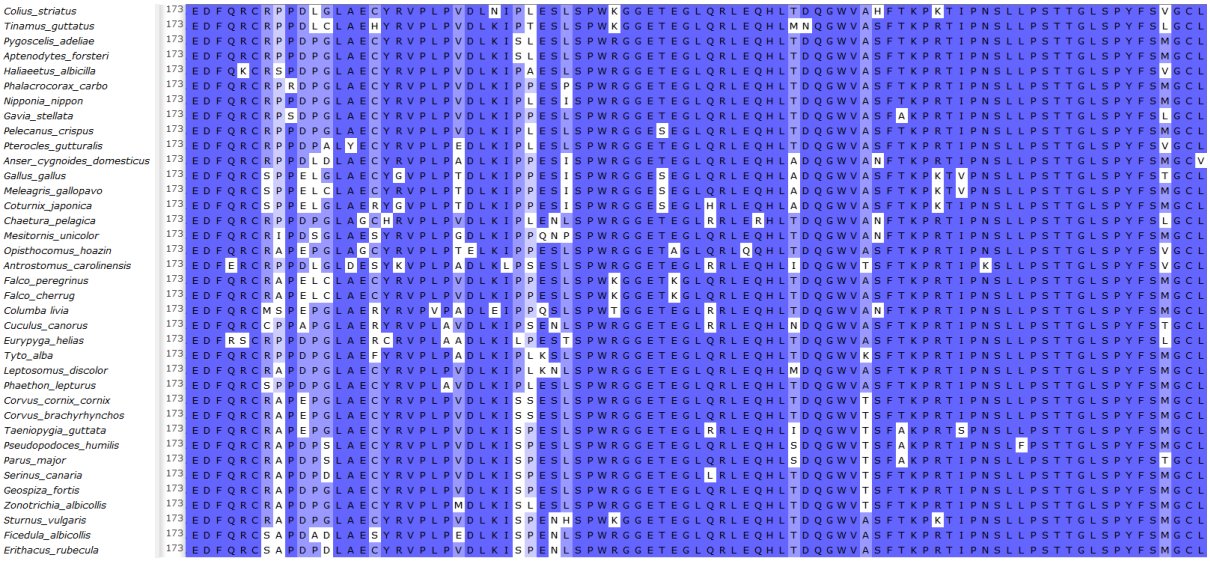
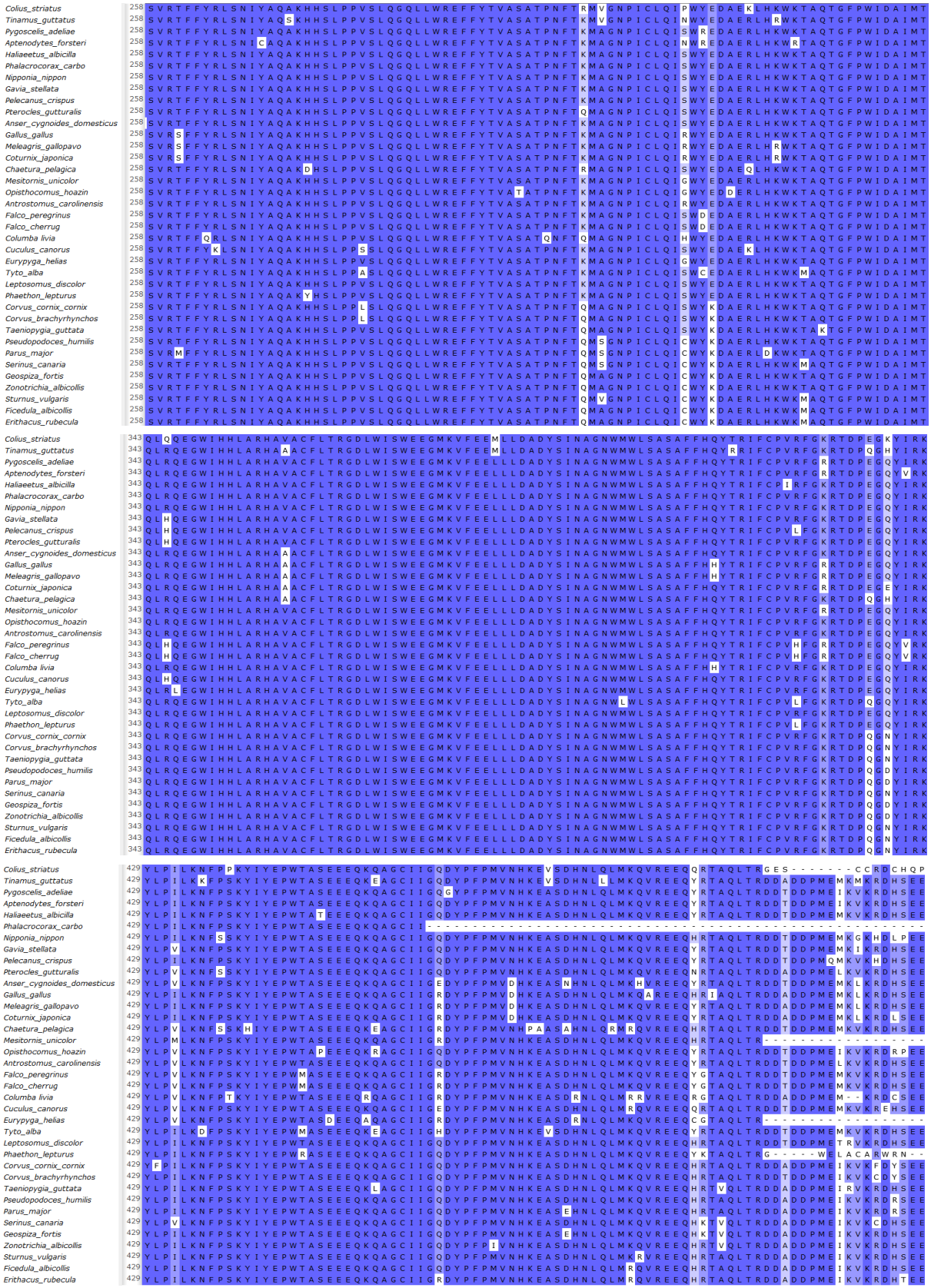


Figure 6.9. Full sequence alignment of different Cryptochromes belonging to the classes: Type I, Type II and Cry4. Type II is represented by *Gg*Cry1a (*Gallus gallus*), *Er*Cry1a (*Erithacus rubecula*), *Er*Cry1b, *Hs*Cry1 (*Homo sapiens*), *Mm*Cry1, (*Mus musculus*), *Hs*Cry2, *Mm*Cry2, *Dp*Cry2 (*Danaus plexippus*). Type I is represented by *Dm*Cry (*Drosophila melanogaster*), *Dp*Cry1, *Ag*Cry1 (*Anopheles gambiae*). The Cry4 class is represented by *Gg*Cry4, *Cl*Cry4 (*Columba livia*), *Er*Cry4 and *Dr*Cry4 (*Danio rerio*).


Colius_striatus
Tinamus_guttatus
Pygoscelis_adeliae
Aptenodytes_forsteri
Haliaeetus_albicilla
Phalacrocorax_carbo
Nipponia_nippon
Gavia_stellata
Pelecanus_crispus
Pterocles_gutturalis
Anser_cygnoides_domesticus
Gallus_gallus
Meleagris_gallopavo
Coturnix_japonica
Chaetura_pelagica
Mesitornis_unicolor
Opisthocomus_hoazin
Antrostomus_carolinensis
Falco_peregrinus
Falco_cherrug
Columba livia
Cuculus_canorus
Eurypyga_helias
Tyto_alba
Leptosomus_discolor
Phaethon_lepturus
Corvus_cornix_cornix
Corvus_brachyrhynchos
Taeniopygia_guttata
Pseudopodoces_humilis
Parus_major
Serinus_canaria
Geospiza_fortis
Zonotrichia_albicollis
Sturnus_vulgaris
Ficedula_albicollis
Erithacus_rubecula


Colius_striatus
Tinamus_guttatus
Pygoscelis_adeliae
Aptenodytes_forsteri
Haliaeetus_albicilla
Phalacrocorax_carbo
Nipponia_nippon
Gavia_stellata
Pelecanus_crispus
Pterocles_gutturalis
Anser_cygnoides_domesticus
Gallus_gallus
Meleagris_gallopavo
Coturnix_japonica
Chaetura_pelagica
Mesitornis_unicolor
Opisthocomus_hoazin
Antrostomus_carolinensis
Falco_peregrinus
Falco_cherrug
Columba livia
Cuculus_canorus
Eurypyga_helias
Tyto_alba
Leptosomus_discolor
Phaethon_lepturus
Corvus_cornix_cornix
Corvus_brachyrhynchos
Taeniopygia_guttata
Pseudopodoces_humilis
Parus_major
Serinus_canaria
Geospiza_fortis
Zonotrichia_albicollis
Sturnus_vulgaris
Ficedula_albicollis
Erithacus_rubecula


Colius_striatus
Tinamus_guttatus
Pygoscelis_adeliae
Aptenodytes_forsteri
Haliaeetus_albicilla
Phalacrocorax_carbo
Nipponia_nippon
Gavia_stellata
Pelecanus_crispus
Pterocles_gutturalis
Anser_cygnoides_domesticus
Gallus_gallus
Meleagris_gallopavo
Coturnix_japonica
Chaetura_pelagica
Mesitornis_unicolor
Opisthocomus_hoazin
Antrostomus_carolinensis
Falco_peregrinus
Falco_cherrug
Columba livia
Cuculus_canorus
Eurypyga_helias
Tyto_alba
Leptosomus_discolor
Phaethon_lepturus
Corvus_cornix_cornix
Corvus_brachyrhynchos
Taeniopygia_guttata
Pseudopodoces_humilis
Parus_major
Serinus_canaria
Geospiza_fortis
Zonotrichia_albicollis
Sturnus_vulgaris
Ficedula_albicollis
Erithacus_rubecula


Colius_striatus
Tinamus_guttatus
Pygoscelis_adeliae
Aptenodytes_forsteri
Haliaeetus_albicilla
Phalacrocorax_carbo
Nipponia_nippon
Gavia_stellata
Pelecanus_crispus
Pterocles_gutturalis
Anser_cygnoides_domesticus
Gallus_gallus
Meleagris_gallopavo
Coturnix_japonica
Chaetura_pelagica
Mesitornis_unicolor
Opisthocomus_hoazin
Antrostomus_carolinensis
Falco_peregrinus
Falco_cherrug
Columba livia
Cuculus_canorus
Eurypyga_helias
Tyto_alba
Leptosomus_discolor
Phaethon_lepturus
Corvus_cornix_cornix
Corvus_brachyrhynchos
Taeniopygia_guttata
Pseudopodoces_humilis
Parus_major
Serinus_canaria
Geospiza_fortis
Zonotrichia_albicollis
Sturnus_vulgaris
Ficedula_albicollis
Erithacus_rubecula

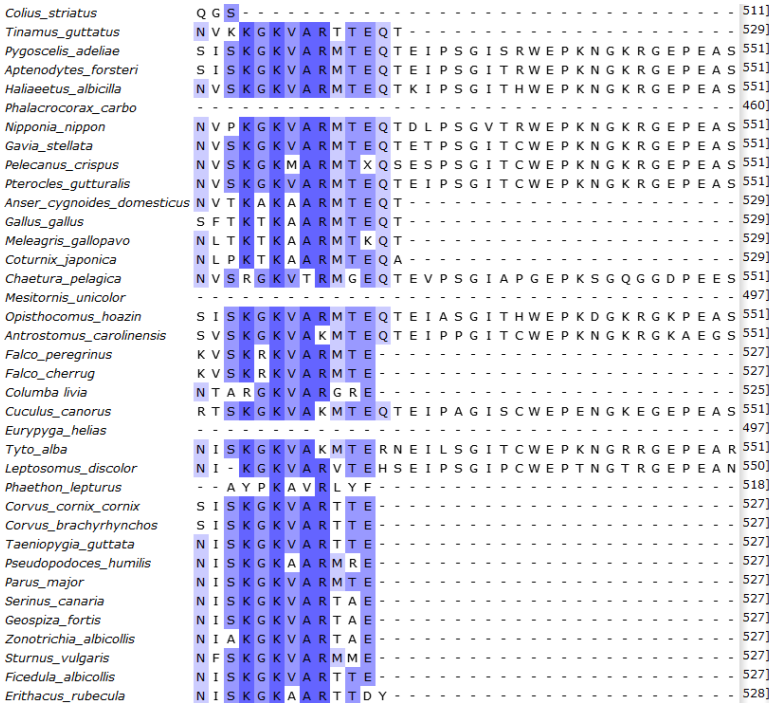


Figure 6.10. Full sequence alignment of different avian Cry4s.

BIBLIOGRAPHY

1. Acosta-Avalos, D. *et al.* Isolation of magnetic nanoparticles from *Pachycondyla marginata* ants. *J. Exp. Biol.* **202**, 2687–2692 (1999).

2. Ahmad, M. & Cashmore, A. R. HY4 gene of *A. thaliana* encodes a protein with characteristics of a blue-light photoreceptor. *Nature* **366**, 162–166 (1993).

3. Ahmad, M., Galland, P., Ritz, T., Wiltschko, R. & Wiltschko, W. Magnetic intensity affects Cryptochrome-dependent responses in *Arabidopsis thaliana*. *Planta* **225**, 615–624 (2007).

4. Alerstam, T. Findings of dead birds drifted ashore reveal catastrophic mortality among early spring migrants, especially rooks *Corvus frugilegus* over the southern Baltic Sea. *Anser* **27**, 181–218 (1988).

5. Angerhofer, A. & Bittl, R. Radicals and radical pairs in photosynthesis. *Photochemistry and Photobiology* vol. 63 11–38 (1996).

6. Armstrong, J. D., Texada, M. J., Munjaal, R., Baker, D. A. & Beckingham, K. M. Gravitaxis in *Drosophila melanogaster*: a forward genetic screen. *Genes, Brain Behav.* **5**, 222–239 (2006).

7. Bae, J.-E. *et al.* Positive geotactic behaviors induced by geomagnetic field in *Drosophila*. *Mol. Brain* **9**, 55 (2016).

8. Bazalova, O. *et al.* Cryptochrome 2 mediates directional magnetoreception in cockroaches. *Proc. Natl. Acad. Sci. U. S. A.* **113**, 1660–1665 (2016).

9. Bazylinski, D. A. & Frankel, R. B. Magnetosome formation in prokaryotes. *Nature Reviews Microbiology* vol. 2 217–230 (2004).

10. Begall, S., Malkemper, E. P., Červený, J., Němec, P. & Burda, H. Magnetic alignment in mammals and other animals. *Mammalian Biology* vol. 78 10–20 (2013).

11. Berndt, A. *et al.* A novel photoreaction mechanism for the circadian blue light photoreceptor *Drosophila* cryptochrome. *J. Biol. Chem.* **282**, 13011–21 (2007).

12. Biskup, T. *et al.* Unexpected electron transfer in cryptochrome identified by time-resolved EPR spectroscopy. *Angew. Chemie - Int. Ed.* **50**, 12647–12651 (2011).

13. Björn, L. O. *Photobiology: The science of light and life, third edition*. *Photobiology: The Science of Light and Life, Third Edition* (Springer New York, 2015). doi:10.1007/978-1-4939-1468-5.

14. Blakemore, R. Magnetotactic bacteria. *Science (80-.).* **190**, 377–379 (1975).

15. Bolte, P. *et al.* Localisation of the putative magnetoreceptive protein Cryptochrome 1b in the retinae of migratory birds and homing pigeons. *PLoS One* **11**, e0147819 (2016).

16. Bottesch, M. *et al.* A magnetic compass that might help coral reef fish larvae return to their natal reef. *Current Biology* vol. 26 R1266–R1267 (2016).

17. Brettel, K. & Byrdin, M. Reaction mechanisms of DNA photolyase. *Current Opinion in Structural Biology* vol. 20 693–701 (2010).

18. C. Martinez, J. *et al.* Isothermal Titration Calorimetry: Thermodynamic Analysis of the Binding Thermograms of Molecular Recognition Events by Using Equilibrium Models. in *Applications of Calorimetry in a Wide Context - Differential Scanning Calorimetry, Isothermal Titration Calorimetry and Microcalorimetry* (InTech, 2013). doi:10.5772/53311.

19. Cailliez, F., Müller, P., Firmino, T., Pernot, P. & De La Lande, A. Energetics of Photoinduced Charge Migration within the Tryptophan Tetrad of an Animal (6-4) Photolyase. *J. Am. Chem. Soc.* **138**, 1904–1915 (2016).

20. Chae, K. S., Oh, I. T., Lee, S. H. & Kim, S. C. Blue light-dependent human magnetoreception in geomagnetic food orientation. *PLoS One* **14**, e0211826 (2019).

21. Chaves, I. *et al.* The Cryptochromes: Blue light photoreceptors in plants and animals. *Annu. Rev. Plant Biol.* **62**, 335–364 (2011).

22. Chernetsov, N. *et al.* Migratory Eurasian Reed Warblers Can Use Magnetic Declination to Solve the Longitude Problem. *Curr. Biol.* **27**, 2647-2651.e2 (2017).

23. Chowdhry, B. Z. & Harding, S. E. *Protein-ligand interactions : hydrodynamics and calorimetry : a practical approach*. *The practical approach series* (Oxford University Press, 2001).

24. Clayton, D. L. Circadian and geotactic behaviors: Genetic pleiotropy in *Drosophila melanogaster*. *J. Circadian Rhythms* **14**, 1–5 (2016).

25. Cooper, M. A. Optical biosensors in drug discovery. *Nature Reviews Drug Discovery* vol. 1 515–528 (2002).

26. Coyne, J. A. *et al.* Long-Distance Migration of *Drosophila*. *Am. Nat.* **119**, 589–595 (1982).

27. Cranfield, C. G. *et al.* Biogenic magnetite in the nematode *Caenorhabditis elegans*. *Proc. R. Soc. B Biol. Sci.* **271**, (2004).

28. Czarna, A. *et al.* Structures of *Drosophila* Cryptochrome and mouse Cryptochrome 1 provide insight into circadian function. *Cell* **153**, 1394–1405 (2013).

29. Davila, A. F., Fleissner, G., Winklhofer, M. & Petersen, N. A new model for a magnetoreceptor in homing pigeons based on interacting clusters of superparamagnetic magnetite. *Phys. Chem. Earth* **28**, 647–652 (2003).

30. Deguen, R. & Lasbleis, M. Fluid dynamics of earth's core: Geodynamo, inner core dynamics, core formation. in *CISM International Centre for Mechanical Sciences, Courses and Lectures* vol. 595 129–212 (Springer International Publishing, 2020).

31. Diebel, C. E., Proksch, R., Green, C. R., Neilson, P. & Walker, M. M. Magnetite defines a vertebrate magnetoreceptor. *Nature* **406**, 299–302 (2000).

32. Dodson, C. A., Hore, P. J. & Wallace, M. I. A radical sense of direction: Signalling and mechanism in Cryptochrome magnetoreception. *Trends Biochem. Sci.* **38**, 435–446 (2013).

33. Dolezelova, E., Dolezel, D. & Hall, J. C. Rhythm defects caused by newly engineered null mutations in *Drosophila'*s cryptochrome gene. *Genetics* **177**, 329–345 (2007).

34. Dommer, D. H., Gazzolo, P. J., Painter, M. S. & Phillips, J. B. Magnetic compass orientation by larval *Drosophila melanogaster*. *J. Insect Physiol.* **54**, 719–726 (2008).

35. Efimova, O. & Hore, P. J. Role of exchange and dipolar interactions in the radical pair model of the avian magnetic compass. *Biophys. J.* **94**, 1565–1574 (2008).

36. Emery, P. *et al. Drosophila* CRY is a deep brain circadian photoreceptor. *Neuron* **26**, 493–504 (2000).

37. Emlen, S. T. Decision making by nocturnal bird migrants: the integration of multiple cues. *Acta XVII Congr. Intern. Ornithol., Berlin* 553–60 (1980).

38. Emlen, S. T. & Emlen, J. T. A Technique for recording migratory orientation of captive birds. *Auk* **83**, 361–367 (1966).

39. Engelhard, C. *et al.* Cellular metabolites enhance the light sensitivity of *Arabidopsis* cryptochrome through alternate electron transfer pathways. *Plant Cell* **26**, 4519–4531 (2014).

40. Engels, S. *et al.* Anthropogenic electromagnetic noise disrupts magnetic compass orientation in a migratory bird. *Nature* **509**, 353–356 (2014).

41. Ernst, D. A. & Lohmann, K. J. Effect of magnetic pulses on Caribbean spiny lobsters: Implications for magnetoreception. *J. Exp. Biol.* **219**, 1827–1832 (2016).

42. Falkenberg, G. *et al.* Avian magnetoreception: Elaborate iron mineral containing dendrites in the upper beak seem to be a common feature of birds. *PLoS One* **5**, e9231 (2010).

43. Fedele, G. *et al.* Genetic analysis of circadian responses to low frequency electromagnetic fields in *Drosophila melanogaster*. *PLoS Genet.* **10**, e1004804 (2014).

44. Fedele, G., Green, E. W., Rosato, E. & Kyriacou, C. P. An electromagnetic field disrupts negative geotaxis in *Drosophila* via a CRY-dependent pathway. *Nat. Commun.* **5**, 4391 (2014).

45. Fleissner, G., Stahl, B., Thalau, P., Falkenberg, G. & Fleissner, G. A novel concept of Fe-mineral-based magnetoreception: Histological and physicochemical data from the upper beak of homing pigeons. *Naturwissenschaften* **94**, 631–642 (2007).

46. Foley, L. E., Gegear, R. J. & Reppert, S. M. Human Cryptochrome exhibits light-dependent magnetosensitivity. *Nat. Commun.* **2**, 356 (2011).

47. Gegear, R. J., Casselman, A., Waddell, S. & Reppert, S. M. Cryptochrome mediates light-dependent magnetosensitivity in *Drosophila*. *Nature* **454**, 1014–1018 (2008).

48. Gegear, R. J., Foley, L. E., Casselman, A. & Reppert, S. M. Animal Cryptochromes mediate magnetoreception by an unconventional photochemical mechanism. *Nature* **463**, 804–807 (2010).

49. Giachello, C. N. G., Scrutton, N. S., Jones, A. R. & Baines, R. A. Magnetic fields modulate blue-light-dependent regulation of neuronal firing by Cryptochrome. *J.*

Neurosci. **36**, 10742–10749 (2016).

50. Giovani, B., Byrdin, M., Ahmad, M. & Brettel, K. Light-induced electron transfer in a cryptochrome blue-light photoreceptor. *Nat. Struct. Biol.* **10**, 489–490 (2003).

51. Glatzmaiers, G. A. & Roberts, P. H. A three-dimensional self-consistent computer simulation of a geomagnetic field reversal. *Nature* **377**, 203–209 (1995).

52. Gould, J. L., Kirschvink, J. L. & Deffeyes, K. S. Bees have magnetic remanence. *Science (80-.).* **201**, 1026–1028 (1978).

53. Günther, A. *et al.* Double-cone localization and seasonal expression pattern suggest a role in magnetoreception for European robin Cryptochrome 4. *Curr. Biol.* **28**, 211–223 (2018).

54. Harris, S. R. *et al.* Effect of magnetic fields on cryptochrome-dependent responses in *Arabidopsis thaliana*. *J. R. Soc. Interface* **6**, 1193–1205 (2009).

55. Hein, C. M. *et al.* Night-migratory garden warblers can orient with their magnetic compass using the left, the right or both eyes. *J. R. Soc. Interface* **7**, (2010).

56. Hein, C. M., Engels, S., Kishkinev, D. & Mouritsen, H. Robins have a magnetic compass in both eyes. *Nature* vol. 471 E11-2; discussion E12-3 (2011).

57. Helfrich-Förster, C. The *Drosophila* clock system. in *Biological Timekeeping: Clocks, Rhythms and Behaviour* 133–176 (Springer India, 2017). doi:10.1007/978-81-322-3688-7_6.

58. Henbest, K. B., Kukura, P., Rodgers, C. T., Hore, P. J. & Timmel, C. R. Radio frequency magnetic field effects on a radical recombination reaction: A diagnostic test for the radical pair mechanism. *J. Am. Chem. Soc.* **126**, 8102–8103 (2004).

59. Henbest, K. B. *et al.* Magnetic-field effect on the photoactivation reaction of Escherichia coli DNA photolyase. *Proc. Natl. Acad. Sci. U. S. A.* **105**, 14395–14399 (2008).

60. Heyers, D., Manns, M., Luksch, H., Güntürkün, O. & Mouritsen, H. A visual pathway links brain structures active during magnetic compass orientation in migratory birds. *PLoS One* **2**, (2007).

61. Heyers, D., Zapka, M., Hoffmeister, M., Wild, J. M. & Mouritsen, H. Magnetic field changes activate the trigeminal brainstem complex in a migratory bird. *Proc. Natl. Acad.*

Sci. U. S. A. **107**, 9394–9399 (2010).

62. Hirsch, J. & Erlenmeyer-Kimling, L. Sign of taxis as a property of the genotype. *Science (80-.).* **134**, 835–836 (1961).

63. Hiscock, H. G. *et al.* The quantum needle of the avian magnetic compass. *Proc. Natl. Acad. Sci. U. S. A.* **113**, 4634–4639 (2016).

64. Hiscock, H. G., Mouritsen, H., Manolopoulos, D. E. & Hore, P. J. Disruption of magnetic compass orientation in migratory birds by radiofrequency electromagnetic fields. *Biophys. J.* **113**, 1475–1484 (2017).

65. Hoang, N. *et al.* Human and *Drosophila* Cryptochromes are light activated by flavin photoreduction in living cells. *PLoS Biol* **6**, 160 (2008).

66. Hogben, H. J., Efimova, O., Wagner-Rundell, N., Timmel, C. R. & Hore, P. J. Possible involvement of superoxide and dioxygen with cryptochrome in avian magnetoreception: Origin of Zeeman resonances observed by in vivo EPR spectroscopy. *Chem. Phys. Lett.* **480**, 118–122 (2009).

67. Hore, P. J. & Mouritsen, H. The radical-pair mechanism of magnetoreception. *Annu. Rev. Biophys.* **45**, 299–344 (2016).

68. Van Der Horst, G. T. J. *et al.* Mammalian Cry1 and Cry2 are essential for maintenance of circadian rhythms. *Nature* **398**, 627–630 (1999).

69. Inagaki, H. K. *et al.* Methods for quantifying simple gravity sensing in *Drosophila melanogaster*. *Nat. Protoc.* **5**, 20–25 (2010).

70. Irwin, W. P. & Lohmann, K. J. Disruption of magnetic orientation in hatchling loggerhead sea turtles by pulsed magnetic fields. *J. Comp. Physiol. A Neuroethol. Sensory, Neural, Behav. Physiol.* **191**, 475–480 (2005).

71. Jacob, J. J. & Suthindhiran, K. Magnetotactic bacteria and magnetosomes – Scope and challenges. *Materials Science and Engineering C* vol. 68 919–928 (2016).

72. Johnsen, S. & Lohmann, K. J. Magnetoreception in animals. *Phys. Today* **61**, 29–35 (2008).

73. Jones, J. S., Bryant, S. H., Lewontin, R. C., Moore, J. A. & Prout, T. Gene flow and the geographical distribution of a molecular polymorphism in *Drosophila pseudoobscura*.

Genetics **98**, 157–178 (1981).

74. Kain, J. S., Stokes, C. & De Bivort, B. L. Phototactic personality in fruit flies and its suppression by serotonin and white. *Proc. Natl. Acad. Sci. U. S. A.* **109**, 19834–19839 (2012).

75. Kalmijn, A. J. Biophysics of geomagnetic field detection. *IEEE Trans. Magn.* **17**, 1113–1124 (1981).

76. Kalmijn, A. J. Electric and magnetic field detection in elasmobranch fishes. *Science (80-.).* **218**, 916–918 (1982).

77. Kattnig, D. R. *et al.* Chemical amplification of magnetic field effects relevant to avian magnetoreception. *Nat. Chem.* **8**, 384–391 (2016).

78. Kavokin, K. *et al.* Magnetic orientation of garden warblers (*Sylvia borin*) under 1.4 MHz radiofrequency magnetic field. *J. R. Soc. Interface* **11**, (2014).

79. Keary, N. *et al.* Oscillating magnetic field disrupts magnetic orientation in Zebra finches, *Taeniopygia guttata*. *Front. Zool.* **6**, 1–7 (2009).

80. Kerpal, C. *et al.* Chemical compass behaviour at microtesla magnetic fields strengthens the radical pair hypothesis of avian magnetoreception. *Nat. Commun.* **10**, (2019).

81. Kirschvink, J. L. & Gould, J. L. Biogenic magnetite as a basis for magnetic field detection in animals. *BioSystems* **13**, 181–201 (1981).

82. Kirschvink, J. L. & Walker, M. M. Particle-size considerations for magnetite-based magnetoreceptors. in 243–254 (Springer, Boston, MA, 1985). doi:10.1007/978-1-4613-0313-8_11.

83. Kirschvink, J. L. Uniform magnetic fields and double-wrapped coil systems: Improved techniques for the design of bioelectromagnetic experiments. *Bioelectromagnetics* **13**, 401–411 (1992).

84. Kirschvink, J. L., Winklhofer, M. & Walker, M. M. Biophysics of magnetic orientation: Strengthening the interface between theory and experimental design. *Journal of the Royal Society Interface* vol. 7 S179-91 (2010).

85. Kishkinev, D., Chernetsov, N., Pakhomov, A., Heyers, D. & Mouritsen, H. Eurasian reed warblers compensate for virtual magnetic displacement. *Current Biology* vol. 25

R822–R824 (2015).

86. Kobylkov, D. *et al.* A newly identified trigeminal brain pathway in a night-migratory bird could be dedicated to transmitting magnetic map information. *Proceedings. Biol. Sci.* **287**, 20192788 (2020).

87. Kobylkov, D. *et al.* Electromagnetic 0.1-100 kHz noise does not disrupt orientation in a night-migrating songbird implying a spin coherence lifetime of less than 10 μs. *J. R. Soc. Interface* **16**, (2019).

88. Komolkin, A. V. *et al.* Theoretically possible spatial accuracy of geomagnetic maps used by migrating animals. *J. R. Soc. Interface* **14**, (2017).

89. Krylov, V. V., Iziumov, I. G., Izvekov, E. I. & Nepomniashchikh, V. A. Magnetic fields and fish behavior. *Zhurnal obshcheĭ biologii* vol. 74 354–365 (2013).

90. Kutta, R. J., Archipowa, N., Johannissen, L. O., Jones, A. R. & Scrutton, N. S. Vertebrate Cryptochromes are vestigial flavoproteins. *Sci. Rep.* **7**, 44906 (2017).

91. Lambinet, V., Hayden, M. E., Reigl, K., Gomis, S. & Gries, G. Linking magnetite in the abdomen of honey bees to a magnetoreceptive function. *Proc. R. Soc. B Biol. Sci.* **284**, (2017).

92. Lee, A. A. *et al.* Alternative radical pairs for cryptochrome-based magnetoreception. *J. R. Soc. Interface* **11**, (2014).

93. Levy, C. *et al.* Updated structure of *Drosophila* cryptochrome. *Nature* vol. 495 E3 (2013).

94. Li, X. *et al.* Arabidopsis cryptochrome 2 (CRY2) functions by the photoactivation mechanism distinct from the tryptophan (trp) triad-dependent photoreduction. *Proc. Natl. Acad. Sci. U. S. A.* **108**, 20844–20849 (2011).

95. Liedvogel, M. *et al.* Chemical magnetoreception: Bird Cryptochrome 1a is excited by blue light and forms long-lived radical-pairs. *PLoS One* **2**, e1106 (2007).

96. Liedvogel, M. *et al.* Lateralized activation of Cluster N in the brains of migratory songbirds. *Eur. J. Neurosci.* **25**, 1166–1173 (2007).

97. Liedvogel, M. & Mouritsen, H. Cryptochromes - A potential magnetoreceptor: What do we know and what do we want to know? *Journal of the Royal Society Interface* vol. 7

(2010).

98. Lohmann, K. J., Cain, S. D., Dodge, S. A. & Lohmann, C. M. F. Regional magnetic fields as navigational markers for sea turtles. *Science (80-.).* **294**, 364–366 (2001).

99. Lohmann, K. J. & Lohmann, C. A Light-Independent Magnetic Compass in the Leatherback Sea Turtle. *Biol. Bull.* **185**, 149–151 (1993).

100. Lohmann, K. J., Lohmann, C. M. F. & Putman, N. F. Magnetic maps in animals: Nature's GPS. *Journal of Experimental Biology* vol. 210 3697–3705 (2007).

101. Maeda, K. *et al.* Magnetically sensitive light-induced reactions in Cryptochrome are consistent with its proposed role as a magnetoreceptor. *Proc. Natl. Acad. Sci. U. S. A.* **109**, 4774–9 (2012).

102. Mann, S., Sparks, N. H., Walker, M. M. & Kirschvink, J. L. Ultrastructure, morphology and organization of biogenic magnetite from sockeye salmon, Oncorhynchus nerka: implications for magnetoreception. *J. Exp. Biol.* **140**, 35–49 (1988).

103. Marley, R., Giachello, C. N. G., Scrutton, N. S., Baines, R. A. & Jones, A. R. Cryptochrome-dependent magnetic field effect on seizure response in *Drosophila* larvae. *Sci. Rep.* **4**, 5799 (2014).

104. Mertens, I. *et al.* PDF receptor signaling in *Drosophila* contributes to both circadian and geotactic behaviors. *Neuron* **48**, 213–219 (2005).

105. Mitsui, H. *et al.* Overexpression in yeast, photocycle, and in vitro structural change of an avian putative magnetoreceptor Cryptochrome4. *Biochemistry* **54**, 1908–1917 (2015).

106. Mora, C. V., Davison, M., Martin Wild, J. & Walker, M. M. Magnetoreception and its trigeminal mediation in the homing pigeon. *Nature* **432**, 508–511 (2004).

107. Moser, C. C., Keske, J. M., Warncke, K., Farid, R. S. & Dutton, P. L. Nature of biological electron transfer. *Nature* **355**, 796–802 (1992).

108. Mouritsen, H. Long-distance navigation and magnetoreception in migratory animals. *Nature* **558**, 50–59 (2018).

109. Mouritsen, H. Magnetoreception in birds and its use for long-distance migration. in *Sturkie's Avian Physiology: Sixth Edition* 113–133 (Elsevier Inc., 2014).

doi:10.1016/B978-0-12-407160-5.00008-7.

110. Mouritsen, H. The Magnetic Senses. in *Neurosciences - From molecule to behavior: a university textbook* 427–443 (Springer Berlin Heidelberg, 2013). doi:10.1007/978-3-642-10769-6_20.

111. Mouritsen, H. Sensory biology: Search for the compass needles. *Nature* vol. 484 320–321 (2012).

112. Mouritsen, H., Feenders, G., Liedvogel, M., Wada, K. & Jarvis, E. D. Night-vision brain area in migratory songbirds. *Proc. Natl. Acad. Sci. U. S. A.* **102**, 8339–8344 (2005).

113. Mouritsen, H., Heyers, D. & Güntürkün, O. The neural basis of long-distance navigation in birds. *Annu. Rev. Physiol.* **78**, 133–154 (2016).

114. Mouritsen, H. & Hore, P. J. The magnetic retina: Light-dependent and trigeminal magnetoreception in migratory birds. *Current Opinion in Neurobiology* vol. 22 343–352 (2012).

115. Müller, P. & Ahmad, M. Light-activated cryptochrome reacts with molecular oxygen to form a flavin-superoxide radical pair consistent with magnetoreception. *J. Biol. Chem.* **286**, 21033–40 (2011).

116. Müller, P., Yamamoto, J., Martin, R., Iwai, S. & Brettel, K. Discovery and functional analysis of a 4th electron-transferring tryptophan conserved exclusively in animal cryptochromes and (6-4) photolyases. *Chem. Commun.* **51**, 15502–15505 (2015).

117. Neil, S. R. T. *et al.* Broadband cavity-enhanced detection of magnetic field effects in chemical models of a cryptochrome magnetoreceptor. *J. Phys. Chem. B* **118**, 4177–4184 (2014).

118. Nielsen, C., Kattnig, D. R., Sjulstok, E., Hore, P. J. & Solov'yov, I. A. Ascorbic acid may not be involved in cryptochrome-based magnetoreception. *J. R. Soc. Interface* **14**, (2017).

119. Nießner, C. *et al.* Avian Ultraviolet/Violet cones identified as probable magnetoreceptors. *PLoS One* **6**, e20091 (2011).

120. Nießner, C. *et al.* Magnetoreception: Activated Cryptochrome 1a concurs with magnetic orientation in birds. *J. R. Soc. Interface* **10**, (2013).

121. Nießner, C. *et al.* Seasonally changing Cryptochrome 1b expression in the retinal ganglion cells of a migrating passerine bird. *PLoS One* **11**, e0150377 (2016).

122. Nießner, C., Denzau, S., Peichl, L., Wiltschko, W. & Wiltschko, R. Magnetoreception in birds: I. Immunohistochemical studies concerning the Cryptochrome cycle. *J. Exp. Biol.* **217**, 4221–4224 (2014).

123. Nießner, C., Denzau, S., Peichl, L., Wiltschko, W. & Wiltschko, R. Magnetoreception: activation of avian cryptochrome 1a in various light conditions. *J. Comp. Physiol. A Neuroethol. Sensory, Neural, Behav. Physiol.* **204**, 977–984 (2018).

124. Nimpf, S. *et al.* A Putative Mechanism for Magnetoreception by Electromagnetic Induction in the Pigeon Inner Ear. *Curr. Biol.* **29**, 4052-4059.e4 (2019).

125. Oh, I.-T. *et al.* Behavioral evidence for geomagnetic imprinting and transgenerational inheritance in fruit flies. *Proc. Natl. Acad. Sci.* 201914106 (2019) doi:10.1073/pnas.1914106117.

126. Özgür, S. & Sancar, A. Purification and properties of human blue-light photoreceptor Cryptochrome 2. *Biochemistry* **42**, 2926–2932 (2003).

127. Ozturk, N. *et al.* Comparative photochemistry of animal type 1 and type 4 Cryptochromes. *Biochemistry* **48**, 8585–8593 (2009).

128. Ozturk, N., Selby, C. P., Annayev, Y., Zhong, D. & Sancar, A. Reaction mechanism of *Drosophila* cryptochrome. *Proc. Natl. Acad. Sci. U. S. A.* **108**, 516–521 (2011).

129. Ozturk, N., Selby, C. P., Zhong, D. & Sancar, A. Mechanism of photosignaling by *Drosophila* cryptochrome role of the redox status of the flavin chromophore. *J. Biol. Chem.* **289**, 4634–4642 (2014).

130. Painter, M. S., Dommer, D. H., Altizer, W. W., Muheim, R. & Phillips, J. B. Spontaneous magnetic orientation in larval *Drosophila* shares properties with learned magnetic compass responses in adult flies and mice. *J. Exp. Biol.* **216**, 1307–1316 (2013).

131. Pakhomov, A. *et al.* Very weak oscillating magnetic field disrupts the magnetic compass of songbird migrants. *J. R. Soc. Interface* **14**, (2017).

132. Paulin, M. G. Electroreception and the compass sense of sharks. *J. Theor. Biol.* **174**,

325–339 (1995).

133. Peschel, N., Chen, K. F., Szabo, G. & Stanewsky, R. Light-dependent interactions between the *Drosophila* circadian clock factors Cryptochrome, Jetlag, and Timeless. *Curr. Biol.* **19**, 241–247 (2009).

134. Phillips, J. B. & Sayeed, O. Wavelength-dependent effects of light on magnetic compass orientation in *Drosophila melanogaster*. *J. Comp. Physiol. A* **172**, 303–308 (1993).

135. Phillips, J. B. Two magnetoreception pathways in a migratory salamander. *Science (80-.).* **233**, 765–767 (1986).

136. Phillips, J. B. & Borland, S. C. Behavioural evidence for use of a light-dependent magnetoreception mechanism by a vertebrate. *Nature* **359**, 142–144 (1992).

137. Picton, H. D. Some responses of *Drosophila* to weak magnetic and electrostatic fields. *Nature* vol. 211 303–304 (1966).

138. Pinzon-Rodriguez, A. & Muheim, R. Zebra finches have a light-dependent magnetic compass similar to migratory birds. *J. Exp. Biol.* **220**, 1202–1209 (2017).

139. Player, T. C. & Hore, P. J. Viability of superoxide-containing radical pairs as magnetoreceptors. *J. Chem. Phys.* **151**, 225101 (2019).

140. Qin, S. *et al.* A magnetic protein biocompass. *Nat. Mater.* **15**, 217–226 (2016).

141. Renn, S. C. P., Park, J. H., Rosbash, M., Hall, J. C. & Taghert, P. H. A pdf neuropeptide gene mutation and ablation of PDF neurons each cause severe abnormalities of behavioral circadian rhythms in *Drosophila*. *Cell* **99**, 791–802 (1999).

142. Ritz, T. *et al.* Magnetic compass of birds is based on a molecule with optimal directional sensitivity. *Biophys. J.* **96**, 3451–3457 (2009).

143. Ritz, T., Adem, S. & Schulten, K. A model for photoreceptor-based magnetoreception in birds. *Biophys. J.* **78**, 707–718 (2000).

144. Ritz, T., Thalau, P., Phillips, J. B., Wiltschko, R. & Wiltschko, W. Resonance effects indicate a radical-pair mechanism for avian magnetic compass. *Nature* **429**, 177–180 (2004).

145. Rodgers, C. T. Magnetic field effects in chemical systems. *Pure and Applied Chemistry* vol. 81 19–43 (2009).

146. Rodgers, C. T., Norman, S. A., Henbest, K. B., Timmel, C. R. & Hore, P. J. Determination of radical re-encounter probability distributions from magnetic field effects on reaction yields. *J. Am. Chem. Soc.* **129**, 6746–6755 (2007).

147. Rosato, E. *et al.* Light-dependent interaction between *Drosophila* CRY and the clock protein PER mediated by the carboxy terminus of CRY. *Curr. Biol.* **11**, 909–917 (2001).

148. Sancar, A. Structure and function of DNA photolyase and cryptochrome blue-light photoreceptors. *Chem. Rev.* **103**, 2203–2237 (2003).

149. Sancar, A. Cryptochrome: The second photoactive pigment in the eye and its role in circadian photoreception. *Annu. Rev. Biochem.* **69**, 31–67 (2000).

150. Schindelin, J. *et al.* Fiji: An open-source platform for biological-image analysis. *Nature Methods* vol. 9 676–682 (2012).

151. Schulten, K., Swenberg, C. E. & Weiler, A. A biomagnetic sensory mechanism based on magnetic field modulated coherent electron spin motion. *Zeitschrift fur Phys. Chemie* **111**, 1–5 (1978).

152. Schwarze, S. *et al.* Weak broadband electromagnetic fields are more disruptive to magnetic compass orientation in a night-migratory songbird (*Erithacus rubecula*) than strong narrow-band fields. *Front. Behav. Neurosci.* **10**, 55 (2016).

153. Sheppard, D. M. W. *et al.* Millitesla magnetic field effects on the photocycle of an animal Cryptochrome. *Sci. Rep.* **7**, 42228 (2017).

154. Solov'yov, I. A., Chandler, D. E. & Schulten, K. Magnetic field effects in Arabidopsis thaliana cryptochrome-1. *Biophys. J.* **92**, 2711–2726 (2007).

155. Solov'yov, I. A. & Schulten, K. Magnetoreception through cryptochrome may involve superoxide. *Biophys. J.* **96**, 4804–4813 (2009).

156. Stanewsky, R. *et al.* The cry(b) mutation identifies Cryptochrome as a circadian photoreceptor in *Drosophila*. *Cell* **95**, 681–692 (1998).

157. Steiner, U. E. & Ulrich, T. Magnetic field effects in chemical kinetics and related phenomena. *Chem. Rev.* **89**, 51–147 (1989).

158. Takahashi, J. S. Molecular components of the circadian clock in mammals. *Diabetes, Obesity and Metabolism* vol. 17 6–11 (2015).

159. Thalau, P., Ritz, T., Stapput, K., Wiltschko, R. & Wiltschko, W. Magnetic compass orientation of migratory birds in the presence of a 1.315 MHz oscillating field. *Naturwissenschaften* **92**, 86–90 (2005).

160. Toma, D. P., White, K. P., Hirsch, J. & Greenspan, R. J. Identification of genes involved in *Drosophila melanogaster* geotaxis, a complex behavioral trait. *Nat. Genet.* **31**, 349–353 (2002).

161. Towe, K. M. & Lowenstam, H. A. Ultrastructure and development of iron mineralization in the radular teeth of Cryptochiton stelleri (mollusca). *J. Ultrasructure Res.* **17**, 1–13 (1967).

162. Treiber, C. D. *et al.* Clusters of iron-rich cells in the upper beak of pigeons are macrophages not magnetosensitive neurons. *Nature* **484**, 367–370 (2012).

163. Treiber, C. D. *et al.* High resolution anatomical mapping confirms the absence of a magnetic sense system in the rostral upper beak of pigeons. *Commun. Integr. Biol.* **6**, (2013).

164. Vácha, M., Půžová, T. & Kvíčalová, M. Radio frequency magnetic fields disrupt magnetoreception in American cockroach. *J. Exp. Biol.* **212**, 3473–3477 (2009).

165. Wang, C. X. *et al.* Transduction of the geomagnetic field as evidenced from alpha-band activity in the human brain. *eNeuro* **6**, ENEURO.0483-18.2019 (2019).

166. Wang, J. & Pantopoulos, K. Regulation of cellular iron metabolism. *Biochemical Journal* vol. 434 365–381 (2011).

167. Weber, S. *et al.* Origin of light-induced spin-correlated radical pairs in cryptochrome. *J. Phys. Chem. B* **114**, 14745–14754 (2010).

168. Wehner, R. & Labhart, T. Perception of the geomagnetic field in the fly *Drosophila melanogaster*. *Experientia* **26**, 967–968 (1970).

169. van Wilderen, L. J. G. W., Silkstone, G., Mason, M., van Thor, J. J. & Wilson, M. T. Kinetic studies on the oxidation of semiquinone and hydroquinone forms of Arabidopsis cryptochrome by molecular oxygen. *FEBS Open Bio* **5**, 885–892 (2015).

170. Wiltschko, R., Gehring, D., Denzau, S., Nießner, C. & Wiltschko, W. Magnetoreception in birds: II. Behavioural experiments concerning the Cryptochrome cycle. *J. Exp. Biol.*

217, 4225–4228 (2014).

171. Wiltschko, R., Stapput, K., Thalau, P. & Wiltschko, W. Directional orientation of birds by the magnetic field under different light conditions. *Journal of the Royal Society Interface* vol. 7 (2010).

172. Wiltschko, R. & Wiltschko, W. Magnetoreception: Why is conditioning so seldom successful? *Naturwissenschaften* **83**, 241–247 (1996).

173. Wiltschko, R. & Wiltschko, W. Magnetoreception. *BioEssays* vol. 28 157–168 (2006).

174. Wiltschko, W. & Wiltschko, R. Magnetic compass of European robins. *Science (80-.).* **176**, 62–64 (1972).

175. Wiltschko, W. Über den Einfluß statischer Magnetfelder auf die Zugorientierung der Rotkehlchen (Erithacus rubecula). *Z. Tierpsychol.* **25**, 537–558 (1968).

176. Wiltschko, W. *et al.* The magnetic compass of domestic chickens, Gallus gallus. *J. Exp. Biol.* **210**, 2300–2310 (2007).

177. Wiltschko, W., Munro, U., Ford, H. & Wiltschko, R. Red light disrupts magnetic orientation of migratory birds. *Nature* **364**, 525–527 (1993).

178. Wiltschko, W., Traudt, J., Güntürkün, O., Prior, H. & Wiltschko, R. Lateralization of magnetic compass orientation in a migratory bird. *Nature* **419**, 467–470 (2002).

179. Wiltschko, W. & Wiltschko, R. Magnetic orientation and magnetoreception in birds and other animals. *J. Comp. Physiol. A Neuroethol. Sensory, Neural, Behav. Physiol.* **191**, 675–693 (2005).

180. Winklhofer, M. & Kirschvink, J. L. A quantitative assessment of torque-transducer models for magnetoreception. *J. R. Soc. Interface* **7**, (2010).

181. Woodward, J. R. Radical pairs in solution. *Prog. React. Kinet. Mech.* **27**, 165–207 (2002).

182. Wu, C. L. *et al.* Magnetoreception regulates male courtship activity in *Drosophila*. *PLoS One* **11**, e0155942 (2016).

183. Xing, W. *et al.* SCF FBXL3 ubiquitin ligase targets cryptochromes at their cofactor pocket. *Nature* **496**, 64–68 (2013).

184. Xu, J. *et al.* Cryptochrome 4 from a night-migratory songbird has the magnetic properties required of a light-dependent magnetoreceptor. *Nat. (submitted, under Revis.*

185. Yoshii, T., Ahmad, M. & Helfrich-Förster, C. Cryptochrome mediates light-dependent magnetosensitivity of *Drosophila*'s circadian clock. *PLoS Biol.* **7**, e1000086 (2009).

186. Yuan, X., Wang, W., Wu, W. & Wang, J. Efficient expression and purification of Cryptochrome1 from Columbia livia in E. coli. *Protein Pept. Lett.* **25**, 986–995 (2018).

187. Zapka, M. *et al.* Visual but not trigeminal mediation of magnetic compass information in a migratory bird. *Nature* **461**, 1274–1277 (2009).

188. Zeugner, A. *et al.* Light-induced electron transfer in Arabidopsis cryptochrome-1 correlates with in vivo function. *J. Biol. Chem.* **280**, 19437–19440 (2005).

189. Zhu, H. *et al.* The two CRYs of the butterfly. *Curr. Biol.* **16**, 730 (2005).

190. Zoltowski, B. D. *et al.* Chemical and structural analysis of a photoactive vertebrate cryptochrome from pigeon. *Proc. Natl. Acad. Sci. U. S. A.* **116**, 19449–19457 (2019).

Acknowledgments

I would like to start thanking Prof. Peter Hore and Prof. Henrik Mouritsen for their support and guidance during my DPhil.

Special thanks to Dr. Daniel Kattnig for all the help at the beginning of my DPhil. Also, to all the people from the Timmel and Mackenzie groups for all the chats and shared ideas in these years.

I would also like to thank Prof. Scott Waddell and all the people I met in CNBC. It has been fun working with you guys.

Many thanks to everyone I met in Oldenburg, especially to Mitya, with whom I shared an office, countless coffees and ideas.

Special thanks to Ale, Giulio, Piotr, Luca and Bianca. These years wouldn't have been the same without you.

E ovviamente, grazie ai miei genitori e alla mia famiglia. Tutto ciò non sarebbe stato possibile senza di voi.